VNIVERSITAT DE VALÈNCIA

DEPARTAMENTO DE BIOQUÍMICA Y BIOLOGÍA MOLECULAR

PROGRAMA DE DOCTORADO:

BIOQUÍMICA Y BIOMEDICINA (3003)

DEVELOPMENT AND VALIDATION OF NEW METHODS FOR THE STUDY OF OXIDATIVE STRESS BY IMAGING FLOW CYTOMETRY

TESIS DOCTORAL

FRANCISCO JOSE SALA DE OYANGUREN

Director

JOSE ENRIQUE O´CONNOR BLASCO

VALENCIA, MARZO 2017

José Enrique O'Connor Blasco, Catedrático del Departamento de Bioquímica y Biología Molecular de la Universidad de Valencia.

CERTIFICA:

Que la presente Tesis Doctoral titulada **"DEVELOPMENT AND VALIDATION OF NEW METHODS FOR THE STUDY OF OXIDATIVE STRESS BY IMAGING FLOW CYTOMETRY"**, presentada para optar al grado de Doctor en Biología por la Universidad de Valencia, ha sido realizada bajo mi dirección por D. FRANCISCO JOSE SALA DE OYANGUREN, licenciado en Ciencias Biológicas por la Universidad de Valencia.

Lo que certifico en Valencia, a 31 de Marzo de 2017.

Fdo. José Enrique O´Connor Blasco

This Ph. D. Thesis has been partially supported thanks to the incentives granted to the following Research Projects:

Nuevas tecnologías para Toxicología in vitro: Diseño y validación de una plataforma integrada ADMETOX de ensayos celulares para predicción de riesgo químico en humanos. Ministerio de Ciencia e Innovación (BIO2010-19870).

Desarrollo de una estrategia de ensayos citómicos para detección temprana y predicción de toxicidad crónica humana de fármacos y xenobióticos. Universitat de València, Convocatòria Accions Especials 2015 (UV-INV-AE15-349700).

ACKOWLEDGEMENTES

Firstly, I would like to express my sincere gratitude to my advisor Professor Jose-Enrique O'Connor for the continuous support of my Ph. D study and related research, for his patience, motivation and immense knowledge. His guidance helped me in all the time of research and writing of this thesis. I could not have imagined having a better advisor and mentor for my Ph. D. study. Thank you for all the moments lived during these years, inside and outside (congresses, workshops, conferences, meetings, courses...) the laboratory.

Second, I would like to express my gratitude to Dr. Guadalupe Herrera, Dr. Alicia Martinez, Domingo Gil, Beatriz Jávega and Jesús Tamarit and to all my colleagues from the Faculty of Medicine of the University of Valencia (UV) and from the Principe Felipe Research Center (CIPF). This work would not have been possible without your help and support throughout these years.

My sincere thanks also go to Dr. Anne Wilson, from the Ludwig Center for Cancer Research of the University of Lausanne, who provided me an opportunity to join her excellent work team as intern, giving me access to apply for the International Mention for this Ph. D thesis. Special thanks to Gabriel Siegert, who gave me the occasion to discover Lausanne...

I could not have reached this stage of my education without the encouragement I received from my parents, Vicente and Marita. Thank you both. I am proud to be your son. Special thanks to my brother Jose Maria and my sister Mar, you have kept me motivated and believed in me no matter what.

Finally I would like to thank Carol, who never once doubted that I would succeed. Her faith and patience throughout these years has been irreplaceable.

Thanks for all your support!

ABSTRACT

Oxidative stress is caused by an imbalance between the production of reactive oxygen species (ROS) and the antioxidant mechanisms within the cell. This imbalance in the normal redox state of the cell may cause toxic effects by producing free radicals and peroxides that damage essential components of the cell such as proteins, lipids and membranes, and DNA. Oxidative Stress is currently considered to be involved in the mechanisms of a large number of degenerative diseases and cancer. It is also thought to have an important role in the process of Aging.

One of the main challenges in the study of oxidative processes derives from the short half-life of ROS and from its localized physiological action, restricted to certain cell types and confined in specific subcellular compartments. The development of novel methods based on single-cell analysis and on co-localization with intracellular compartments may be relevant for this purpose.

In the last twenty years, multi-parametric analysis of single cells by conventional Flow Cytometry has been applied to the study of oxidative stress. Recent advances in charge-coupled device camera technology, optical filters and digital computing have now made possible imaging of all the cells in the flow stream. Imaging Flow Cytometry combines the strengths of Microscopy and Flow Cytometry in a single system for quantitative image-based cellular assays in large and heterogeneous cell populations. The combination of both techniques offers novel analytical capabilities and allows a large number of new possible applications beyond the current limitations of Flow Cytometry.

However, this methodology has not yet been significantly applied to the study of oxidative stress and its physiological and pathological implications. The development and validation of an Imaging Cytometry-based method for the evaluation of oxidative processes may help in the understanding of the biological outcomes that ROS are responsible for.

RESUMEN

El estrés oxidativo se origina debido a un desequilibrio entre la producción de especies reactivas de oxígeno (ROS) y los mecanismos celulares antioxidantes. Este desequilibrio en el estado normal redox puede causar efectos tóxicos a través de la producción de radicales libres y peróxidos, que dañan a componentes esenciales de la célula, como proteínas, lípidos y ADN. Actualmente se cree que el estrés oxidativo está relacionado con los mecanismos en un gran número de enfermedades degenerativas y cáncer, y también se le atribuye un papel importante en el proceso de envejecimiento.

Las principales dificultades en el estudio de los procesos del estrés oxidativo derivan de la corta vida media de los ROS y de la localización de su acción fisiológica, restringida a ciertos tipos celulares, y confinada en compartimentos subcelulares específicos. Por ello, el desarrollo de métodos basados en el análisis de células individuales y de sus compartimentos subcelulares es de gran importancia. Asimismo, el estudio de la implicación del estrés oxidativo en las respuestas inmunitarias se vería favorecido por el desarrollo de métodos que permitan el análisis en muestras de sangre entera.

En los últimos veinte años, la capacidad de análisis multiparamétrico de células individuales de la Citometría de Flujo (FCM), que permite evaluar simultáneamente parámetros funcionales y bioquímicos, se ha aplicado al estudio del estrés oxidativo. Más recientemente, una nueva tecnología de análisis celular; la Citometría de Imagen en Flujo (IFCM) aporta sustanciales mejoras con respecto a la FCM convencional, al combinar en un único sistema las capacidades de la microscopia y la citometría. Esta tecnología ofrece nuevas capacidades analíticas y permite multitud de aplicaciones más allá de los límites actuales de la Citometría de Flujo y la Microscopia.

El objetivo principal de este trabajo es comprobar la capacidad de esta nueva tecnología mediante la optimización, puesta a punto y validación de un método basado en Citometría de Imagen en Flujo para evaluar las respuestas oxidativas asociadas a la fagocitosis y a la activación de NF-κB. Para ello hemos desarrollado una serie de ensayos *in vitro* en muestras de sangre entera y modelos celulares de relevancia inmunológica.

INDEX

LIST OF ABBREVIATIONS 9

1. INTRODUCTION 11

1.1 ROS and RNS: definition and physiological functions 13

1.1.1 Sources of ROS and RNS 14

1.1.2 Oxidative stress: causes and consequences 15

1.2 Phagocytosis 18

1.3 Oxidative Burst 26

1.3.1 Brief history of oxidants and phagocytes 26

1.3.2 Enzymes and agents involved 27

1.4 Deficiencies in phagocytic function 31

1.4.1 Chronic Granulomatous disease (CGD) 31

1.4.2 Myeloperoxidase deficiency 33

1.4.3 Leukocyte adhesion deficiency (LAD) 33

1.4.4 Wiskott-Aldrich syndrome (WAS) 34

1.5 Nuclear Factor-kappa B (NF-κB) 34

1.6 Cytomic Strategies 38

1.6.1 Flow Cytometry (FCM) 38

1.6.2 Imaging Flow Cytometry (IFCM) 40

2. HYPOTHESIS 45

3. OBJECTIVES 47

4. MATERIALS AND METHODS 49

4.1 Phagocytosis and oxidative burst assays 51

4.1.1 Biological Systems 51

4.1.1.1 U937 cell line 51

4.1.1.1.1 Routine culture medium 51

4.1.1.1.2 Cell Culture procedures 51

4.1.1.1.3 Cell counting 51

4.1.1.1.4 Cell Freezing 51

4.1.1.2 Peripheral Blood Samples 51

4.1.1.3 Fluorescent bacteria 52

4.1.2 Reagents 52

4.1.2.1 Leukocyte subpopulation markers 52

4.1.2.2 Oxidative burst indicator 53

4.1.3 Instrumentation 53

4.1.4 Assay validation in whole blood samples 56

4.1.5 Data Analysis 57

4.2 NF-κB Immunotoxicity assays 58

4.2.1 Biological Systems 58

4.2.2 Reagents 58
4.2.2.1 Monoclonal antibodies and fluorescent markers 58
4.2.2.2 Positive and negative controls 59
4.2.2.3 Test compounds 59
4.2.3 Instrumentation 60
4.2.4 Assay optimization in the U937 cell line 60
4.2.4.1 Viability Assays 60
4.2.4.2 Preparation of U937 cells for assays 61
4.2.4.3 Preparation of Test compounds dilutions for the assays 61
4.2.4.4 Nuclear Translocation Assays 62
4.2.5 Assay validation in whole blood samples 62
4.2.5.1 Whole blood incubation with test compounds 62
4.2.5.2 Cytotoxicity measurements. Viability assays 63
4.2.5.3 Nuclear Translocation assays 63
4.2.6 Statistical Analysis 64
5. RESULTS AND DISCUSSION 65
5.1 Phagocytosis and oxidative burst assays 67
5.1.1. Assay optimization in the U937 cell line 67
5.1.2. Assay Validation in whole blood samples 74
5.2 NF-κB Immunotoxicity assays 85
5.2.1 Assay optimization in U937 cells 85
5.2.2 Assay Validation in whole blood samples 92
6. CONCLUSIONS 101
7. BIBLIOGRAPHY 103

LIST OF ABBREVIATIONS

ARPs: Actin related proteins

ADN: Deoxyribonucleic acid

APC: Allophycocyanin

ATP: Adenosine triphosphate

AUF: Arbitrary units of fluorescence

CD: Cluster of differentiation

CGD: Chronic granulomatous disease

CR1: First complement receptor

C3: Third complement protein

CR3: Third complement receptor

DC: Dendritic cell

DMSO: Dimethyl sulfoxide

ER: Endoplasmic reticulum

FCM: Flow cytometry

FcR: Fc receptor

FSC: Forward scatter

GFP: Green fluorescent protein

GSH: Glutathione

GTP: Guanosine triphosphate

HE: Hydroethidine

HOCl: Hypochlorous acid

H_2O: Hydrogen peroxide

IgG: Immunoglobulin G

IFCM: Imaging flow cytometry

IFN-γ: Interferon gamma

JNK_S: c-Jun N-terminal kinases

LAD: Leukocyte adhesion deficiency

LBP: Lipopolysaccharide binding protein

LPS: Lipopolisaccharides

MAPK: Mitogen-activated protein kinase

MHC: Major histocompatibility complex

MPO: Myeloperoxidase

MR: Mannose receptor

NADPH: Nicotinamide adenine dinucleotide phosphate

NETs: Neutrophil extracellular traps

NBT: Nitro blue tetrazolium chloride

NF-κB: Nuclear factor kappa-light-chain-enhancer of activated B cells

NO: Nitric oxide

NOS: Nitric oxide synthases

PAMP: Pathogen-associated molecular pattern

PBS: Phosphate-buffered saline

PerCP: Peridinin chlorophyll

PDTC: Ammonium pyrrolidinedithiocarbamate

PI: Propidium iodide

PMA: Phorbol 12-myristate 13-acetate

PMN: Polymorphonuclear leukocyte

RNS: Reactive nitrogen species

ROS: Reactive oxygen species

RT: Room temperature

SBF: Fetal bovine serum

SOD: Superoxide dismutase

SSC: Side scatter

TCR: T-cell receptor

TLRs: Toll-like receptors

TNF-α: Tumor necrosis factor- α

WASP: Wiskott-Aldrich syndrome protein

WAVE: Wasp-family verprolin-homologous protein

INTRODUCTION

1.1 ROS and RNS: definition and physiological functions

Life on Earth has evolved by creating organisms that need oxygen to live. Most living organisms depend on oxygen to obtain large amounts of metabolic energy from the oxidation of biomolecules (Fridovich 1998). Paradoxically, the oxygen functions essential to living things depend on a chemical property dangerous to them: the structure of the oxygen molecule (O_2) has two unpaired electrons, and O_2 can accept individual electrons to generate highly unstable and highly reactive molecular forms known as reactive oxygen species (ROS). The term ROS may be applied to a variety of molecules not only derived from O_2 but including both free radicals and species derived from free radicals (Forman, Augusto et al. 2015).

Major ROS molecules include singlet oxygen radical, superoxide anion radical, hydrogen peroxide (H_2O_2), hydroxyl radical, hypochlorous acid (HOCl), lipid peroxides (ROOH) and ozone (O_3), (Clancy and Birdsall 2013). There are also free radicals and reactive nitrogen-containing molecules, the Reactive Nitrogen Species (RNS), including nitric oxide (NO) and peroxynitrite (Di Meo, Reed et al. 2016). Because they also contain oxygen and their generation is connected to ROS generation, they are often considered as ROS. Thus, ROS and RNS are not single entities but represent instead a broad range of chemically distinct reactive species with diverse biological reactivities.

Reactive oxygen species (ROS) and reactive nitrogen species (RNS) are well known for exerting a dual role as both harmful and beneficial species. The generation of ROS and RNS has been implicated in cellular senescence and aging (Vina, Borras et al. 2007); (Halliwell and Whiteman 2004), as well as in the onset and progression of genetic (Hayashi and Cortopassi 2015) and acquired diseases and conditions including, but not limited to, inflammatory conditions (Li, Tan et al. 2015); (Beltran, Nos et al. 2010), cardiovascular diseases (Siti, Kamisah et al. 2015) and thrombosis (Fuentes and Palomo 2016), cancer (Collado, Ivars et al. 2014), (Oh, Figtree et al. 2016) and anticancer chemotherapy (Ivanova, Zhelev et al. 2016), HIV-progression (Ivanov, Valuev-Elliston et al. 2016), neurodegenerative diseases (Henchcliffe and Beal 2008); (Barnham, Masters et al. 2004) and metabolic disorders (Rani, Deep et al. 2016).

However, ROS and RNS also serve important regulatory roles, mediated by intercellular and intracellular signaling (Forman 2016); (Dugas, Debre et al. 1995) and cell-function modifying processes involved both in the destruction of invading pathogens (El-Benna, Hurtado-Nedelec et al. 2016) and in the fine tuning of cellular adaptation to endogenous and exogenous stress (Lionaki, Markaki et al. 2013). Phagocytes use ROS and NOS as a powerful antimicrobial weapon (Valko, Leibfritz et al. 2007) and, in low concentrations, ROS and NOS also serve as second messengers of signal transduction.

Most cytoplasmic proteins contain free SH- groups, which may undergo oxidation/reduction cycles. ROS, in coordination with antioxidant proteins and

molecules may turn functional proteins on and off by redox cycling (Ritz and Beckwith 2001). A large number of such proteins are involved in signal transduction or in the regulation of gene expression in eukaryotes and prokaryotes. (Choi, Kim et al. 2001)

ROS signaling is involved in cell survival adaptation to stress. Signaling through mitogen-activated protein kinases (MAPKs) leads to the generation of H_2O_2 from several enzymes, including NADPH oxidases (Park, Park et al. 2006), and production of H_2O_2 at nanomolar levels is required for proliferation in response to growth factors (Burch and Heintz 2005). In synchronized cells ROS increase during the cell cycle, peaking at the G2/M phase (Havens, Ho et al. 2006). It has been suggested that small increases of H_2O_2 result in increased reentry into the cell cycle, while sustained high levels of H_2O_2 lead to cell arrest and apoptosis (Burhans and Heintz 2009). Apoptosis induced by prolonged activation of c-Jun N-terminal kinase (JNK) can be caused by exposure to ROS (Nakano, Nakajima et al. 2006). Conversely, autophagy is also triggered as an adaptive response, among other stressors, to intracellular ROS (Navarro-Yepes, Burns et al. 2014).

ROS have also recently been related to signaling in platelets. ROS, which are produced after platelet stimulation with collagen, are responsible for a series of platelet activating events due to oxidative inactivation of SHP-2, which promotes tyrosine phosphorylation-based signal transduction (Jang, Min et al. 2014).

NO plays a critical role as molecular mediator of a variety of physiological processes, including blood-pressure regulation and neurotransmission (Massaad and Klann 2011). NO that diffuses into smooth muscle cells binds to the heme group of guanylate cyclase. Peroxynitrite, a RNS considered as an inflammatory mediator in various cardiovascular pathologies, has more recently been recognized as a modulator of signal transduction pathways due to its ability to nitrate tyrosine residues, thereby influencing responses dependent on tyrosine phosphorylation (Speckmann, Steinbrenner et al. 2016).

1.1.1 Sources of ROS and RNS

The generation of ROS and RNS can be endogenous, associated with oxidative processes; such as the mitochondrial chain of electronic transport, NADPH oxidase, xanthine oxidase and various flavoproteins (Dickinson and Chang 2011), or it can be exogenous, derived from inflammatory pathologies, exposure to xenobiotics, ionizing radiation, etc. (Rahal, Kumar et al. 2014)

Most ROS and RNS are physiologically generated in specific subcellular compartments. The intracellular location of ROS and RNS is of great importance, as its microenvironment will affect both the intrinsic functions of the reactive species and the population of molecules and structures that will be eventually affected by the interaction with ROS and RNS. In higher organisms, the major generation of ROS takes

place in the mitochondria, during the tetravalent reduction of O_2 occurring in the electron transport chain associated with oxidative phosphorylation, especially through electron leakage from Complexes I and III. In prokaryotic cells, this mechanism takes place on the plasma membrane. This process, directed to the production of ATP, gives rise to H_2O as the final product, via a sequence of univalent reductions that generate ROS. Other organelles with localized ROS generation include the phagosome, where ROS and RNS are focused on pathogen killing, and the peroxisomes, where many catabolic oxidation reactions are confined (Dickinson and Chang 2011). These other cellular reactions may contribute to the steady state of [$O_2^{\bullet-}$] and [H_2O_2] but mitochondria seem to be the main cellular source (Cadenas and Davies 2000).

Nitric oxide (NO) is synthesized from L-arginine in a reaction catalyzed by NO synthase (Erusalimsky and Moncada 2007). NO reacts readily with superoxide to form the peroxynitrite anion, a RNS with strong oxidant properties (Speckmann, Steinbrenner et al. 2016), and activated macrophages and neutrophils produce NO and superoxide, and thus peroxynitrite, at similar rates.

1.1.2 Oxidative stress: causes and consequences

The beneficial effects of ROS and RNS occur at low concentrations and involve physiological roles in cellular responses as mentioned beforehand. Nevertheless, overproduction of ROS results in oxidative stress, a deleterious process that can damage cell structures.

Oxidative stress is caused by an imbalance between the production of reactive oxygen species (ROS) and the ability of a biological system to readily detoxify the reactive intermediates or to repair the resulting damage (Dickinson and Chang 2011). This imbalance in the normal redox state of the cell may cause toxic effects by producing free radicals and peroxides that damage essential components of the cell such as proteins, lipids and membranes, and DNA.

Oxidative stress can result from two separate but not exclusive processes. On one hand, it can be due to the decrease in levels or activity of enzymes of the antioxidant defense (by mutation or destruction of the active center) induced by the ROS themselves (Rahal, Kumar et al. 2014). Deficiencies in the dietary supply of soluble antioxidants can also cause oxidative stress. On the other hand, increased production of ROS, exposure of cells or organisms to elevated levels of exogenous ROS or their metabolic precursors, and even excessive induction of protective (immunological, detoxifying) systems that produce ROS can lead to oxidative stress (Di Meo, Reed et al. 2016).

Superoxide anion radicals (or superoxide or $O_2^{\bullet-}$) and hydrogen peroxide (H_2O_2) are produced during normal aerobic metabolism by mitochondria and constitute physiological intracellular metabolites. Both of them are free radicals with one or more

unpaired electrons in their atomic or molecular orbitals. Free radicals are very unstable and react quickly with other compounds or with themselves, trying to capture the needed electron to gain stability. They attack the nearest stable molecule trying to "steal" its electron. When the attacked molecule loses its electron, it will become a free radical itself, beginning a chain reaction.

Because of their reactivity, most ROS and RNS are short-lived molecules. For example, the half-life of hydroxyl radicals within a cell is only about 10^{-9} seconds, compared to about 10^{-3} seconds for H_2O_2 (Dickinson and Chang 2011). This means that hydroxyl radicals will react with or very near to their origin, whereas H_2O_2 can diffuse away from its source.

To prevent the harmful effects of in vivo production of ROS and RNS, evolution has provided prokaryotes and higher organisms with complex and effective antioxidant systems that include enzymatic antioxidant mechanisms and antioxidant molecules, broadly understood as those molecules that protect a biological target against oxidative stress (Table 1).

The first line of antioxidant enzymes is the superoxide dismutase family of enzymes (SOD) that catalyzes the dismutation of superoxide to H_2O_2. Catalase converts H_2O_2 to water and O_2, and thus completes the detoxification initiated by SOD. Glutathione (GSH) peroxidase includes a group of Se-containing enzymes that also catalyze the decomposition of H_2O_2, as well as of organic peroxides. In the GSH peroxidase process, GSH is consumed by oxidation, so that GSH reductase is required to transform oxidized GSH (GSSG) into GSH (Rahal, Kumar et al. 2014).

The non-enzymatic antioxidants are a large group of molecules that exert various protective antioxidant mechanisms, and include molecules that react with ROS, such as GSH, tocopherol and β-carotene, or proteins such as transferrin and ceruloplasmin, capable of chelating transition metals. GSH is the most important intracellular defense against the toxic effects of ROS. Vitamin C or ascorbic acid is a water-soluble molecule capable of reducing ROS, while vitamin E (α-tocopherol) is a lipid soluble molecule that has been suggested to play a similar role in cell membranes (Rahal, Kumar et al. 2014).

Free radicals		Non radicals	
Reactive oxygen species (ROS)			
Superoxide	$O_2^{\bullet-}$	Hydrogen peroxide	H_2O_2
Hydroxyl	$OH^{\bullet}$	Hypobromous acid	HOBr
Hydroperoxyl	$HO_2^{\bullet-}$	Hypochlorous acid	HOCl
		Ozone	O_3
Peroxyl	$RO_2^{\bullet}$	Singlet oxygen	O_2^1
Alkoxyl	$RO^{\bullet}$	Organic peroxides	ROOH
Carbonate	$CO_3^{\bullet-}$	Peroxynitrite	$ONOO^-$
Carbon dioxide	$CO_2^{\bullet-}$	Peroxynitrous acid	ONOOH
Reactive chlorine species (RCS)			
Atomic chlorine	$Cl^{\bullet}$	Hypochlorous acid	HOCl
		Nitryl chloride	NO_2Cl
		Chloramines	
		Chlorine gas	Cl_2
Reactive Nitrogen species (RNS)			
Nitric oxide	$NO^{\bullet}$	Nitrous acid	HNO_2
Nitrogen dioxide	$NO_2^{\bullet}$	Nytrosil cation	NO^+
		Nitroxyl anion	NO^-
		Dinitrogen tetroxide	N_2O_4
		Peroxynitrous acid	ONOOH
		Alkyl peroxynitrites	ROONO

Table 1: Nomenclature of Radical species (Adapted from Halliwell et al 2004).

Oxidative damage to cells and tissues produced by ROS is associated with free radical chain reactions with all kinds of biomolecules, such as carbohydrates, lipids, proteins and DNA.

Protein oxidation plays an important role in many of the effects of oxidative and nitrosative stress. The modifications produced may be irreversible, such as carbonylation of lysine (Lys) and arginine (Arg), formation of di-tyrosine bonds, protein-protein bonds and nitration of Tyr and tryptophan (Ghezzi and Bonetto 2003). These changes generally result in loss of permanent function of damaged proteins. In complex enzymes, free radical interaction can also be damaging at the level of the prosthetic group, leading to functional inactivation (Imlay 2013).

Lipid peroxidation is a process that occurs in three phases: initiation, propagation and termination. The initiation phase involves the reaction of the free radicals with cellular lipids, generating peroxyl radicals. In the propagation phase, the reaction of these newly formed peroxyl radicals with intact lipids triggers a chain reaction that may be terminated by the action of antioxidants. It is a phenomenon detrimental to the cell, since changes in the physical-chemical properties of the membrane, as its fluidity, as well as the inactivity of transporters and membrane enzymes can occur (Bielski, Arudi et al. 1983).

More than 100 different free radical-induced DNA modifications have been described, either in nitrogenated bases or in deoxyribose. The hydroxyl ion seems to be the main cause of these lesions, an effect that is facilitated by the polyanionic character of the phosphodiester bond, since it is attracted by metals such as Fe^{2+}, favoring the Fenton reaction. NO and its derivatives have the capacity to induce lesions in the DNA, mainly through the deamination of bases, although other processes are involved (Gros, Saparbaev et al. 2002).

In some cases, production of reactive oxygen species is not an undesirable phenomenon and is part of normal cell function. Certain leukocytes constitute part of the first line of defense against infectious agents by performing phagocytosis. This process is followed by an oxidative burst and a rapid increase in oxygen uptake. Most of this oxygen will be reduced to superoxide anions and oxygen peroxide that contribute to the destruction of the ingested particle.

In addition, ROS signalling plays a major role in the translation and transcription of target genes regulated by NF-κB (nuclear kappa-light-chain-enhancer of activated B cells), related to the production of pro- inflammatory cytokines and chemokines that support microbicide responses (Vernon and Tang 2013). This transcription factor acts as a key responder to changes in the environment and plays a major role in many biological processes. It is found in almost all animal cell types and is involved in both innate and adaptive immune responses, inflammation, secondary lymphoid organ development, cell survival, stress responses and osteoclastogenesis (Hoffmann, Natoli et al. 2006). A number of reports published during recent years show that some ROS are able to affect the activation and activity of NF-κB (Valko, Leibfritz et al. 2007).

1.2 Phagocytosis

The plasma membrane is a highly dynamic structure composed by a bilayer of glycerophospholipid molecules and proteins, which protects and defines the cell from the extracellular environment by regulating the traffic of small and large molecules necessary for cell metabolism. It is the interface between cells and their variable extracellular milieu.

The selective permeability of the plasma membrane to small molecules allows cells to maintain their internal composition. Only small, uncharged molecules can diffuse freely through the plasma membrane. Small, non-polar molecules (O_2, CO_2) are soluble in the lipid bilayer and consequently can readily cross the cell membrane. Small, uncharged polar molecules (H_2O, ethanol) can also diffuse through cell membranes, however the bilayer is impermeable to large polar molecules (such as glucose and amino acids) and to ions. Essential small molecules (sugars, ions and amino acids) have to pass across cell membranes via the action of specific transmembrane proteins (channel proteins or carrier proteins) that act as transporters.

Macromolecules must be transported into the cell in membrane-bound vesicles derived by the invagination of pieces of the plasma membrane in a process named endocytosis. This term involves several different mechanisms by which cells internalize macromolecules and particles. These mechanisms fall into two broad categories: “phagocytosis” (or cell eating) and “pinocytosis” (or the uptake of fluid and solutes). Phagocytosis is typically restricted to specialized mammalian cells while pinocytosis occurs in all cells (Conner and Schmid 2003). Endocytosis is thought to have been one of the first trafficking events that evolved during the prokaryote-to-eukaryote transition. In his book “Blueprint for a Cell: The nature and origin of life” (1991), Christian De Duve suggested that when primitive cells moved from the concentrated primordial soup to more diluted environments (primitive oceans), new mechanisms evolved to take up extracellular macromolecules and secrete digestive enzymes directly into an endocytic vacuole containing the appropriate nutrient pumps (a lysosome precursor) to digest the internalized macromolecules. Subsequently the acquisition of mitochondria and chloroplasts is believed to have happened by phagocytosis of eubacteria and/or blue-green algae respectively (Margulis and Bermudes 1985).

Phagocytosis is the process by which cells engulf large particles (typically ≥0.5 μm), digest them and expel the waste products. It is used for different purposes by a broad range of organisms from amoeba to vertebrates (Jutras and Desjardins 2005). Phagocytosis was first described by the Canadian physician William Osler and later studied and named by the Russian zoologist Elie Metchnikoff in 1882, as a result of his experiments with the transparent larvae of starfish. Metchnikoff demonstrated the process when he introduced small thorns from a tangerine tree into the starfish larvae and found unusual “motile” cells surrounding the thorns (Gordon 2008). He hypothesized that these cells would be able to recognize and internalize external pathogens. Later he discussed his hypothesis with the zoologist Carl Friedrich Whilhelm Claus, who suggested the term “phagocyte” for these mobile cells that could surround and attack external pathogens. In 1903, the British bacteriologist Almroth Wright discovered that phagocytosis was enhanced by specific antibodies that he named “opsonins” (from Greek opsōnein, additive or condiment).

The importance of these findings was recognized in 1908 when Metchnikoff and Paul Erlich were awarded the Nobel Prize in Medicine in recognition of their work on immunity. Nevertheless, the interactions of phagocytes with and all the other components of the immune system were not elucidated until the 1980s.

The ability to ingest large particles is thought to be a nutritional function in unicellular organisms. In the amoeba Dictyiostelium discoideum phagocytosis is a way to ingest bacteria and yeast that are used as food source. The internalized microorganism is trapped in a phagosome that will ultimately be delivered to a lysosome to form a phagolysosome, where the microorganism will be degraded by a

cocktail of hydrolytic enzymes (Bozzaro and Eichinger 2011). Phagocytosis was primarily used for the acquisition of nutrients but in mammals is performed mainly by "professional" cells (including dendritic cells, monocytes, macrophages and neutrophils) specialized in the removal of pathogens, such as bacteria or yeast, arterial deposits of fat or remnants from apoptotic cells. Additionally, professional phagocytes can present to lymphoid cells antigens derived from the degradation of engulfed particles. Although they are unable to internalize microbes, fibroblasts, epithelial and endothelial cells can also ingest apoptotic bodies, thereby contributing to tissue homeostasis and remodelling.

Optimal phagocytosis relies on a variety of surface receptors, signalling processes, participation of the cytoskeleton (actin and actin-related proteins) and vesicle trafficking and fusion processes. Pathogens in turn, have evolved different mechanisms to interfere with these processes, some can block maturation of the phagosome, manipulate its composition or escape into the cytosol, by covering the surface of the bacterial cell with a component recognized as "self" by the host phagocyte. In mammalian immune cells the process is activated by the attachment to pathogen-associated molecular patterns (PAMPs), which also leads to NF-κB activation.

Opsonins such as C3b and antibodies can act as attachment sites and support phagocytosis of pathogens. Engulfment of the invading particle is assisted by the actin-myosin contractile system. The phagosome with the ingested particle will fuse with a lysosome, to form the phagolysosome that will lead to degradation of the particle. This degradation can be:

A. Oxygen-dependent: depends on the activity of a membrane-associated NADPH oxidase that generates superoxide leading to other ROS with microbicidal and inflammatory actions.
B. Oxygen-independent: by the release of granules containing proteolytic enzymes such as lysozyme, lactoferrin, defensins and antimicrobial peptides.

Phagocytosis is a highly conserved and regulated process involving specific cell-surface receptors and signalling cascades mediated by Rho-family GTPases. These receptors not only trigger engulfment but also act to modulate the consequences of phagocytosis as either proinflammatory or anti-inflammatory responses (Stuart and Ezekowitz 2005). From an evolutionary perspective, modern organisms have restricted phagocytosis to specific cell types involved with the immune response (Aderem and Underhill 1999). Phagocytic machinery is also involved in the removal and turnover of apoptotic cells during embryonic development and in cellular homeostasis.

Unlike pinocytosis, phagocytosis is an adhesion-dependent process (Jaumouille and Grinstein 2011). The phagocytic vacuole is formed after association of the ligands

on the surface of the target particle with cellular receptors present on the phagocyte's cell membrane (Table 2). The ligands can be endogenous components of the target particle or adherent serum-derived opsonins. In fact, there are multiple modes of phagocytosis, depending on the nature of the particle to be ingested and on the class of receptor that will recognize that particle. This ensures that phagocytosis operates cooperatively with other aspects of the cell´s physiological response (Conner and Schmid 2003). Phagocytosis is a heterogeneous process whose molecular mechanisms have not been unravelled yet. One of the main difficulties is the large diversity of ligands and receptors that can trigger the process with so many different molecular and morphological consequences (Underhill and Ozinsky 2002). Most of our current understanding of the signalling pathways leading to phagocytosis derives from the studies of Fc receptors (in particular the FcγR), from the complement receptor 3 (CR3) protein and from the macrophage mannose receptor (MMR) in mammal phagocytes (Aderem 2003). Based on these studies, phagocytosis can be described as the sucession of several stages.

In a preliminary stage, at sites of infection or tissue injury, pro-inflammatory cytokines will be released and act as chemoattractants to orchestrate the migration of phagocytes towards the release site, driven by the cytokine gradient (Iijima, Huang et al. 2002).

The first stage is the interaction and binding of the target particle with the receptors on the phagocyte's cell membrane (Figure 1). These receptors either directly recognize the particle or recognize targets coated in opsonic molecules, such as immunoglobulin G (IgG) or CR3 (or integrin $\alpha_M\beta_2$ or CD11b/CD18). There are multiple receptors that can recognize simultaneously conserved motifs on pathogens that are not present in higher eukaryotes.

These motifs are essential to the biology of the invading agent and, therefore, are not subject to high mutation rates. These ligands were initially referred to as pathogen-associated molecular patterns (PAMPs) and include mannans in the yeast cell wall, formylated peptides in bacteria, and lypopolysaccharides and lipoteichoic acids on the surface of Gram negative and Gram positive bacteria. However, this designation did not include the recognition of commensal bacteria or apoptotic cells (Stuart and Ezekowitz 2005).

Receptors	Ligands	Reference
Pattern recognition receptors		
Mannose receptor (CD206)	Mannan	(Ezekowitz, Sastry et al. 1990)
Dectin-1 (CLEC-7A)	β1,3-glucan	(Herre, Marshall et al. 2004)
CD14	Lipopolysaccharide-binding protein	(Schiff, Kline et al. 1997)
Scavenger receptor A (CD204)	Lipopolysaccharide, lipoteichoic acid	(Thomas, Li et al. 2000)
CD36	*P. falciparum*-infected erythrocytes	(Patel, Serghides et al. 2004)
MARCO	Bacteria	(van der Laan, Dopp et al. 1999)
Opsonic receptors		
FcγRI (CD64)	IgG1 = IgG3 > IgG4	(Anderson, Shen et al. 1990)
FcγRIIa (CD32a)	IgG3 ≥ IgG2 > IgG1	(Anderson, Shen et al. 1990)
FcγRIIc (CD32C)	IgG	(Alevy, Tucker et al. 1993)
FcγRIIIa (CD16a)	IgG	(Anderson, Shen et al. 1990)
FcαRI (CD89)	IgA1, IgA2	(van Spriel, van den Herik-Oudijk et al. 1999)
FcεRI	IgE	(Daeron, Malbec et al. 1994)
CR1 (CD35)	Mannan-binding lectin,C1q,C4b,C3b	(Ghiran, Barbashov et al. 2000)
CR3 ($\alpha_M\beta_2$, CD11b/CD18)	iC3b	(Ross, Reed et al. 1992)
CR4 ($\alpha_V\beta_2$, CD11c/CD18)	iC3b	(Ross, Reed et al. 1992)
$\alpha_5\beta_1$	Fibronectin, vitronectin	(Blystone, Graham et al. 1994)
Apoptotic receptors		
T cell immunoglobulin mucin-1	Phosphatidylseryne	(Kobayashi, Karisola et al. 2007)
T cell immunoglobulin mucin-4	Phosphatidylseryne	(Kobayashi, Karisola et al. 2007)
Brain specific angiogenesis inhibitor -1	Phosphatidylseryne	(Park, Tosello-Trampont et al. 2007)
Stabilin-2	Phosphatidylseryne	(Park, Jung et al. 2008)
Mer	Gas6, protein S	(Anderson, Maylock et al. 2003)
$\alpha_V\beta_3$	Milk fat globule-E8	(Hanayama, Tanaka et al. 2002)
$\alpha_V\beta_5$	Apoptotic cells	(Albert, Kim et al. 2000)
CD36	Oxidized lipids	(Greenberg, Sun et al. 2006)

Table 2: Human receptors mediating phagocytosis and their ligands. Abbreviations: CR, complement receptor; Ig, immunoglobulin.

The effectiveness of the interaction between receptors and their ligands is modulated by their affinity and by their density on the surface of both phagocyte and the target. Phagocytic receptors differ not only in the nature of ligands they can recognize but also in the signals they trigger.

After binding the ligand, the attached-receptor triggers many different signalling cascades that will lead to differential maturation of phagosomes, antigen presentation and either proinflammatory or anti-inflammatory responses (Figure 1).

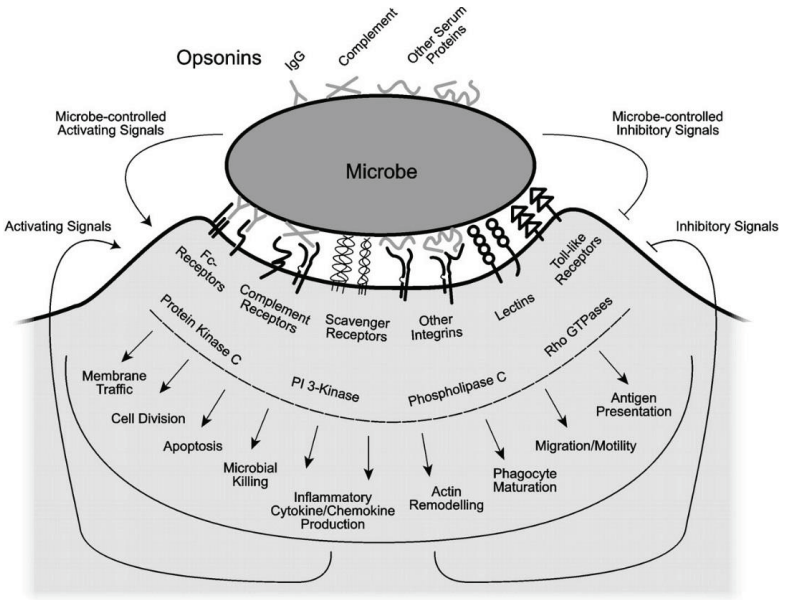

Figure 1: Receptor and signalling interactions during phagocytosis of microbes. Adapted with permission from "*Phagocytosis of Microbes"*. Written by David Underhill and Adrain Ozinsky. Annual Review of Immunology. Vol.20:1-885. April 2002

One of the first responses is rearrangement of the actin cytoskeleton that will drive engulfment of the particle (Figure 2). Actin filaments are dynamic polymers formed by a constant association of actin monomers at one end and dissociation from the other end, a process named as "treadmilling". Filament formation requires the activity of nucleators. Phosphoinositides and Rho-family GTPases play also key roles in this signalling cascade (Ali, Chen et al. 2013). The inositides (alongside with newly phosphorylated proteins) trigger the recruitment and activation of nucleotide-exchange factors that activate small GTP-ases (such as Rac and CDC42 in the case of FcγR stimulation). These in turn will start actin nucleation (the first step in actin polymerization) via ARP 2/3, WASP, WAVE and membrane extension (Jaumouille and Grinstein 2011). The ARP2/3 nucleator complex is a seven-protein complex that promotes the formation of branched actin filaments by nucleating polymerization from the side of an existing filament (Flannagan, Jaumouille et al. 2012).

The WASP family consists of two main classes of protein: WASPs and SCAR/WAVEs. WASPs are named due to Wiskott-Aldrich syndrome, in which mutations in the gene encoding WASP cause immune and blood deficiencies. The dual name of SCAR/WAVE emerged since the same protein was discovered independently by two research groups: 'SCAR' through "Dictyostelum discoideum" genetics (Bear, Rawls et al. 1998) and 'WAVE' by homology with WASP (Miki, Miura et al. 1996). It has also been described that other components of the cytoskeleton (such as microtubules and some atypical myosins) participate in the process (Araki 2006).

The membrane surface required to enclose the particles that professional phagocytes can ingest may correspond to an area equivalent to the entire cell surface. This is well exemplified by the fact that macrophages can internalize beads larger than themselves without affecting their basic functions (Cannon and Swanson 1992). Capacitance measurements assayed in the murine-macrophage cell line J774, after incubation with latex beads, showed that phagocytosis is associated with an increase rather than a decrease in the cell surface area (Holevinsky and Nelson 1998).

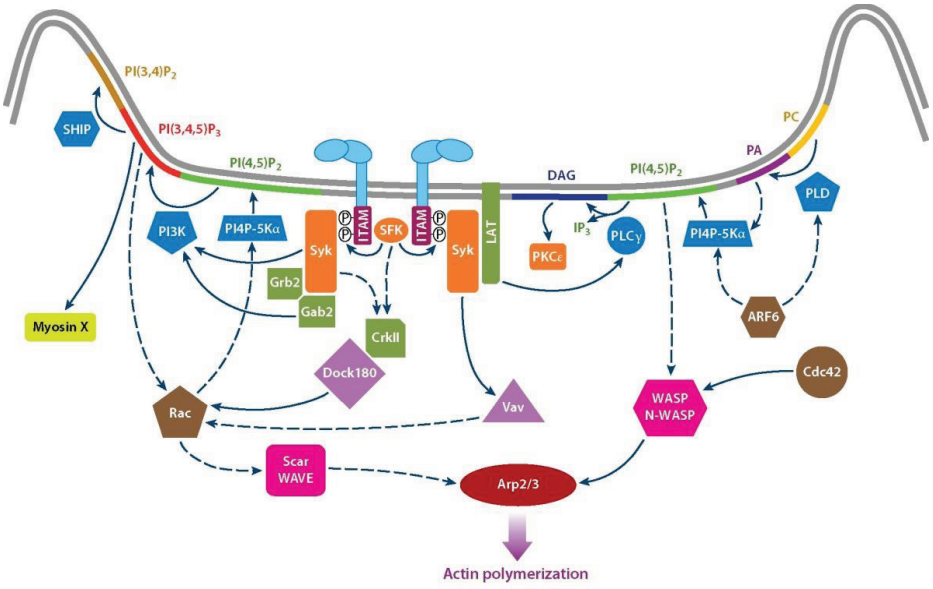

Figure 2: Signalling leading to actin polymerization during Fcγ receptor-mediated phagocytosis (Flannagan, Jaumouille et al. 2012). Aggregated receptors trigger activation of tyrosine kinases (*orange*), including Src-family kinases (SFKs), followed by recruitment of adaptor proteins (*green*). The resulting signalling platforms activate multiple lipid-modifications enzymes (*blue*) and guanine nucleation exchange factors (*lavender*) for small GTPases (*brown*). Nucleation-promoting factors (*purple*) activate the actin nucleation complex Arp2/3 (*red*), which in turn elicits actin polymerization that drives pseudopod extension. Abbreviations: DAG, diacylglycerol; ITAM, immunoreceptor tyrosine-based activation motif; LAT, linker of activated T cells; PA, phosphatidic acid; PC, phosphatidylcholine; PI3K, phosphatidylinositol 3-kinase; PI(3,4)P2, phosphatidylinositol-3,4-bisphosphate; PI(3,4,5)P3, phosphatidylinositol-3,4,5-trisphosphate; PI(4,5)P2, phosphatidylinositol-4-5 bisphosphate; PKC, protein kinase C; PLC, phospholipase C; PLD, phospholipase D; SHIP, Src homology 2 domain-containing inositol 5'-phosphatase; Syk, spleen tyrosine kinase; WASP, Wiskott-Aldrich syndrome protein. Reproduced with permission from "*The Cell Biology of Phagocytosis"* published in the Annual Review of Pathology: Mechanisms of Disease, 7:61–98, (2012). http://www.annualreviews.org (doi: 10.1146/annurev-pathol-011811-132445).

These observations were the first to suggest that intracellular endomembranes (from endosomes, lysosomes and endoplasmic reticulum) are recruited to the cell surface in order to contribute to the formation of nascent phagosomes (Bajno, Peng et al. 2000).

Membrane reorganization drives engulfment of the particle which will be released to the cytoplasm inside a phagosome. The compartments formed by phagocytosis can be very heterogeneous depending on the type of the particles and the type of receptors triggered at the cell membrane. However, phagosomes are particularly dynamic organelles that are continuously modified during their formation. The composition of the phagosomal lumen (and its protein content) changes significantly during the maturation process. After a series of fusion and fission events, the phagosomal lumen and its contents mature, fusing with late endosomes and ultimately with lysosomes to form a phagolysosome. Microtubules serve as tracks for vesicular traffic in both phagosome formation and maturation. Fusion processes during phagosome biogenesis are modulated by a subset of Rab GTPases, including Rab5 and Rab7, which are thought to regulate the fusion processes with early and late endosomes, respectively (Duclos, Diez et al. 2000).

Amongst the different signalling cascades triggered by the phagocytic receptors, activation of the respiratory burst by professional phagocytes will kill the internalized pathogens by the production of reactive superoxide anion (and other ROS) produced by the assembly of the NADPH oxidase on phagosomal membranes.

In many cases the decisions to activate inflammatory responses during phagocytosis are regulated by additional receptors that are not phagocytic themselves. Amongst these receptors, recent studies have been focused on the family of Toll-like receptors (TLRs), that are specifically recruited to phagosomes during their maturation (Aderem and Underhill 1999). TLRs are a family of receptors that recognize microbial molecules (PAMPs) and induce the expression of inflammatory cytokines (upon activation), therefore contributing to the innate immune system. TLR specificity identifies certain organisms: TLR4 recognizes LPS from Gram negative bacteria; TLR5 identifies flagellin from motile bacteria; and TLR3 recognizes viral nucleic acids. As a result, differences in the signals triggered by different TLRs may sense the microbial contents of the phagosome to elicit an appropriate immune response against the particular type of threat detected. Inversely, recognition of apoptotic ligands by phagocytic receptors may be associated with an anti-inflammatory and anti-immunogenic response (Erwig and Henson 2008).

In the final stage of phagocytosis, the target particle is killed and digested in the low pH of the phagolysosome by hydrolytic enzymes in preparation for antigen presentation. In jawed vertebrates, peptides generated through the degradation of exogenous proteins can be loaded in the phagosome lumen onto Major histocompatibility complex (MHC) molecules and presented at the cell surface to initiate an adaptive immune response. This response involves recognition of MHC-associated peptides by TCR molecules, which have co-evolved with the MHC (Du Pasquier 2004). Phagosomes in jawed vertebrates represent thus a compartment that has evolved to integrate functions of the innate and adaptive immune system.

Phagocytosis is commonly measured using either fluorescence microscopy or flow cytometry (Hampton and Winterbourn 1999). However both methods have some limitations. Quantification of internalized particles by manual fluorescence microscopy is subjective and allows examination of only a limited number of cells per sample, making statistical analysis difficult. In contrast, flow cytometry objectively quantifies statistically thousands of cells per sample but the localization of internalized particles within the cell is not feasible. Moreover, with both techniques, discrimination between external or internalized particles is often difficult to discern (Drevets and Campbell 1991).

1.3 Oxidative Burst

1.3.1 Brief history of oxidants and phagocytes

The first evidence that oxygen may be related to the function of phagocytes was the discovery in 1935 of the "respiratory burst". Baldridge and Gerard found that when neutrophils were exposed to bacteria, they exhibited a sharp increase in oxygen uptake. This increase was initially attributed to an increase in oxidative phosphorylation by the mitochondria, apparently to supply the added energy required for the ingestion of the microorganism (Babior 2000).

In 1959, Svarra and Karnovsky published an article that opened the field of phagocytes and oxidants. These researchers found that the respiratory burst was not affected by cyanide. Their discovery ruled out the possibility that mitochondrial function was involved in the process and raised the question as to the purpose of this increase in oxygen uptake when phagocytes were exposed to their targets. The answer was provided by Iyer and Islam in 1961, who found out that H_2O_2 was produced by the stimulated cells. Then, Klebanoff showed that myeloperoxidase was involved in the process, catalyzing the reaction between H_2O_2 and Cl^- to generate HClO, a highly potent microbicidal compound.

The discrepancy between the healthy state of patients with myeloperoxidase deficiency and the high susceptibility to infections exhibited by patients with Chronic Granulomatose disease (CGD), an hereditary condition in which the patient's phagocytes cannot produce H_2O_2, led to the discovery of the O_2^- produced by these cells (Babior, Kipnes et al. 1973), completing the phagocyte oxidant story, in general terms.

These reactive oxidants are manufactured with the purpose of killing invading microorganisms but they also inflict damage on nearby tissues, and are thought to be of pathogenic relevance in a large number of diseases.

1.3.2 Enzymes and agents involved

Phagocytes produce a broad battery of reactive oxidants that will be used for the destruction of invading microorganisms (Figure 4). These oxidants are generated by four enzymes: NADPH oxidase, superoxide dismutase, nitric oxide synthase and myeloperoxidase (in the case of eosinophils, eosinophil peroxidase).

NADPH Oxidase

The nicotinamide adenine dinucleotide phosphate (NADPH) oxidase expressed in phagocytes is a multi-subunit enzyme complex that generates superoxide from oxygen and NADPH:

$$2\ O_2 + NADPH \longrightarrow O_2^{\bullet -} + NADPH^+ + H^+$$

The phagocyte oxidase is the first identified and best studied member of the NOX family of NADPH oxidases (Babior 2000). It is highly expressed in granulocytes and monocyte/macrophages and contributes to the destruction of microbes.

It is dormant in resting phagocytes but is activated when the cell detects a variety of stimuli, including bacteria and certain inflammatory polypeptides (e.g., C5a). The active phagocyte oxidase (*phox*) complex consists of five subunits with a small GTPase Rac. The catalytic core of the complex, which displays no activity in resting phagocytic cells, is composed of two transmembrane subunits, $gp91^{phox}$ (91-kDa *glycoprotein of phagocyte oxidase*, or NOX2) and $p22^{phox}$. These proteins form a heterodimer known as flavocytochrome b_{558} in vesicular and plasma membranes of neutrophils and other leukocytes. In response to stimuli, the regulatory subunits $p67^{phox}$, $p47^{phox}$ and $p40^{phox}$, which are located in the cytosol, will translocate along with Rac-GTP to form the membrane-bound catalytic core and assemble the active enzyme complex (Figure 3).

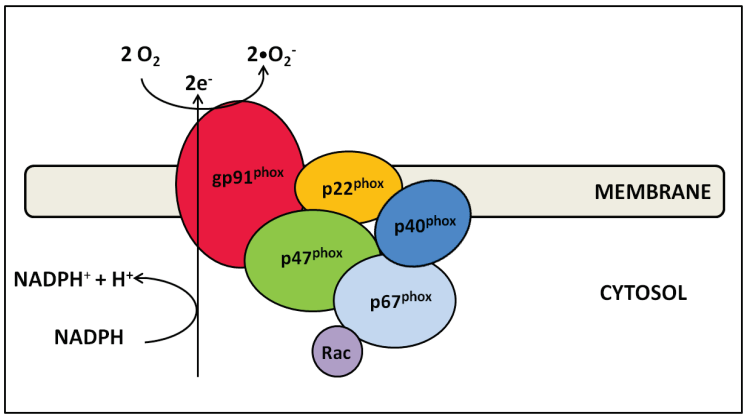

Figure 3: NADPH oxidase structure. This multi-subunit enzyme complex is present in the vesicular and plasma membranes of leukocytes. Two transmembrane subunits, $gp91^{phox}$ and $p22^{phox}$ comprise flavocytochrome b_{558}, the catalytic core of the complex. This heterodimer catalyzes the transfer of

electrons from cytosolic NADPH to molecular oxygen, generating superoxide. Flavocytochrome b_{558} is regulated by association of the subunits $p47^{phox}$, $p67^{phox}$, and $p40^{phox}$, along with the small GTPase Rac. These regulatory subunits are located in the cytosol of resting cells and translocate to the catalytic core after being stimulated.

Once activated, there is a fusion of vesicles with the plasma membrane of the phagosomal membrane. The active enzymatic complex transports electrons from cytoplasmic NADPH to extracellular or phagosomal oxygen to generate superoxide, that serves as a precursor to other, more reactive ROS, such as hydrogen peroxide and singlet oxygen (de Oliveira-Junior, Bustamante et al. 2011).

Superoxide Dismutase (SOD)

The discovery of superoxide dismutase by Irwin Fridovich and Joe McCord in 1968, was the turning point from which emerged the entire field of reactive oxidant biology (Babior 2000). SOD is a family of metalloproteins that catalyze the reaction:

$$2\ O_2^{\bullet -} + 2\ H^+ \longrightarrow O_2 + H_2O_2$$

It is called a dismutation, because the substrate ($O_2^{\bullet -}$) reacts with itself to give an oxidized product (oxygen) and a reduced product (H_2O_2). Although hydrogen peroxide plays a key role in the destruction of invading pathogens, SOD is not only expressed in phagocytes but in most of eukaryotic cells, constituting an important antioxidant defence mechanism. SOD activity increases by 9 the speed of the superoxide anion dismutation process, compared to its spontaneous dissociation to molecular oxygen and hydrogen peroxide.

There are two types of SOD in humans: a copper-zinc enzyme present in the cytoplasm and a manganese enzyme that is located in mitochondria. The Cu-Zn-SOD is present in the cytoplasm of all eukaryotic cells. Nearly all mitochondria and many bacteria contain a form with manganese.

One of the most reactive free radicals is the hydroxyl radical (•OH). In biological systems, the •OH is produced by the reaction between H_2O_2 and iron or copper in a low valence state (Fenton reaction):

$$H_2O_2 + Fe^{2+} \longrightarrow \bullet OH + OH^- + Fe^{3+}$$

The metal is then re-reduced by any of the many reducing agents in biological systems (e.g. ascorbic acid), and in the resulting low-valence state is ready to react with another molecule of H_2O_2, generating another hydroxyl radical.

A feature of free radical reactions is that when a free radical reacts with a molecule with no unpaired electrons (trying to capture the needed electron to gain stability) the product is another free radical, beginning a chain reaction. The chain will only terminate when a free radical reacts with another molecule with an unpaired electron (a free radical or a transition metal).

Nitric Oxide Synthase (NOS)

This enzyme catalyzes the production of nitric oxide (NO) from arginine, oxygen and NADPH.

$$\text{Arginine + oxygen + NADPH} \longrightarrow \text{NO + citruline + } NADP^+$$

There are two general varieties of NO synthase: constitutive and inducible. The constitutive forms are low-activity enzymes that make small amounts of NO as signalling molecules (Marletta 1994). These are found in vascular endothelium and in the central nervous system. The inducible form is a high-activity enzyme that is produced by phagocytes when they are adequately stimulated, by LPS or cytokines (Weinberg, Misukonis et al. 1995). NO synthase is soluble and no deficiency of NO synthase has been recognized in humans.

Reactive Nitrogen Species (RNS) are manufactured by the reaction of NO with O_2^- and other oxidizing species produced by phagocytes. The first characterized of these species is peroxynitrite, formed in a reaction NO with O_2^-, both of which are free radicals:

$$NO\bullet + O_2^{\bullet -} \longrightarrow ONOO^-$$

$ONOO^-$ then undergoes a secondary reaction to produce a radical agent that is able to nitrate tyrosine from the proteins.

Myeloperoxidase (MPO)

Myeloperoxidase is only expressed in neutrophils and monocytes and catalyzes the oxidation of halide ions (Cl^-, Cr^-, I^-) to hypohalous acids at the expense of hydrogen peroxide (Hampton, Kettle et al. 1998):

$$Cl^- + H_2O_2 \longrightarrow HOCl + OH^-$$

The H_2O_2 employed in this reaction is produced by the dismutation of O_2^-. The enzyme can oxidize any of the three halide ions mentioned, and in addition can oxidize thiocyanate (SCN^-), a “pseudohalide” that is abundant in saliva. OCl^- is the principal product, however, because of the high concentration of Cl^- in body fluids.

Myeloperoxidase is a heme enzyme containing as prostetic group, the same heme group that is found in hemoglobin, however myeloperoxidase is green and is the substance that provides the greenish colour to pus.

Peroxidases, including MPO, can catalyze halogenation reactions, whereby a halogen can be included in a biological substrate such as tyrosine. MPO is unique among the animal peroxidases in supporting chlorination of substrates at physiological pH (Klebanoff, Kettle et al. 2013), a property that can be used as a biochemical fingerprint for the presence of enzymatically active MPO in tissues. The presence of

chlorinated proteins in atheromatous plaques has been presented as evidence that MPO contributes to the initiation or persistence of a variety of cardiovascular diseases (Nicholls and Hazen 2005).

Eosinophil peroxidase:

This enzyme is unique to eosinophils in humans and mammals. Unlike myeloperoxidase, eosinophil peroxidase is red. It is unable to catalyze the oxidation of Cl^-, so it employs Br^- and SCN^- as its major substrates, oxidizing Br^- to OBr^- and SCN^- to $OSCN^-$.

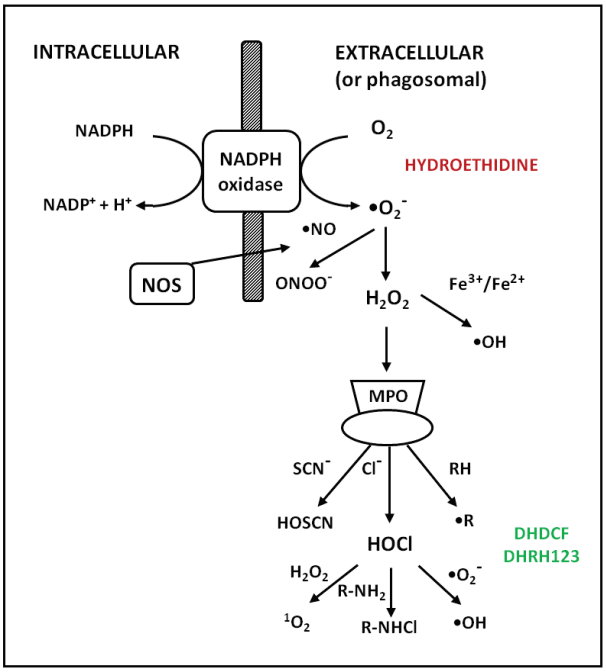

Figure 4: Possible oxidant generating reactions in stimulated neutrophils and Flow Cytometry probes useful for their detection. (NOS, nitric oxide synthase; MPO, myeloperoxidase; DHDCF, dihydrodichlorofluorescein; DHR, dihydrorhodamine).

In addition to the battery of enzymes mentioned, other antioxidant mechanisms (enzymatic and non-enzymatic) are necessary to balance ROS generation, after phagocytosis and oxidative burst, in order to decrease ROS levels and to avoid excessive cell or tissue injury (Splettstoesser and Schuff-Werner 2002).

1.4 Deficiencies in phagocytic function

1.4.1 Chronic Granulomatous disease

Inherited defects in NADPH oxidase are the cause of chronic granulomatous disease (CGD), a primary immunodeficiency characterized by severe recurrent infections and granulomatous inflammation. Phagocytes lacking functional NADPH oxidase are unable to produce ROS, which are necessary to kill pathogenic bacteria and fungi. Thus, patients with CGD patients suffer from early and recurrent severe bacterial and fungal infections, that mainly affect the natural barriers of the human body, such as the skin, lymph nodes and liver, structures of hollow organs (e.g. pylorus, ureters, bladder), and the respiratory tract (Babior 2000).

CGD was originally characterized in 1957 as a clinical entity affecting male infants and termed 'fatal granulomatous disease of childhood (de Oliveira-Junior, Bustamante et al. 2011). Aspergillus pneumonia is especially common and serious among these patients. CGD used to be fatal in early to middle childhood, but treatment with prophylactic antibiotics and gamma interferon (IFNγ) has resulted in the survival of most patients into adulthood, with a decrease in severity as they age, most probably because they can develop antibodies against many microorganisms increasing their resistance.

The estimated incidence per live birth varies: 1/200,000 in the USA, 1/450,000 in Sweden, 1/300,000 in Japan and 1/250,000 in Europe (van den Berg, van Koppen et al. 2009).

Mutations in all of the five structural genes of the NADPH oxidase have been found to cause CGD. X-linked CGD, the most common genetic subgroup, is caused by mutations in $gp91^{phox}$ and accounts for about 65% of cases, mutations in $p47^{phox}$ about 25%, and the remainder is divided between $p67^{phox}$ and $p22^{phox}$; there are no autosomal dominant cases of CGD (de Oliveira Junior, Saud et al. 2011). Interestingly, CGD, CGD carrier status and gene polymorphisms have all been associated with autoinflammatory and autoimmune disorders, suggesting a potential role for NADPH oxidase in regulating adaptive responses (Gardiner, Deffit et al. 2013).

Reeves et al. (Reeves, Lu et al. 2002) have shown that phagocyte production of ROS leads to microbial killing through the activation of certain primary granule proteins inside the phagocytic vacuole (including elastase and cathepsin G). The $O_2^{\bullet -}$ generating system causes an influx of K^+ into the phagocytic vacuole with an associated rise in pH to the optimal level for the activity of proteases. This paradigm for NADPH oxidase-mediated killing, suggests that ROS also act as intracellular signalling molecules, leading to activation of other non-oxidative pathways. One implication is that, in the absence of NADPH activity, phagocyte enzymes are present but hypofunctional. This model suggests that phagocytes are capable of a spectrum of

microbicidal activity that can be modulated by regulating different processes, rather than encompassing distinct oxidative and non-oxidative mechanisms (Holland 2013).

The provisional diagnosis of CGD is usually made by techniques that measure superoxide anion and hydrogen peroxide production. Nitroblue tetrazolium (NBT) reduction by Microscopy (Ayatollahi, Tabei et al. 2006), or dihydrorhodamine oxidation (DHR) by flow cytometry are routinely employed. DHR is preferable to use of its relative ease of use, its ability to distinguish X-linked from autosomal patterns of CGD on flow cytometry, and its sensitivity to even very low frequencies of functional neutrophils (Holland 2010). However, the definitive diagnosis of CGD must be corroborated by immunoblotting for the components of NADPH-oxidase and by DNA-based molecular techniques.

Inflammation is frequent in patients with CGD, and in some cases it can be the first clinical manifestation. The disease is so named due to the exuberant chronic granuloma formation observed in patients. Current data indicate that either increased or decreased NOX2 activity may lead to inflammatory complications.

A deficiency in the NADPH oxidase system in CGD patient phagocytes leads to reduced degradation of phagocytosed material or apoptotic cells, which implicates either the remaining pathogen or apoptotic neutrophils phagocytosed by macrophages, such as pathognomonic eosinophilic crystals. The main consequence is a persistent activation and hyperinflammation at the cellular level (Roxo-Junior and Simao 2014).

Upon activation, neutrophils release neutrophil extracellular traps (NETs). NETs are extracellular structures composed of chromatin and granular proteins that bind and kill microorganisms (gram-positive and –negative as well as fungi). NETs are abundant at inflammatory sites and provide a high local concentration of antimicrobial molecules that kill microbes effectively. This process depends on the generation of ROS by NADPH oxidase (Brinkmann, Reichard et al. 2004) and CGD patients are unable to make NETs.

Fuchs et al. showed that neutrophils isolated from CGD patients and exposed to *S. aureus* were able to induce NETS after treatment with exogenous hydrogen peroxide (Fuchs, Abed et al. 2007). After NETs formation, *S. aureus* was killed efficiently. Their data indicates that NADPH oxidase is essential not only for phagosomal killing but also is required to trigger a signal that culminates in NETs formation.

GCD treatment consists of trimethropin/sulfamethoxazole for the bacterial infections, antifungal therapy (itraconazole,) and gamma interferon (IFNγ). Until recently, fungal infections due to Aspergillus species were the leading cause of mortality in CGD. However, with the advent of current therapies, mortality from Aspergillus infections in CGD is now unusual and therefore, overall mortality is diminished (Holland 2013).

1.4.2 Myeloperoxidase deficiency

Myeloperoxidase deficiency is an extremely common inherited condition, affecting 1/2,000 in the USA, 1/4,000 in Europe and 1/57,000 people in Japan. Neutrophils deficient in MPO produce superoxide and H_2O_2 properly but are unable to convert H_2O_2 to HOCl. Patients are generally asymptomatic; however those who have symptoms generally experience enhanced susceptibility to *Candida* spp. infections, particularly in patients who have myeloperoxidase deficiency and diabetes (Hampton, Kettle et al. 1998). This contrasts considerably with CGD, where the NADPH oxidase is absent and common pathogens cause life-threatening problems. The absence of such complications has been offered as evidence that MPO oxidant system may be a secondary mechanism for neutrophil-mediated antimicrobial activity. Nevertheless, this argument fails to consider observations from humans and knockout mice that demonstrate that microbial killing by MPO-deficient cells is less efficient than that of normal neutrophils. Seymour J. Klebanoff et al. proposed that the contribution of MPO to normal host defence is manifested only when exposure to pathogens overwhelms the capacity of the other host defence mechanisms (Klebanoff, Kettle et al. 2013).

1.4.3 Leukocyte adhesion deficiency (LAD)

LAD is a rare autosomal recessive disorder characterized by immunodefiency resulting in recurrent infections due to a number of defects in adhesion molecule expression and function. The adhesion defects result in poor leukocyte chemotaxis, particularly neutrophils inability to form pus and neutrophilia. LAD is divided into three subtypes: LAD1, LAD2 and LAD3 (also known as LAD-1/variant).

LAD 1 is the most common subtype and is due to mutations in the gene encoding CD18 (ITGB2) that lead to absent, reduced or aberrant CD18 protein expression in the leukocyte membrane of the β-2 integrins. There are four members in this family of adhesion molecules: LFA-1 (CD11a/CD18), Mac-1 (CD11b/CD18, CR3), p150 (CD11c/CD18, CR4) and CD11d/CD18 (Ibbotson, Doig et al. 2001). The main function of these proteins is to participate in the adhesion of neutrophils to endothelial cells. In the absence of this adhesion step, transendothelial migration to the site of inflammation is deficient, and neutrophils cannot extravasate and fight against bacteria in tissues. The disorder is characterized by a high resting neutrophils count and recurrent infections with frequent dissemination and sepsis (Andrews and Sullivan 2003). In the case of this subtype, specific diagnosis is performed by Flow Cytometry to detect absent or reduced CD18 expression in the leukocyte membrane.

1.4.4 Wiskott-Aldrich syndrome (WAS)

WAS is a rare X-linked primary immunodeficiency that is characterized by recurrent infections, hematopoietic malignancies, eczema and thrombocytopenia. A variety of hematopoietic cells (such as lymphocytes, neutrophils, monocytes and platelets) are affected by this genetic defect. The Wiskott-Aldrich syndrome protein (WASp) is a member of a family of cytoplasmic proteins that share similar domain structures and are thought to be responsible for the transduction of signals from the plasma membrane to the actin cytoskeleton. Interactions between WASp, the Rho family GTPase CDC42, and the cytoskeleton organizing complex Arp2/3 appear to be critical to this function and when altered translates into measurable defects of cell polarization and motility. Several studies have demonstrated that WASp-family molecules are associated with numerous signaling molecules known to alter the actin cytoskeleton (Snapper and Rosen 1999). WASp may depolymerize actin directly and/or serve as a scaffold for these signaling molecules in a cascade that regulates the assembly and dissolution of the cytoskeleton. It has been described that WAS macrophages exhibit a defective formation of phagocytic cups (Lorenzi, Brickell et al. 2000). Patients with this syndrome contain a mutant copy of the WAS gene and in most cases there is no detectable expression of WASp in primary hematopoietic cells.

1.5 Nuclear Factor-kappaB (NF-κB)

Transcription factors of the nuclear factor kappa B (NF-κB) family play a main role in the regulation of diverse immune and inflammatory responses in mammalian cells. NF-κB family members control the transcription of cytokines and antimicrobial effectors (Hayden, West et al. 2006) as well as genes that regulate cellular differentiation, survival and proliferation. In addition, NF-κB also contributes to the development and survival of the cells and tissues that carry out immune responses in mammals.

In vertebrates, NF-κB proteins include five structurally related monomers: NF-κB2 p53/p100, NF-κB1 p50/p105, C-Rel, RelA/p65, and Rel B (Figure 5). These proteins form a variety of homo- and heterodimers in different activation states, though the NF-κB complex commonly refers to the heterodimer of p65/RelA and p50 as it is the most prevalent protein dimer found in cells (Hoffmann, Natoli et al. 2006).

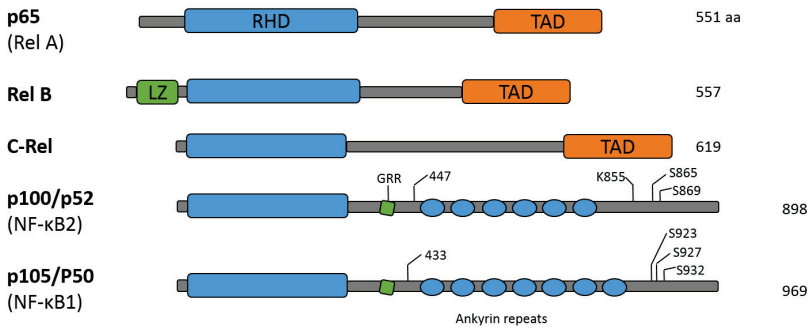

Figure 5: Schematic representation of the NF-κB family of proteins. The number of amino acids in each protein is indicated on the right. Presumed sites of cleavage for p100 (amino acid 447) and p105 (amino acid 433) are shown. Phosphorylation and ubiquitination sites for p100 and p105 are indicated. (GRR; glycine rich region, LZ; leucine zipper domain, RHD; Rel homology domain, TAD; transactivation domain).

These proteins share a highly conserved 300 amino acid domain termed Rel Homology Domain (RHD) which is located towards the extreme amino terminus (Baldwin 1996). This domain is responsible for DNA binding, dimerization, inhibitor binding and nuclear localization (Huxford, Malek et al. 1999).

NF-κB was originally identified in 1986 as an activator of the immunoglobulin kappa light chains in B cells. Nowadays, it is known to be found in almost all animal cell types and is involved in cellular responses to stimuli such as stress, cytokines, free radicals, ultraviolet irradiation, oxidized LDL and bacterial or viral antigens. These stimuli may trigger innate and adaptive immune responses, inflammation, secondary lymphoid organ development, cell survival, stress responses and osteoclastogenesis (Hoffmann, Natoli et al. 2006).

Although there are many ways of activating NF-κB, two main signaling pathways (Figure 6) have been described that lead to the activation of NF-κB target genes. These are referred as the canonical (or classical) and non-canonical (or alternative) pathways (Scheidereit 2006).

The activity of NF-κB is tightly regulated by interaction with inhibitory proteins (IκB). In unstimulated cells, NF-κB complexes are inactive, residing in the cytoplasm in a complex with any of the family of inhibitory IκB proteins. When the pathway is activated, the IκB protein is degraded through the ubiquitin-proteasome pathway, releasing NF-κB to enter into the nucleus to modulate target gene expression. In almost all cases, the common step in this activating process is mediated by an IκB kinase (IKK) complex, which phosphorylates IκB and targets it for proteasomal degradation. The IKK complex consists of two catalitically active kinases (IKKα and IKKβ) and a regulatory scaffold protein (IKKγ or NEMO). In the canonical pathway, IKKβ and NEMO are required for the activation of complexes such as p50/Rel A, p50/c-Rel, etc., whereas IKKα is relatively dispensable.

Conversely, in the non-canonical pathway IKKα alone controls the activation of complexes that are inhibited by the IkB protein p100 (Senftleben, Cao et al. 2001).

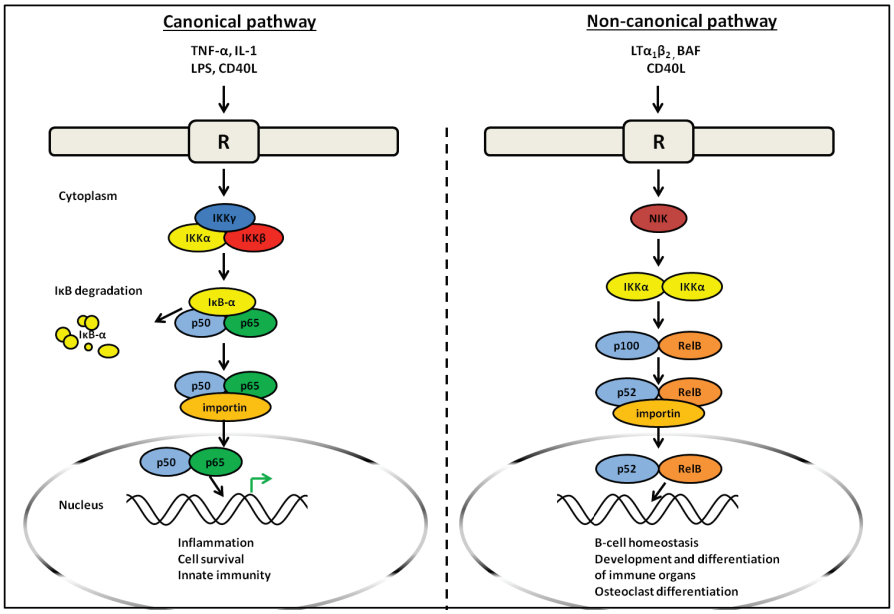

Figure 6: Canonical and non-canonical NF-κB activating pathways.

Expression of NF-κB has been shown to promote cell proliferation, whereas inhibition of NF-κB activation blocks cell proliferation. Reactive oxygen species have been implicated as second messengers involved in the activation of NF-κB via tumor necrosis factor α (TNFα) and interleukin-1 (Baud and Karin 2001).

As mentioned previously, ROS are toxic in cells at certain levels, due to the oxidative stress they exert by reacting with proteins, lipids and nucleic acids. The appropriate cellular response to ROS production is consequently critical in order to prevent further oxidative damage, and to maintain cell survival. However, if the cellular antioxidant mechanisms are overwhelmed by ROS production, the cell will be eliminated for the benefit of the surrounding cells. ROS can therefore trigger both apoptotic and necrotic cell death depending on the severity of the oxidative stress (Saito, Nishio et al. 2006). Although there are a few exceptions where NF-κB induces cell death (Perkins and Gilmore 2006), in most cases the expression of NF-κB target genes typically promotes cell survival. Thus, is not surprising that ROS may modulate NF-κB response and that NF-κB target genes may attenuate ROS to promote survival.

NF-κB Signalling pathways

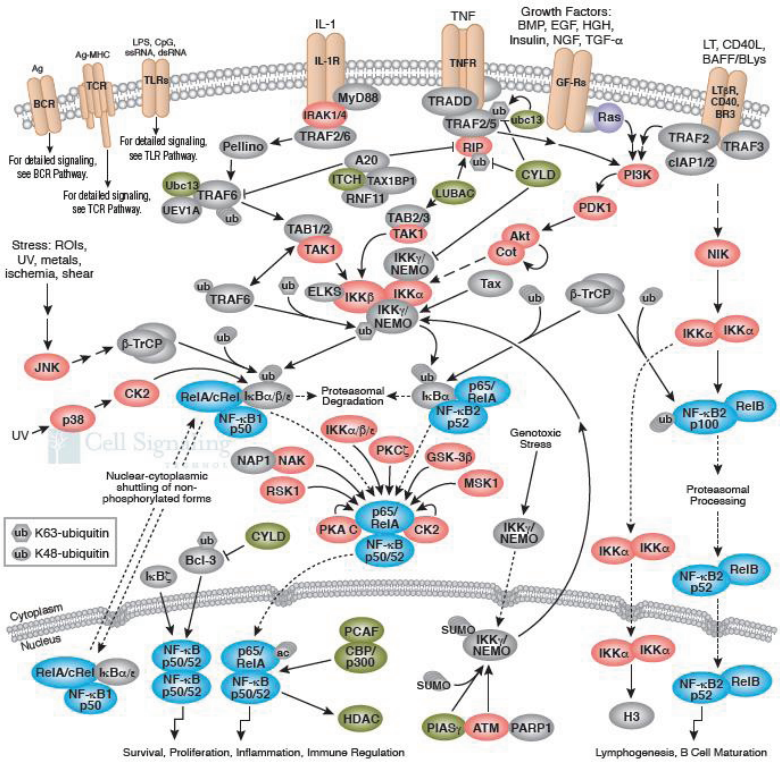

Figure 7: Nuclear factor-κB (NF- κB)/Rel proteins include NF-κB2 p52/p100, NF-κB1 p50/p105, c-Rel, RelA/p65 and Rel B. These proteins function as dimeric transcription factors that regulate the expression of genes influencing a broad range of biological processes including innate and adaptive immunity, inflammation, stress responses, B-cell development, and lymphoid organogenesis. Illustration reproduced courtesy of Cell Signaling Technology, Inc. (www.cellsignal.com)

Identifying immunotoxicants is difficult because chemicals can cause a wide variety of complicated effects on immune function. Observations in humans and studies in rodents have clearly demonstrated that a number of environmental and industrial chemicals can adversely affect the immune system (Boverhof, Ladics et al. 2014).

In vitro detection of human immunotoxicity is relevant to basic and regulatory toxicology but is usually complex (e.g., multiple cytokine detection, complex signaling pathways) while steps central to integrative processes may become simple and suitable endpoints. Abnormal activation of NF-κB is a promising therapeutic target in cancer biology and in immunotoxicity studies; therefore quantitative measurement of its activity is an important endpoint.

Conventional methods employed to determine nuclear translocation of NF-κB are not statistically robust (microscopy), or lack the ability to discern heterogeneity within the sampled populations (Western blotting and gel shift assays). Flow cytometric analysis of phospho-protein-specific staining measures the degree of subunit phosphorylation, but does not assess the intracellular localization of the molecule (Krutzik and Nolan 2003).

Recent advances in imaging instrumentation technology (Basiji, Ortyn et al. 2007) and image processing have enabled the numerical determination of large populations of cells, allowing statistically robust quantitation of nuclear translocation events to this traditionally time-consuming and subjective process

1.6 Cytomic Strategies:

1.6.1 Flow Cytometry (FCM): is a technology that simultaneously measures and analyzes multiple physical characteristics of single particles (usually cells) as they Flow in a fluid stream through a laser beam. The properties measured include a particle's relative size (Forward Scatter, FSC), relative granularity or internal complexity (Side Scatter, SSC) and relative fluorescence intensity. These parameters are determined using an optical-to-electronic coupling system that records how the particle scatters incident laser light and emits fluorescence (Figure 8). A Flow cytometer is made up of three main systems:

1. Fluidics system: transports particles in a stream to the laser beam for interrogation.
2. Optics system: consists of lasers to illuminate the particles in the sample stream and optical filters to direct the emitted light signals to the appropriate detectors.
3. Electronics system: converts the detected light signals into electronic signals that can be processed by the computer.

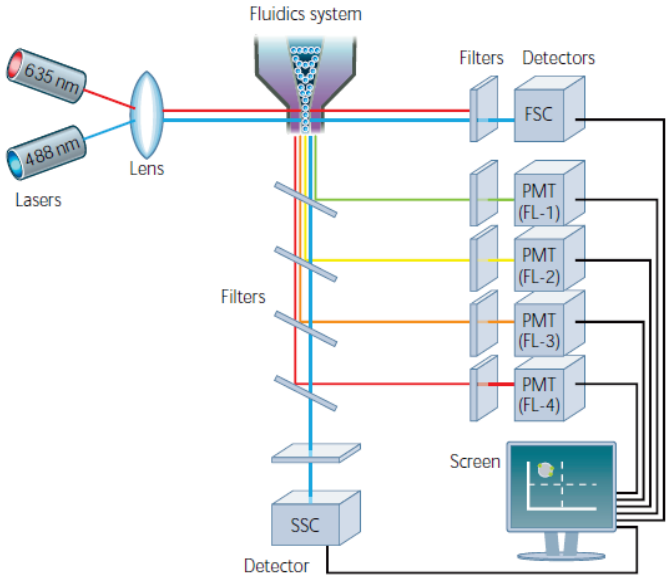

Figure 8: Schematic overview of a typical Flow cytometer setup. Reproduced from https://www.bio-rad-antibodies.com/introduction-to-flow-cytometry.html

By using appropriate fluorescent markers, FCM is unique in that multiple structural and functional parameters can be quantified simultaneously on a single-particle basis, while up to thousands of biological particles per second may be examined. The main strengths of Flow Cytometry can be summarized as follows: (O'Connor, Callaghan et al. 2001)

a) *Multiparametric data acquisition*. Most standard biochemical procedures determine a single parameter per assay and are not sensitive enough for single-cell analysis. FCM instruments routinely allow two morphology-related parameters (FSC and SSC) and up to 18 fluorescence signals per single particle. In this way, in a single-tube assay, one or more parameters may be used to identify and select ("gated analysis") cell subsets in heterogeneous populations (e.g., live, apoptotic or necrotic cells; cells of different origin or lineage; cells in different cell cycle stage and so on), whereas other markers may be assigned to analyze specific structures or functions.

b) *Multivariate Data Analysis*. Due to the hardware and software design of modern cytometers, multiparametric acquisition is interfaced to multivariate data analysis. In this way, a cell population is not described by mere enumeration of the individual properties measured but by their correlation on a single cell-basis, thus increasing the discrimination power.

c) *Fast analysis of large numbers of live cells.* FCM may be performed on a large variety of biological material in different conditions of vitality (e.g., intact fresh cells, fixed and/or permeabilized cells). The use of live cells allows one to probe multiple

biochemical parameters in minimally perturbed intracellular environments, as well as under near-physiological extracellular conditions. The fast rate of data acquisition and the possibility of examining millions of individual particles in a reasonable time allows the detection and accurate analysis of infrequent or rare cells, down to 1 event per 10^8 cells (Gross, Verwer et al. 1993). Such a possibility is in contrast with bulk standard fluorimetric determinations in which millions of cells are analyzed at the same time, yielding a single mean concentration value.

d) *Non-invasive technique.* Most cytometry applications are non-invasive in terms of cell integrity, so the examined cell populations may be found under close to physiological conditions at the moment of their analysis.

In the last twenty years, multi-parametric analysis of single cells by conventional FCM has been applied to the study of oxidative stress (O'Connor, Callaghan et al. 2001).

The use of Flow Cytometry to asses phagocytosis and oxidative burst was first described in 1944 as a two-color assay involving isolated polymorphonuclear (PMN) cells and labeled bacteria (Van Amersfoort and Van Strijp 1994). Since this first experiment, Flow Cytometry assays for this purpose have become routine. In most published reports the fluorescence quenching technique has been used to discriminate between adherent and ingested particles.

Fluorescence-based analysis of oxidative stress and related processes is also an extended application of Flow Cytometry (Martinez-Pastor, Mata-Campuzano et al. 2010). Imaging approaches, including confocal microscopy (Liegibel, Abrahamse et al. 2000), high-content analysis by automated microscopy (Manshian, Abdelmonem et al. 2016) and the more recent Imaging Flow Cytometry (Ploppa, George et al. 2011), that allows in addition visualization and quantification of image-based features of intracellular ROS production and action.

1.6.2 Imaging Flow Cytometry (IFCM):

Recent advances in charge-coupled device (CCD) camera technology, optical filters and digital computing have now made feasible imaging of all the cells in the flow stream. (Basiji, Ortyn et al. 2007). Imaging Flow Cytometry combines the strengths of Microscopy and Flow Cytometry in a single system for quantitative image-based cellular assays in large and heterogeneous cell populations (Figure 9). The combination of both techniques offers novel analytical capabilities and allows a large number of new possible applications beyond the current limitations of Flow Cytometry.

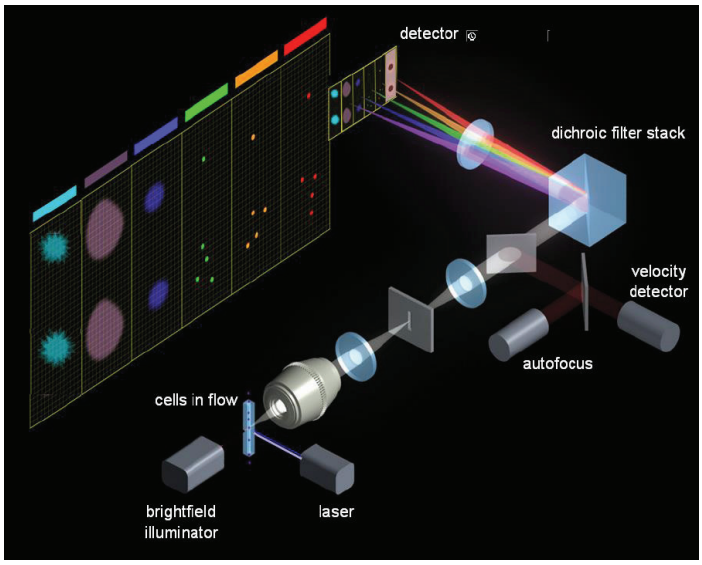

Figure 9: Schematic representation of the ImageStream100 (Amnis corp, EMD Milliore) multispectral imaging cytometer. Hydrodynamically focused cells are trans-illuminated by a brightfield source and orthogonally by a laser(s). An objective lens collects fluorescence emissions, scattered and transmitted light from the cells. Prior to projection on the CCD camera, the light is passed through a spectral decomposition optical system that directs different spectral bands to different lateral positions across the detector. With this technique an image is optically decomposed in a subset of six sub images, each corresponding to a different color component and spatially isolated from the remaining sub-images. Reproduced with permission from www.amnis.com

Examples of these new applications include the analysis of molecule co-localization and/or translocation, the analysis of cell-to-cell contact regions and its signaling interactions, the detection of rare molecules within the cells, the analysis of bacterial or parasite internalization, spot counting, morphology-based cell classification and many other analytical approaches.

Thus Imaging Flow Cytometry combines the statistical power and fluorescence sensitivity common to Flow Cytometry with the spatial information of microscopy in a single system, allowing the digitalization of thousands of cells per minute, while measuring fluorescence as a conventional flow cytometer.

The Amnis ImageStream100 instrument (Amnis, Merck Millipore) acquires up to six images of each cell in different imaging modes. Cells can be magnified by a 20, 40 or 60x objective allowing a wide range of applications. The six images of each cell comprise: a side-scatter (SSC) image, a transmitted light (brightfield) image and four fluorescence images corresponding to the FL1, FL2, FL3 and FL4 spectral bands of conventional flow cytometers (Basiji, Ortyn et al. 2007).

The imaging objective has a numeric aperture of 0.75 and image quality is compared to a 60X microscope when using the highest magnification power, with a pixel size of 0.025 μm^2.

In addition to obtaining classical fluorescence Flow Cytometry data, image-based parameters are also measured from each cell in flow (Figure 10), such as cell shape, texture, size, probe distribution heterogeneity, nuclear translocation, subcellular localization of proteins, etc. Most dyes used in conventional Flow Cytometry can be detected and compensation is applied to the images in a pixel-by-pixel and cell-by-cell basis, thus allowing for the use of more colors compared to microscopy. The system is equipped with 3-lasers (405nm, 488nm and 640nm) and 4 different fluorescent channels can be analyzed simultaneously. Data analysis is performed using IDEAS software, which allows the analysis of more than 100 parameters per single cell.

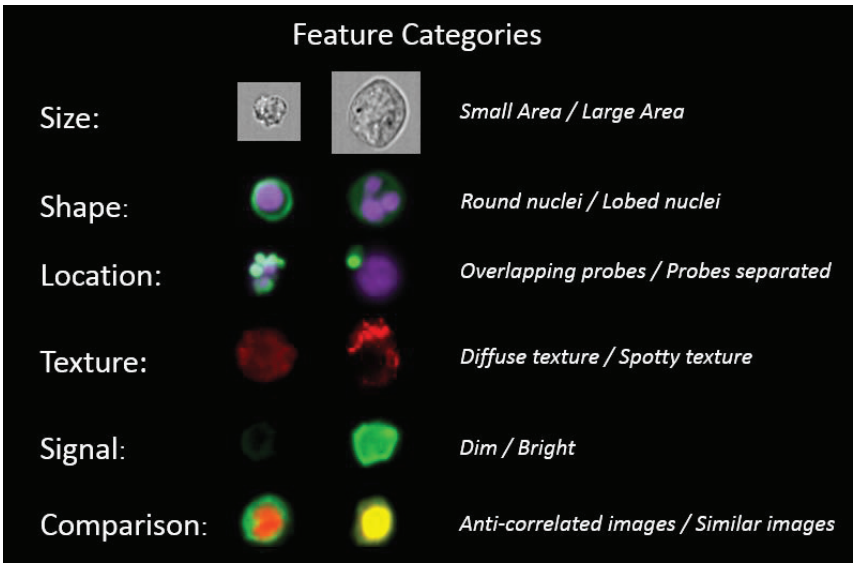

Figure 10: Features categories used by IDEAS® 6.0 software (Amnis, EMD Millipore).

Six channel images are collected using a 10 bit CCD (charge-coupled device) camera operated in TDI (time delay integration) mode. Light is quantified for all the pixels in the image, and identifies both the intensity and location of the fluorescence. Each pixel has an X coordinate, a Y coordinate and an intensity value that corresponds to the amount of light captured at that location.

A digital image can be defined as a two dimensional grid of pixels, with each pixel having a value (intensity) that can be represented in a third dimension. Working with pixelated imagery allows numerical measurements of parameters associated with an image to be performed on thousands of images per sample and permits statistical discrimination of cells based on appearance. Pixelated imagery also allows for the

statistical analysis of cell morphology by using mathematical functions (called features) which contain quantitative and positional information about the images. Features are applied to specific locations of an image by the use of a mask that identifies pixels within the region of interest of the image

One of the main challenges in the study of oxidative processes is the short half-life of ROS and its localized physiological action, restricted to certain cell types and confined in specific subcellular compartments. The development of novel methods based on single-cell analysis and on co-localization with intracellular compartments may be relevant for this purpose. Furthermore, understanding of the involvement of oxidative stress in the immune responses would be enhanced by the development and implementation of new methods that allow the analysis of whole blood samples.

However, this methodology has not yet been significantly applied to the study of oxidative stress and its physiological and pathological implications. Therefore, the development of new applications by Imaging-Flow Cytometry for ROS analysis and quantification may help in the understanding of the biological outcomes that ROS are responsible for.

HYPOTHESIS

One of the main challenges in Biomedicine is the study of oxidative stress and its consequences.

This Ph. D thesis is based on the hypothesis that the development of novel methods based on single-cell analysis, image-derived features and co-localization with intracellular compartments may be relevant for understanding the involvement of oxidative stress in immune responses.

OBJECTIVES

1. Development and validation of an Imaging Cytometry-based method for the evaluation of oxidative processes associated with phagocytosis in whole blood samples and in cellular models with immunological relevance.

2. Set-up and validation of an Imaging Flow Cytometric method to asses NF-κB nuclear translocation in whole blood samples and in cellular models.

3. Optimization and validation of an *in vitro* assay of immunotoxicity dependent upon oxidative stress based on NF-κB nuclear translocation in whole blood samples and in cellular models with immunological relevance.

MATERIALS AND METHODS

4.1 Phagocytosis and oxidative burst assays

4.1.1 Biological systems

4.1.1.1 U937 cell line: the human monocytic U937 cell line was obtained from American Type Culture Collection (ATCC CRL-1593.2, Manassas, VA). Cells were thawed by introducing the cryotube in a water bath at 37 °C, then re-suspended and transferred to a tissue culture flask (Corning Inc., US) containing pre-warmed Routine culture medium. This cell line was isolated from a 37-year-old male patient with histiocytic lymphoma and is commonly employed in biomedical research to study the behavior and differentiation of monocytes.

4.1.1.1.1 Routine culture medium: U937 cells were maintained in suspension culture in RPMI 1640 (Life Technologies, US) supplemented with 10% (v/v) FCS, 2 mM L-glutamine, 1mM sodium pyruvate, 4.5 g/L glucose and 100 U/ml Penicillin/Streptomycin at 37 °C in a humidified atmosphere of 5% CO_2.

4.1.1.1.2 Cell Culture procedures: Cells were maintained and sub-cultured at 37 °C in a humidified atmosphere of 5% CO_2. U937 cells were sub-cultivated in conventional T-25 culture flasks (Corning Inc., US) and cell density was maintained at 10^6 viable cells/ml by Trypan blue exclusion (Strober 2001). The flasks were examined on a daily basis under a phase contrast microscope and after 12 passages a new cryotube from the stock was thawed. Fresh medium was added every 2 to 3 days after centrifugation at 300xg for 5 minutes at room temperature.

4.1.1.1.3 Cell counting: after centrifuging at 300xg and re-suspending in 12 ml of fresh media, an aliquot (100 µL) was removed*/pipetted* and diluted by half with trypan blue (Sigma-Aldrich, US) solution in PBS (0.2% w/v). Cells were incubated for 30 seconds to stain dead cells and a coverslip was placed onto the Neubauer chamber. The counting chamber was filled with the cell suspension. A total of 4 (0.1 mm^3) squares were counted. To count viable cells, any non-viable cells stained with trypan blue were excluded. An average of the counts was made and this equates to the number of cells $x10^4$ per ml, this is doubled to account for the trypan blue dilution to give the number of cells/ml in the suspension (i.e. average of 4 squares x 2 = cells/ml x 10^4).

4.1.1.4 Cell Freezing: stocks of U937 cells were regularly frozen and stored in sterile cryotubes in liquid N_2 to maintain stocks. To freeze cells, a cell suspension was first counted to give numbers of viable cells, re-centrifuged, and the resulting pellet was then re-suspended in FBS containing 10% dimethyl sulfoxide (DMSO) to obtain $1x10^6$ cells/ml. Then 2.5 ml of this cell suspension was added to a cryogenic vial and placed in a polystyrene box which was maintained at -80 °C overnight. Finally the vial was placed in liquid N_2.

4.1.1.2 Peripheral blood samples: Blood from healthy volunteers was collected into heparinized tubes (BD, Vacutainer) and held at room temperature for maximal 2 hours

until processed. Stock solutions of positive and negative controls were prepared in pyrogen-free polypropylene reaction tubes and kept at -20°C until use. Samples were provided by the hematological service of the Hospital Clinico Universitario de Valencia (Valencia).

4.1.1.3 Fluorescent bacteria

A plasmid harboring the pMEK91 GFP gene containing vector was transformed into a capsular serum-resistant strain of *Escherichia coli* (ATCC 11775) by electroporation (Palazzolo, Suquet et al. 2005). The GFP has two excitation peaks at 395 and 475 nm and its emission peak is at 509 nm. Transformed cells were selected by growth on kanamycin (Sigma-Aldrich, US)-containing nutrient agar plates, the construct readily expressed GFP without induction. The GFP-plasmid containing *E. coli* were subsequently grown on Luria broth or LB (Life Technologies, US) at 37 °C. For daily experiments, cells were grown from isolated colonies on the nutrient plate with 5 ml of LB and 90 µg/ml kanamycin during 18 hours at 37 °C. Bacterial concentration was determined after serial dilutions in the same medium by using an Accuri C6 (BD Biosciences) flow cytometer. The percentage of GFP-expressing bacteria was about 95% and remained stable throughout the assays. After counting, cells were harvested by centrifugation, washed once in 50 mM PBS buffer at pH 7.4, and re-suspended in the same buffer. The final suspension (50,000 bacteria/µl) was kept on ice and used immediately following harvesting. For each assay, fluorescent-labeled bacteria were thawed and adjusted to a final ratio of 1:4 bacteria per leukocyte and 1:10 bacteria per cell in the optimization assays with the U937 cell line.

4.1.2 Reagents

4.1.2.1. Leukocyte subpopulation markers:

CD45-APC (Biolegend, US): CD45 is a 180-240 kD single chain type I glycoprotein also known as leukocyte common antigen (LCA). It is a tyrosine phosphatase expressed on the plasma membrane of all hematopoietic cells, except erythrocytes and platelets. CD45 is a signaling molecule that regulates a variety of cellular processes including cell growth, differentiation, cell cycle and oncogenic transformation. It is also essential for T and B cell antigen receptor mediated activation. Allophycocyanin (APC) is a bright phycobiliprotein isolated from red algae that exhibits far red fluorescence with high quantum yields. It is excited by laser lines at 594 and 633 nm, with a fluorescence peak emission at 660 nm.

CD45-Phycoerythrin (Molecular Probes, US): it was used for the Imaging-Flow cytometry assays. Phycoerythrin (PE) is a red protein-pigment present in red algae with two absorption peaks at 565/498 nm and a maximum emission at 573 nm.

4.1.2.2. Oxidative burst indicator

Hydroethidine (HE): it is widely used as a fluorogenic substrate for detecting intracellular superoxide anion (Benov, Sztejnberg et al. 1998). HE is membrane-permeant and cytosolic HE exhibits blue fluorescence, but once oxidized by superoxide, it originates 2-hydroxy-ethidium (2-OH-E^+), a fluorescent compound with an excitation/emission wavelength at 520/610 nm. It is retained in the nucleus, intercalating with the DNA, a fact that increases its fluorescence (Gomes, Fernandes et al. 2005). It was purchased from Life Technologies (Carslbad, US), titrated and used to a final concentration of 3.3 µg/ml in the whole blood assays and 2.5 µg/ml in the U937 experiments. Stock solutions from HE (10 µg/ml) were prepared by dissolving in DMSO and stored at -20 °C until further use.

HE may have important limitations when used for analysis of intracellular superoxide. It has been shown that cytochrome c is able to oxidize HE, an aspect that might be important in situations where the detected superoxide is mainly of mitochondrial origin or in conditions leading to apoptosis, where cytochrome c is released to cytosol (Tarpey, Wink et al. 2004). Due to the interconnection between oxidative stress and the apoptotic process, it will be difficult, in these situations, to assume that the HE oxidation to E^+ depends only on superoxide. Furthermore, HE can also be oxidized by a variety of reactive species, including peroxynitrite. Thus, HE should be considered as an indicator of ROS and RNS production (Wardman 2007).

4.1.3 Instrumentation

Flow Cytometry

Conventional flow cytometric analysis was performed using an Accuri C6 (BD Biosciences, US) equipped with with a blue (488nm) and red (640 nm) laser, two light scatter detectors (FSC and SSC) and four fluorescence detectors. Data is digitally collected over a six-decade dynamic range. A non-pressurized peristaltic pump system drives the fluidics. The system accurately monitors the sample volume pulled per run, and can calculate absolute counts (or sample concentration per µL) directly without the use of counting beads. Absolute cell counting of U937 cells and leukocytes was performed by using the Accuri C6 flow cytometer, in order to establish/set the optimal bacteria to cell ratio for the assays.

Because this flow cytometer employs non-pressurized peristaltic pumps in an open fluidic system, open tubes can be used to add test compounds to the cell suspension without interrupting sample acquisition. This “continuous-flow” method enables nonstop monitoring of thousands of cells to facilitate/*provide* accurate, gap-free kinetic analysis of cellular responses that occur within seconds, such as analysis of calcium flux, pH and ROS/RNS generation.

Validation and quality control of the cytometer was performed each day by using 6 and 8-peak Spherotech™ validation beads (BD Bioscieces, US), according to manufacturer's instructions.

Based on previous data from our group (Tamarit 2014), GFP-*E. coli* was mixed with U937 cells in a 10:1 bacteria to cell ratio for assay optimization. After incubation at 37°C for different time points, 400 µL of RPMI-1640 (Sigma-Aldrich) were added and samples were acquired by using the Accuri C6 flow cytometer. 10,000 total events were acquired per sample and analyzed with CFlow Plus (BD Biosciences, US) software.

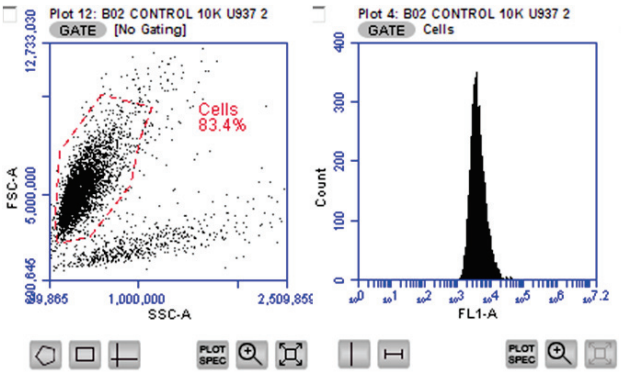

Plot 12: B02 CONTROL 10K U937 2	Count	Events / µL	% of This Plot	% of All
All	5,000	49	100.00%	100.00%
U937 GFP-E. coli	4,170	40	83.40%	83.40%
GFP+	396	4	7.92%	7.92%

Figure 11: Representative dot plot, histogram and data table showing percentages, absolute cell counting and sample concentration (events/µL) of U937 cells incubated for 5 minutes at a 10:1 bacteria to cell ratio. GFP fluorescence is detected in FL1.

Imaging Flow Cytometry

The ImageStream multispectral imaging flow cytometer (Amnis, Merck Millipore) combines the quantitative power of large sample sizes common to Flow Cytometry with the high information content of microscopy in a single system.

This platform acquires up to six images of each cell in different imaging modes). Cells can be magnified by a 20, 40 or 60x objective allowing a wide range of applications. The six images of each cell comprise: a Side-scatter (SSC, darkfield) image, a transmitted light (brightfield) image and four fluorescence images corresponding to the FL1, FL2, FL3 and FL4 spectral bands of conventional flow cytometers (Basiji, Ortyn

et al. 2007). With the 60x objective, light is quantified for each 0.25 μm^2 pixel in the image, and identifies both the intensity and location of the fluorescence. Each pixel has an X and Y coordinate and an intensity value that corresponds to the amount of light captured at that location.

Validation and quality control of the cytometer was performed by daily running of SpeedBeads™ reagent (Amnis, Merck Millipore) and using INSPIRE™ 2.2 software. SpeedBeads are 1 micron, non-fluorescent beads that are continuously run through the flow cell during the operation of the cytometer. Daily operation involves an initial calibration and testing of the system using this reagent followed by sample run and data acquisition. Run-time information from the SpeedBeads is used to maintain continuous synchronization between the camera and the sample flow rate and to automatically focus on the sample core stream. The ImageStream100 uses syringe pumps to drive the sample, so the volume consumed during data acquisition is well-defined. Since the system also images every object in the core, both absolute counting and sample concentration (events per µL) are calculated without the need of calibration beads.

The images can then be analyzed for fluorescence intensity, shape and area of the fluorescence, and localization with respect to other fluorescence-labeled cell compounds or structures, and therefore is well suited to measuring phagocytosis and oxidative burst in whole blood samples.

Asynchronously-growing U937 cells were centrifuged at 300xg for 5 minutes and re-suspended at $50x10^4$ viable cells/ml by Trypan blue exclusion. After cell counting, phagocytosis was initiated by mixing suspensions of U937 cells and GFP-*E. coli* at a 10:1 bacteria to cell ratio. Samples were incubated at 37 °C in a humidified atmosphere of 5% CO2. Incubation at 0°C was performed as negative control.

For oxidative burst quantification and co-localization assays, U937 cells were stained prior to bacterial incubation with 2.5 µg/ml hydroethidine for 20 minutes at room temperature. Incubation at 0°C was performed as negative control. Single GFP- and HE-color controls were used to create a compensation matrix that was applied to all files correct for spectral crosstalk.

Samples were acquired on an ImageStream100 (Amnis, Merck Millipore) exciting with the blue (488 at 20 mW). Cell imagery was obtained after acquiring a minimum of 10,000 total events per sample.

4.1.4 Assay Validation in Whole Blood samples

Internalization Assays:

a) Conventional FCM: Phagocytosis was initiated by mixing suspensions of whole blood and bacteria at 37 °C. Firstly, leukocyte counting was performed after staining heparinized whole blood with CD45-APC antibody (5% v/v). After incubation for 30 min at room temperature, 1 ml of BD FACS lysing solution (BD Biosciences, US) was added. 10,000 total events were acquired for each sample by the Accuri C6 flow cytometer at low flow speed. By plotting SSC intensity vs. CD45-APC fluorescence intensity (FL4) the different leukocyte subpopulations can be distinguished (Figure 12). As this flow cytometer informs about the exact sample volume (µL) run, absolute leukocyte counting can be calculated (cells/ µL) for each sample.

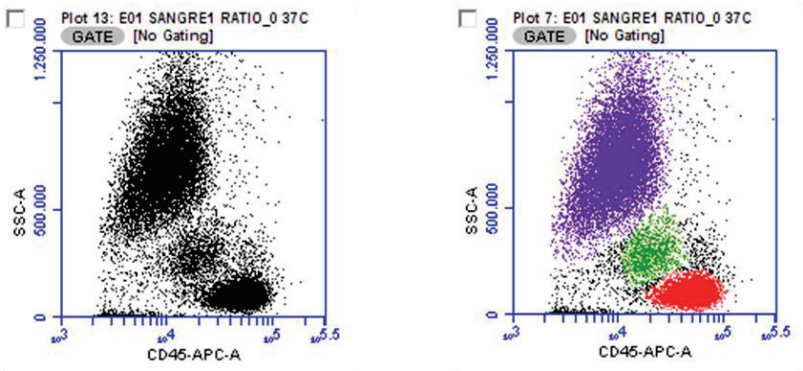

Figure 12: Biparametric dot plots of SSC intensity vs CD45-APC fluorescence intensity showing identification of leukocyte subpopulations. Three different leukocyte subpopulations can be defined by their different SSC/CD45-APC intensities: neutrophils (purple), monocytes (green) and lymphocytes (red). Neutrophils and monocytes are both professional phagocytes.

Afterwards, 1 ml aliquot of GFP-*E. coli* bacteria was centrifuged at 3,000 rpm for 10 minutes. After discarding the supernatant, the pellet was re-suspended in 1 ml of RPMI medium (Life Technologies, US) in order to obtain a final concentration of 50,000 bacteria per µl.

GFP-*E. coli* bacteria was added at different bacterium:leukocyte ratios (1, 0.5 and 0.25) to 50 µl of heparinized whole blood incubated with CD45-APC antibody for the identification of leukocyte subpopulations. For oxidative burst quantitation, HE was titrated and added prior bacterial incubation at 37°C.

Aliquots of heparin-treated blood (50 µL) were added to individual 1.5 ml tubes and incubated at different time points (0, 5, 10, 20, 30 and 60 min). Erythrocytes were lysed by incubating samples with 2 ml Lysing solution (Becton-Dickinson, US) for 5 minutes at room temperature. Incubation at 0°C was performed as negative control.

Positive controls were samples stimulated with 200 nM PMA (Sigma-Aldrich, US) for 30 minutes at 37°C. Samples were acquired by the Accuri C6 exciting with the

blue (488nm) and red (642 nm) lasers and the fluorescence emission of GFP, HE and CD45-APC was detected at FL1, FL2 and FL4 respectively.

b) Imaging Flow Cytometry: Samples were processed by using the same protocol for conventional FCM and acquired on an ImageStream100 exciting with the blue (488 nm) laser at 40 mW. Cell imagery was obtained on 10,000 total events per sample. GFP-and CD45-PE single color controls were used to create a compensation matrix that was applied to all files correct for spectral crosstalk

4.1.5 Data Analysis

After correcting for the spectral overlap, data was subsequently analyzed using two different approaches:

1 Conventional gating technique: Identification of the percentage of cells positive for phagocytosis (GFP+) and/or oxidative burst. Absolute counts of bacteria and cells were performed using BD Accuri C6 software as shown in Figure 11. For the determination of phagocytosis and oxidative burst in whole blood samples, neutrophils were identified by their characteristic side scatter pattern and CD45 intensity. Unstained samples were used to determine the appropriated compensation. Phagocytosis activity was determined as fluorescence intensity of intracellular bacteria, oxidative burst was determined as fluorescence intensity of HE.

2 Image-based gating technique: Data from ImageStream Cytometry were processed by using IDEAS 6.0™ software (Amnis corp, US). Unstained samples and singe color controls were acquired to generate a compensation matrix. After acquisition, the compensation matrix was applied to all data to correct for spectral overlap. All analyses were completed on a population of spectrally-compensated, single, focused cells. Figures 14 to 17 show the image-based gating protocol and features used to gate on the subpopulation of cells of interest.

4.2 NF-κB Immunotoxicity assays

4.2.1 Biological Systems

U937 Cell line: this cell line was isolated from the histiocytic lymphoma of a 37-year old male patient and is commonly employed in biomedical research to study the behavior and differentiation of monocytes. The human monocytic U937 cell line was obtained from American Type Culture Collection (ATCC CRL-1593.2, US). U937 cells were maintained, subcultured and cryopreserved as described previously in section 4.1.1.

Peripheral blood samples: Blood from healthy volunteers was collected into heparinized tubes (BD, Vacutainer) and held at room temperature for maximal 2 hours until processed. Samples were provided by the hematological service of the Hospital Clinico Universitario de Valencia (Valencia).

4.2.2 Reagents

4.2.2.1 Monoclonal antibodies and fluorescent markers

Anti-human NF-κB/p50 Alexa Fluor 488 (Biolegend, US): this nuclear protein is one subunit of the Nκ-kappa B complex consisting of a 65 kD transactivating subunit and a 50 kD DNA binding subunit. The heterodimer p50/p65 is the most prevalent protein, being found in almost all cell types (Hoffmann, Natoli et al. 2006). Alexa Fluor 488 has a maximum emission of 519 nm when it is excited at 488 nm. The antibody was used at a final concentration of 2 µg/ml in U937 assays and 2.5 µg/ml in whole blood assays.

CD14-PerCPVio700 (Miltenyi Biotec, Germany): CD14 is a 53-55 kDa glycosylphosphatidylinositol (GPI)-linked glycoprotein with leucine-rich repeats. The CD14 antigen is a high affinity receptor for lipopolysaccharides (LPS) and LPS-binding protein (LBP)-complexes. It is expressed on cells of myelomonocytic lineages. CD14 antigen is strongly expressed on human monocytes, macrophages, and weakly on neutrophils. It is also weakly expressed on B lymphocytes, but is absent from T lymphocytes, NK cells, red blood and platelets. Although LPS is considered to be the main ligand of this antigen, other PAMPs like lipoteichoic acid (Ranoa, Kelley et al. 2013) can also bind to it. PerCP-Vio700 dye is a tandem conjugate that combines the peridinin chlorophyll protein (PerCP) and Vio700 dye to emit a strong fluorescence with a maximum emission peak at 704 nm upon blue laser excitation at 488 nm.

Propidium Iodide (PI): PI (Sigma-Aldrich, US) is a fluorescent intercalating agent (excitation/emission at 535/635 nm). PI is membrane non-permeant and therefore excluded from viable cells. It was a used for the U937 viability assays at a final concentration of 2.5 µg/ml.

7-Amino-Actinomycin D (7AAD): this dye intercalates between cytosine and guanine bases of DNA. 7-AAD/DNA complexes can be excited by the 488 nm laser and have an emission maxima of 640 nm. It was purchased from Molecular Probes (US) and used at

a final concentration of 12 µg/ml. This dye is generally excluded from live cells, but can be used with fixed and permeabilized cells for nuclear staining.

4.2.2.2 Positive and negative controls

Lipopolysaccharide (LPS): Bacterial LPS are the major outer surface components present in the cell wall of almost all Gram-negative bacteria and act as strong stimulators of innate or natural immunity in diverse eukaryotic species ranging from insect to humans (Alexander and Rietschel 2001). LPS stimulates cells of the innate immune system by the Toll-like receptor 4 (TLR4). LPS from *Salmonella enterica* was purchased from Sigma-Aldrich (US) and used at a dose range from 10 to 50 µg/ml.

Phorbol 12-myristate 13-acetate (PMA): is a diester of phorbol and a potent tumor promoter often employed in biomedical research to activate the signal transduction enzyme Protein Kinase C (PKC), and hence NF-κB (Niedel, Kuhn et al. 1983). PMA (Sigma-Aldrich) was used at a final concentrations of 20, 200 and 400 nM.

Ammonium pyrrolidinedithiocarbamate (PDTC): It is an antioxidant that has been shown in previous works to selectively inhibit NF-κB activation (Foulds 1997); prevents induction of nitric oxide synthetase (NOS) by inhibiting translation of NOS mRNA. Inhibition of NF-κB activation was performed by pre-incubation of samples with 200 µM PDTC (Sigma-Aldrich, US) for one hour followed by treatment with the different test compounds. It has been reported to induce apoptosis in rat smooth muscle cells (Tsai, Jain et al. 1996) but also to inhibit it in Leukemia HL-60 cells (Chen, Lin et al. 2008).

4.2.2.3 Test Compounds

All test compounds were purchased from Sigma-Aldrich (US) unless otherwise noted.

Diazepam (DZP): first marketed as Valium, is a medication of the benzodiazepine family with central nervous system-depressant properties. It is used to treat anxiety, alcohol withdrawal and seizures. It has been described that DZP inhibits human T-cell function through peripheral benzodiazepine receptors, decreasing interferon (IFN)-γ production (Wei, Li et al. 2010).

Mercury (II) Chloride ($HgCl_2$): Mercury is a widespread environmental pollutant that can produce severe negative effects even at very low concentrations. In addition to its well-characterized effects on the nervous system, mercury (Hg) has also been described to affect immune function, including the induction of lupus-like autoimmune pathology in genetically susceptible mouse strains after exposure to inorganic Hg (Gardner, Nyland et al. 2010). Exposure to $HgCl_2$ induces developmental damage, oxidative stress and immunotoxicity in zebrafish embryos-larvae (Zhang, Li et al. 2016).

Hexachlorobenzene (HCB): is an organochloride with the molecular formula C_6Cl_6. It is a fungicide previously used as a seed treatment. It was banned globally under the Stockholm Convention on persistent organic pollutants (2009). HCB is an animal carcinogen and is considered to be a probable human carcinogen. This compound has been classified by the international Agency for Research on Cancer (IARC) as a group 2B carcinogen (possibly carcinogenic to humans). Animal carcinogenicity data for hexachlorobenzene show increased incidences of liver, kidney and thyroid cancers. Histopathological studies in rats and dogs have shown that HCB has immunotoxic properties (Vos 1986).

Lindane: is an organochlorine chemical variant of hexachlorocyclohexane that has been used both as an agricultural insecticide and as a pharmaceutical treatment for lice and scabies only after safer medications have failed or cause side effects. In 2009, the production and agricultural use of lindane was banned by the Stockolm Convention on persistent organic pollutants. Lindane is a neurotoxin that interfers with GABA neurotransmitter function by interacting with the $GABA_A$ receptor-chloride channel complex at the picrotoxin binding site. In humans, lindane affects the nervous system, liver and kidneys and may be well a carcinogen (Nolan, Kamrath et al. 2012).

tert-Butyl Hydroperoxide (t-BuOOH or t-BHP): is an organic peroxide used in a variety of oxidation processes. It has been shown to induce endothelial apoptosis and necrosis in a dose- and time-dependent manner (Zhao, Feng et al. 2017). In low concentrations induce caspase-dependent apoptosis and reactive oxygen species (ROS) generation while necrosis is induced after treatment with high concentrations.

4.2.3 Instrumentation

For the U937 Viability assays, samples were analyzed using a FC500 MCL Flow Cytometer (Beckman Coulter, US) equipped with two lasers (488 and 635 nm) and 5 fluorescence detectors. PI orange fluorescence was detected in FL3 using logarithmic amplification (FL3 Log). A minimal number of 5,000 events per sample were acquired. The IC50 was obtained using Phototox version 2.0 software to establish the concentration range of each test compound.

4.2.4 Assay optimization in the U937 cell line

4.2.4.1 Viability Assays: To establish the concentration range of test compounds in the human U937 cell line, the half maximal inhibitory concentration (IC50) of each test compound was calculated. The IC50 is a measure of the effectiveness of substance in inhibiting a specific biological or biochemical function .IC50s were calculated by a flow cytometric viability assay with Propidium iodide (PI). PI staining and subsequent flow cytometric analysis of orange fluorescence allow for the detection of cytotoxic effects of different compounds that might be mediated by plasma membrane alterations. The

IC50 of each toxic compound was calculated to establish the optimal dose range of each toxic compound. The IC50 is the molar concentration of a toxicant producing 50% of cell death measured with PI.

Procedure:

1) Prepare a cell suspension of 10^5 cells/ml in U937 culture medium. Dispense 200 µl of cell suspension in the wells in routine culture medium with 5% FBS (final cell number per well = $5x10^4$ cells).
2) Incubate at 37°C for 24 hours.
3) Treat with test compounds during the appropriate time points.
4) Prepare a PI (Sigma-Aldrich) solution to 1 mg/ml in distilled H_2O. Keep commercial powder and stock solutions frozen at -20°C. Immediately before use, prepare a solution in culture medium of 10 µg/ml PI in culture medium (4x solution).
5) Add 100 µl of PI 4x solution to 300 µl of cell suspension. The final PI concentrations are 2.5 µg/ml per tube.
6) Incubate at 37°C in the dark for 15 minutes.
7) Analyze immediately by FCM with appropriate cytometer settings

4.2.4.2 Preparation of U937 cells for assays

For testing, U937 cells were seeded at a density of $1x10^6$ cells/ml and pre-cultured in culture flasks overnight. The day after, a cell suspension of $5x10^5$ cells/ml in culture medium was prepared. Using a multi-channel pipette, 100 µl culture medium only were dispensed into the peripheral wells of 96 well plate (= blanks). In the remaining wells 100 µl of the cell suspension were pipetted (= $5x10^4$ cells/well).

4.2.4.3 Preparation of Test compounds dilutions for the assays

A) **DMSO-soluble chemicals**: (e.g. Lindane, Diazepam and Hexachlorobenzene)
    1) Prepare a stock 200x of highest toxicant concentration in DMSO.
    2) Do dilutions from 200x solutions. Do 4 serial dilutions in DMSO applying the appropriate dilution factor for each desired concentration.
    3) Realize 1/100 dilutions in culture medium from each one of previous dilutions.
    4) Add per well: 100 µl of cell medium with 5% FBS to the cells.
B) **Medium-soluble chemicals**: (e.g. t-BHP, Mercury Chloride)
    1) Prepare a stock 2x of highest concentration in culture medium with 5% FBS.
    2) Do dilutions from 2x solutions. Do 5 serial dilutions in culture medium applying the appropriate dilution factor for each desired concentration.
    3) Add per well: 100 µl of cell medium with 5% FBS to the cells.

Per well, 100 µl of treatment medium (with 5% SBF) containing either the appropriate concentration of test chemical, or nothing but vehicle were added. For chemicals

dissolved in DMSO, the final DMSO concentration never exceeded 0.5% in the vehicle controls and in all of the test concentrations. U937 cells were incubated for different time points at 37 °C in a humidified atmosphere of 5% CO_2.

4.2.4.4 Nuclear Translocation Assays

The degree of NF-κB nuclear translocation was quantified in U937 cells treated with different compounds affecting *in vitro* NF-κB-dependent immune functions, including activators (LPS and PMA), inhibitors (PDTC) and test compounds. U937 cells in exponential growth phase were treated with the indicated concentrations of activators and test compounds for the indicated time points in 96 well-plates (Costar, US). Test immunotoxicants included lindane, hexachlorobenzene, t-butylhydroperoxide and mercury chloride. Negative controls were cell cultures treated with appropriate solution vehicles. To analyze the effects of PDTC, samples were pre-incubated with or without 200 µM PDTC for 1h and then stimulated with activating or test compounds.

Procedure:

1) After drug treatments, U937 cells were collected into 5ml sterile polypropilene tubes and centrifuged at 300xg for 5 minutes at room temperature.
2) After discarding the supernatant, cells were fixed with 500 µl 2% PFA-PBS (Merck Millipore, Germany) for 15 min at room temperature.
3) Wash with 500 µl PBS, centrifuge for 5 minutes at 300xg, discard the supernatant and permeabilize the cells with 0.1% PBS-Triton X-100 (Sigma-Aldrich, US) solution for 15 min at room temperature.
4) Incubate the cells with 1.75 µl Anti-human NF-κB p50-AF488 (Biolegend, US) for 20 minutes in the dark at room temperature.
5) Wash with 500 µl PBS and re-suspend the pellet in 10 µg/ml 7-AAD (Molecular probes, US).
6) Acquire a minimum of 5,000 total events on ImageStream100 (Amnis, US) exciting with the blue (488nm) laser at 40mW.

4.2.5 Assay validation in whole blood samples

4.2.5.1 Human whole blood incubations with test-compounds

Blood from healthy volunteers was collected into heparinized tubes and was kept at room temperature for maximal 2 hours until use. Stock solutions of positive and negative controls and test compounds were prepared in pyrogen-free polypropylene reaction tubes and kept at -20°C until use. If not water soluble, the compounds were solved in DMSO. The concentration was 130-fold of the highest concentration, from which serial dilutions were made in RPMI 1640 culture medium supplemented with 2.5 IU/ml heparin, 100 IU/ml Penicillin/Streptomycin and 2mM L-glutamine. The final

DMSO concentration per well never exceeded 0.5% v/v, in control and treated wells. Water soluble compounds were dissolved in culture medium, the stock concentration was 1.3-fold of the highest concentration. Serial dilutions in culture medium at 1.3 times the final concentration were made. Then 155 µl compound/solvent were transferred into 96-well plates (Costar, US). Finally, 45 µl human whole blood were pipetted to each well. Three replicates for each condition were performed. The final volume in each well was 200 µl. The plates were incubated for 24 hours at 37 °C with 5% CO_2. Controls included wells with blood incubated without test compounds to control basal NF-κB activation. After blood incubation with test compounds, 130 µl of the supernatant was collected and stored at -80°C for further analysis of secreted proteins. The rest of the supernatant in the wells (70 µl) containing all blood cells, was re-suspended by gently tapping against the sides of the plate and transferred to a new plate for measuring either cell viability (MABA) or NF-κB subcellular localization (ImageStream cytometry).

4.2.5.2 Cytotoxicity measurements. Viability assays

The rest of supernatant in the wells (70 µl), containing all blood cells, was re-suspended and transferred to a new 96 well-plate for measuring cell viability by the microplate Alamar blue assay (MABA). Alamar Blue (Thermo fisher Scientific, US) was diluted 10-fold with pre-warmed non-supplemented RPMI 1640 from which 150 µl were added to each well and incubated for 2 hours at 37°C. The outer perimeter wells were filled with sterile water to prevent dehydration during incubation. Afterwards, the wells were read using a Sinergy H1 Multi-Mode microplate reader (BioTek Instruments, US). Resofurin formation, as endpoint for cell viability, was detected at 544 nm excitation and 590 emission wavelengths. The IC50 of each test compound was obtained using Phototox version 2.0 software to establish the optimal concentration range for the assays.

4.2.5.3 Nuclear Translocation assays

Surface staining was performed for 100 µl whole blood samples using 1,75 µl anti-human CD14-PerCPVio700 (Miltenyi Biotec, Germany), then erythrocytes were lysed by addition of 2 ml BD FACS Lysing Solution 1X (Becton Dickinson). Samples were then washed with 500 µl PBS and centrifuged at 400xg for 5 minutes in room temperature. Afterwards, the pellet was re-suspended in 500 µl 2% PFA in PBS for 15 min at room temperature. Samples were subsequently permeabilized by the addition of 100 µl 0.1 % Triton-PBS (Sigma-Aldrich, US) for 15 minutes at room temperature. For intracellular staining, fixed and permeabilized cells were stained with 2.5 µg/ml Alexa Fluor 488 anti-NF-κB p50 (Biolegend) for 25 minutes at room temperature. Afterwards cells were washed and stained with 12 µg/ml 7AAD (Molecular Probes) for 10 minutes and then ran on the ImageStream 100.

Cell imagery was obtained using a 6-channel ImageStream100. A minimum of 10,000 total events was collected per sample exciting with the 488 laser (40 mW). After acquisition, a compensation matrix was applied to correct the spectral overlap. Cell populations were gated for single cells that were in focus and were positive for both 7AAD and NF-κB/p50. In the whole blood assays, leukocyte subpopulations were gated based on their different SSC and CD14 intensities (Figure 13). Following data acquisition, the spatial relationship between the NF-κB and nuclear images was measured using the Similarity Score. This score, a log-transformed Pearson's correlation coefficient between the pixels of two image pairs, provides a measure of the degree of nuclear localization of NF-κB by measuring the pixel intensity correlation between the NF-κB-AF488 and 7AAD images. Cells with low similarity scores (negative values or close to 0) exhibit no correlation between the images (corresponding with a main cytoplasmic distribution of NF-κB), whereas cells with high scores exhibit a positive correlation between the images (corresponding with a nuclear distribution of NF-κB).

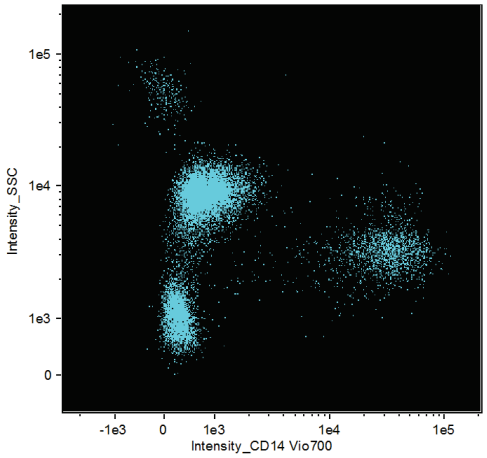

Intensity_CD14 Vio700, Intensity_SSC

Population	Count	%Gated
Single cells & Best Nuclear...	10300	100

Figure 13: CD14 Vio700 vs. SSC (Side Scatter) intensity dot plot showing identification of leukocyte subpopulations in a control whole blood sample.

4.2.6 Statistical Analysis:

All experiments were performed in triplicate. Data from ImageStream Cytometry were processed in IDEAS analysis software (Amnis-Merck Millipore, US) and are presented as mean and standard deviation. Statistical analysis was made by performing the t-Student test using IBM SPSS version 12.0 statistical software. All the treatments had a statistically significant effect (p-value<0.05) when compared with their respective controls.

RESULTS AND DISCUSSION

5.1 Phagocytosis and oxidative burst assays

5.1.1 Assay Optimization in the U937 cell line

Internalization Assays:

First, objects with high gradient RMS histogram values were gated to obtain focused cells (Figure 14). This feature measures the sharpness of an image by detecting large changes in pixels values and allows us to distinguish fuzzy or out of focus events from crisp or in focus objects.

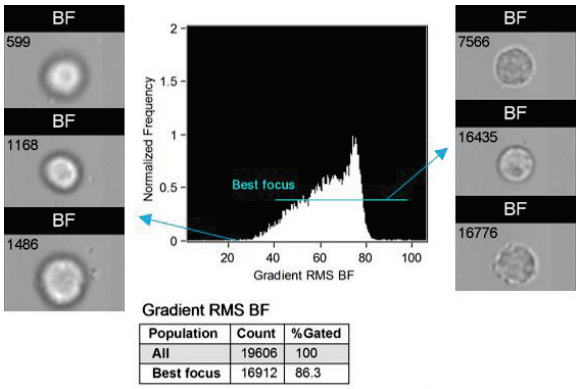

Population	Count	%Gated
All	19606	100
Best focus	16912	86.3

Figure 14: The Gradient RMS is computed using the average gradient of a pixel normalized for variations in intensity levels. Images with low (left) and high (right) values are shown above.

Second, single cells are located by plotting the area of the brightfield image vs. the aspect ratio (the ratio of the minor axis divide by the major axis, i.e. the shape) of the brightfield (BF) channel (Figure 15).

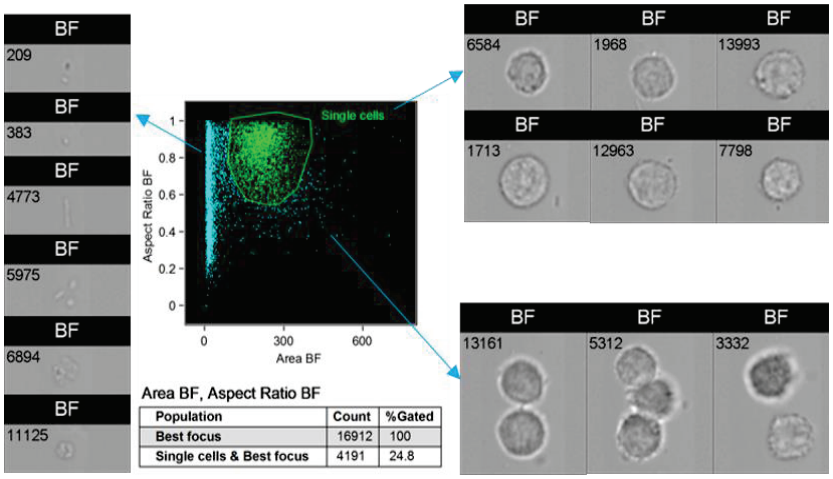

Population	Count	%Gated
Best focus	16912	100
Single cells & Best focus	4191	24.8

Figure 15: Single cells can be distinguished from cell aggregates and debris based on their high aspect ratio and their BF area. Aspect ratio is the minor axis divided by the major axis and describes how round a mask is. Images of single cells, debris and cell aggregates are shown.

For the determination of bacterial localization, the Internalization score was calculated in the subpopulation of cells with bright GFP spots. To discern the subpopulation with GFP-*E.coli* spots, the Max Pixel parameter from the FL1 channel (GFP) was plotted vs. the intensity of the same channel (Figure 16). The Max pixel feature is the largest value of the background-subtracted pixels contained in the input mask. For a concentrated signal, Max Pixel is more sensitive than intensity. After gating on the populations of cells with GFP-*E.coli* spots the internalization feature was calculated.

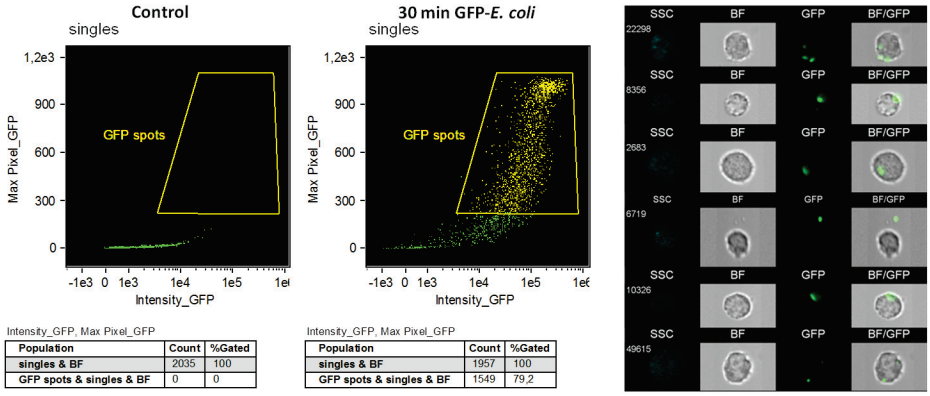

Intensity_GFP, Max Pixel_GFP

Population	Count	%Gated
singles & BF	2035	100
GFP spots & singles & BF	0	0

Intensity_GFP, Max Pixel_GFP

Population	Count	%Gated
singles & BF	1957	100
GFP spots & singles & BF	1549	79,2

Figure 16 Dot plot showing GFP fluorescence intensity vs. Max Pixel GFP in control and U937 cells incubated with GFP-*E. coli* for 30 minutes. Images of cells with bright GFP fluorescence and high Max pixel values are shown (GFP spots). Each cell is represented by a row of images that include: Side-scatter (SSC, blue), Brightfield (BF, grey), GFP-*E. coli* (green) and a composite overlay of the BF and GFP channels.

The Internalization score is defined as the ratio of the intensity inside the cell compared to the intensity of the entire cell, defined as the brightfield cell image. The higher the score is, the greater the concentration of intensity inside the cell. Internalized cells typically have positive scores while cells with little internalization have negative scores. Cells with scores around 0 have a mix of internalization and membrane intensity. This parameter allows the discrimination of cells with internalized bacteria, which have the majority of their fluorescence signal within the mask boundary, from cells with surface-bound bacteria, which have the majority of their fluorescence signal outside the mask boundary.

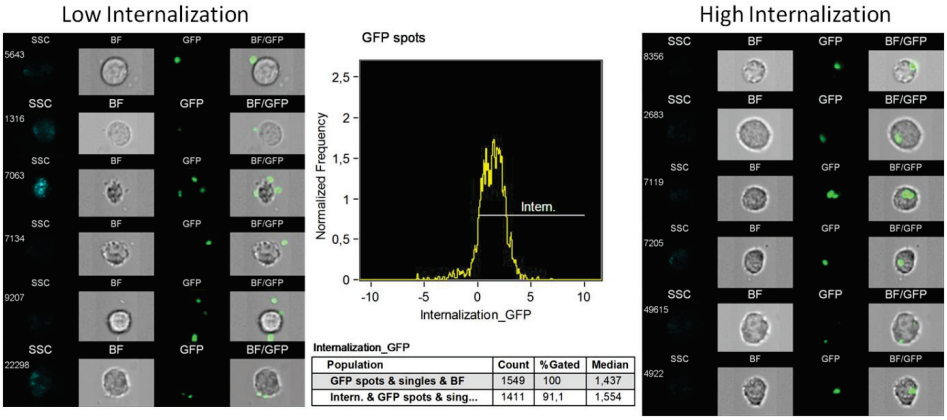

Figure 17: GFP-Brightfield Internalization histogram and associated-imagery after 30 min incubation of U937 cells with GFP-*E. coli* bacteria. Representative images of cells with low and high internalization scores are shown. Each cell is represented by a row of images that includes: Side-scatter (SSC, blue), Brightfield (BF, grey), GFP-*E. coli* (green) and a composite overlay of the BF and GFP-*E. coli* images.

Then a spot mask was created to identify the region of interest: the bright pixels of GFP-*E. coli* within the cells (Figure 18). The spot mask was applied within the cells with internalized bacteria which masked any particles that meet the following criteria: a radius of 3 pixels or less, a spot to background intensity of 6.5 or greater, and an area greater than 2 pixels.

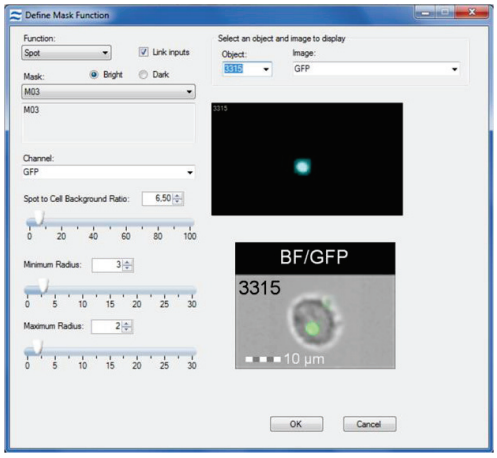

Figure 18: Masking description by using IDEAS (Image Data Exploration and Analysis Software) of the Spot count mask created to identify GFP-*E.coli* bacteria within the cells. Scale bar represents 10 microns.

The number of independent green bacteria within each cell was then determined in the subpopulation of cells positive for the internalization score by using the spot count feature (Figure 19). This feature provides the number of connected components in an image. The connected component algorithm examines the connectivity of each pixel based on whether this pixel is connected to a particular spot or to the background.

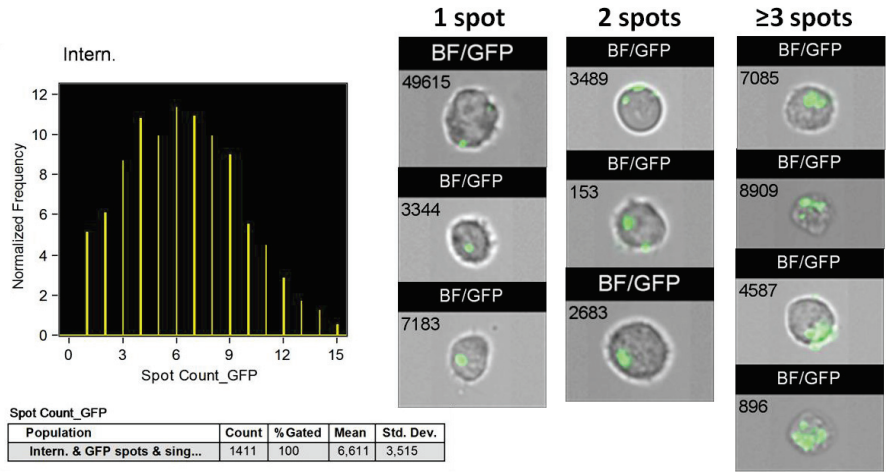

Figure 19: Determination of the number of ingested bacteria in each cell after 30 minutes incubation of U937 cells with GFP-*E. coli* bacteria.. Representative cells with 1, 2 or more than 3 ingested bacteria are displayed above.

Table 3 shows the mean number of ingested bacteria at different time points of phagocytosis. With longer exposure of bacteria to cell samples, the number of ingested bacteria per cell increased, consistent with the increase of fluorescence intensity of the intracellular bacteria. Incubation at 0°C decreased the percentage of cells with internalized bacteria but not the non specific bacterial adherence.

	% of GFP+ cells	GFP Fluorescence (AUF)	% of cells with Internalized GFP	Spot number per cell
Control U937 (no bacteria)	0%	531±133	0%	0
15 min GFP-*E. coli* 37°C	50.4%	10,974±270	47.8%	2.6±0.9
30 min GFP-*E. coli* 37°C	79.2%	15,242±335	91.1%	6.6±3.5
30 min GFP-*E. coli* 0°C	10.6%	12,579±325	8.4%	1.3±0.6
60 min GFP *E. coli* 37°C	82.3%	16,391±778	54.3%	4.3±1.4
90 min GFP *E. coli* 37°C	60.5%	11,564±976	29.7%	3.3±1.1

Table 3: Effect of GFP-*E.coli* incubation with U937 cells at different time points. Data represent mean ± SD of three independent experiments.

Oxidative Burst assays:

In agreement with our previous data on phagocytosis and oxidative burst, HE fluorescence intensity increased over time with longer exposure of U937 cells to bacteria (Table 4). Imaging-Flow cytometry allows quantifying the degree of co-localization between two spectrally distinct images of a single cell (Figure 21). In our case, we measured the correlation between the bright GFP-*E. coli* pixels and the HE images on a pixel-by-pixel and cell-by-cell basis

To determine whether phagosomes containing ingested bacteria co-localize to sites of oxidative burst, the Bright Detail Similarity algorithm (BDS) was used in the population of U937 cells positive for both GFP and HE. This algorithm quantifies the degree of correlation between any two channels images on a pixel-by-pixel and cell-by-cell basis. It is derived from the Pearson's correlation coefficient (ρ), which is based on a linear regression analysis of pairs of values taken from different data sources. The data pairs are the pixel intensities at the same location (x,y) in each image of the GFP and HE channels respectively. The score is negative in sign for images that are opposites, close to zero for uncorrelated images and positive for similar images. High values (≥1) indicate that the fluorescence of bacteria and hydroethidine appear in the same location (same pixel coordinates). The algorithm is applied in the subpopulation of cells positive for GFP and hydroethidine.

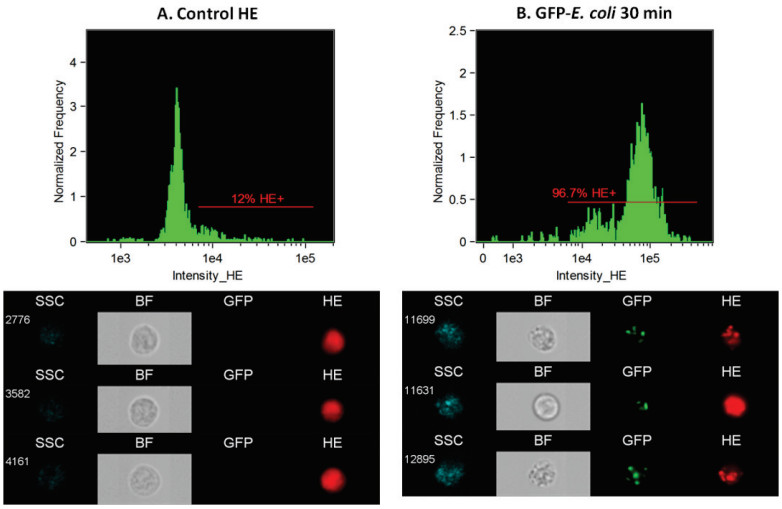

Figure 20: HE Histograms in Control U937 cells vs. cells incubated with GFP-*E. coli* for 30 minutes. Representative imagery of control and treated-samples are shown. Each cell is represented by a row of images that includes: Side-scatter (SSC, blue), Brightfield (BF, grey), GFP-*E. coli* (green) and Hydroethidine (HE, red).

The BDS measures the degree of co-localization between the bacteria and sites of oxidative burst. By analyzing the mean BDS value in the histogram bins, we determined that a score of 2.04 or higher corresponded to cells with degree of co-localization (Figure 21)

$$\text{Similarity} = \ln\left(\frac{1+\rho}{1-\rho}\right) \qquad \rho = \frac{\sum_i (x_i - X)(y_i - Y)}{\sqrt{\sum_i (x_i - X)^2 \sum_j (y_j - Y)^2}}$$

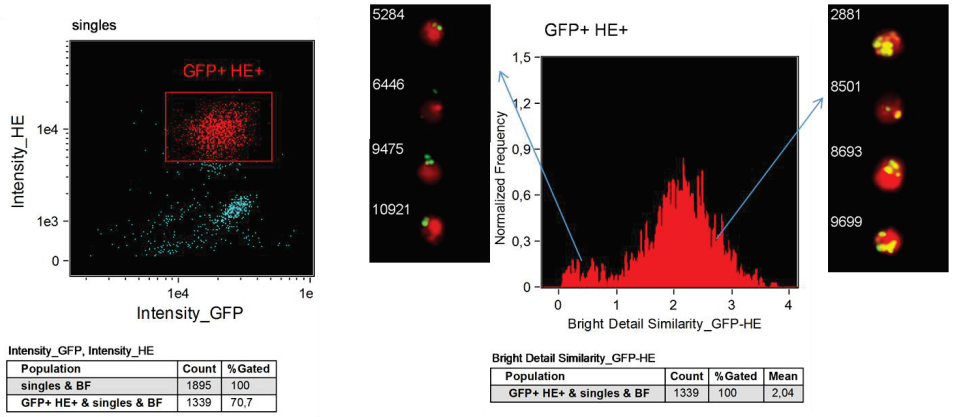

Intensity_GFP, Intensity_HE

Population	Count	%Gated
singles & BF	1895	100
GFP+ HE+ & singles & BF	1339	70,7

Bright Detail Similarity_GFP-HE

Population	Count	%Gated	Mean
GFP+ HE+ & singles & BF	1339	100	2,04

Figure 21: GFP vs. hydroethidine Fluorescence intensity dot plot and Bright Detail Similarity histogram after 30 min incubation with GFP-*E. coli* bacteria. The BDS score is derived from the Pearson's correlation coefficient (ρ). X and Y are the corresponding mean intensity values; x_i and y_i are the per-pixel intensity values of the two images. Imagery of U937 cells with low and high GFP-HE co-localization is shown.

Combining the GFP-HE co-localization score (BDS) with the Internalization feature is possible to identify and quantitate the subset of phagocytic cells with intracellular bacteria co-localized to sites of oxidative burst activity. Three subpopulations were distinguished: cells with surface-bound bacteria, cells with internalized bacteria but not co-localized and cells with ingested bacteria co-localized to sites of oxidative burst response (Figure 22).

Percentages of HE positive cells and HE mean fluorescence increased in a time-dependent manner during the first 30 minutes after incubation. No time-dependent increase of the co-localization of reactive oxygen species to ingested bacteria was observed after 30 minutes incubation (Table 4).

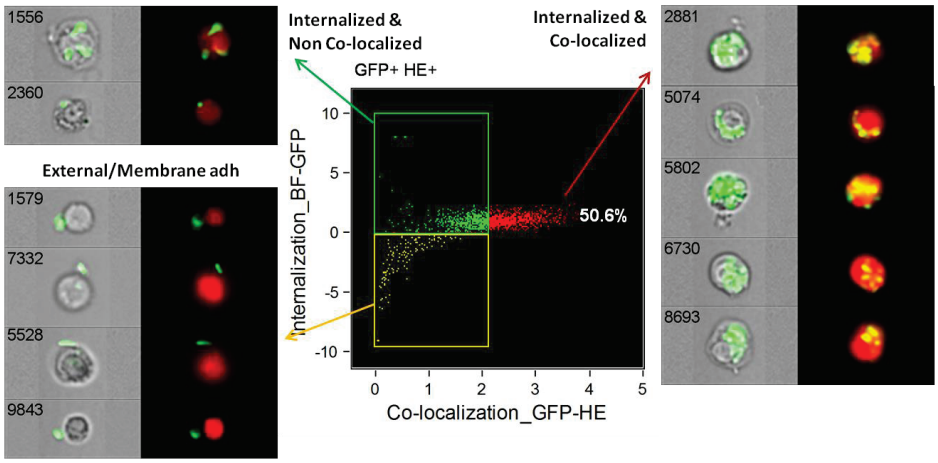

Figure 22: GFP-HE co-localization score (BDS) vs. BF-GFP Internalization feature in U937 cells incubated with GFP-*E .coli* bacteria for 30 minutes at 37 °C.

Double positive cells for both Internalization and Co-localization scores were gated to exclude cells with extracellular/adhered bacteria. Incubations up to 45 minutes may be sufficient for detecting changes in phagocytosis when using *E. coli*. Incubations of as little as 15 minutes are sufficient to detect phagocytosis, but it takes a minimum of 30 min to elicit a maximal oxidative burst response (Table 4).

	% of GFP+ cells	GFP Fluorescence (AUF)	% of cells with Intern. GFP	HE+ cells (%)	HE Fluorescence (AUF)	% Internalized and co-localized
Control U937 15 (no bacteria)	0%	731.59±260	0%	12.7%	16,123±1,240	0%
15 min GFP-*E. coli* 37°C	54.5%	14,496±1437	43.4%	80.2%	24,582±2,210	35.1%
30 min GFP-*E. coli* 37°C	79.2%	15,242±902	91.1%	96.7%	72,411±4,441	50.6%
45 min GFP-*E. coli* 37°C	80.6%	12,500±1040	24.8%	74.06%	59,450±3,650	32.4%
60 min GFP *E. coli* 37°C	68.8%	10,938±932	34.3%	62.3%	67,775±4,690	25.3%

Table 4: Simultaneous measurements of phagocytosis and oxidative burst in U937 cells stained with hydroethidine (HE) and incubated with GFP-*E. coli* at different time points. Data represent mean ± SD of three independent experiments.

5.1.2 Assay Validation in Whole Blood samples

Internalization Assays by conventional FCM: Neutrophils were gated based on their characteristic side-scatter pattern and CD45 expression (Figure23).

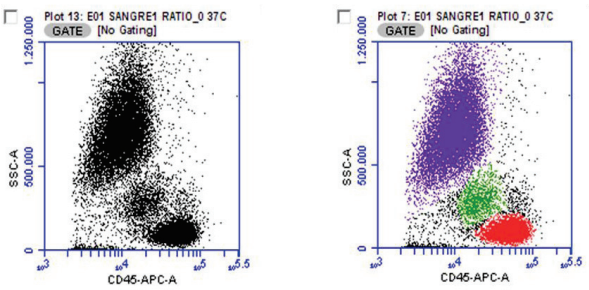

Figure 23: SSC vs. CD45-APC intensity dot plots showing identification of leukocyte subpopulations: neutrophils (57.8%, purple), monocytes (5.7%, green) and lymphocytes (28.7%, red).

The first parameter we consider was the number of bacteria per leukocyte necessary to detect *GFP-E. coli* internalization (ratio bacteria:leukocyte). A ratio as low as 0.25 was enough to trigger phagocytosis by neutrophils in blood samples. Higher ratios increase the percentages of GFP positive neutrophils but also produce a higher non-specific signal (neutrophils at 0°C and lymphocytes at any temperature).

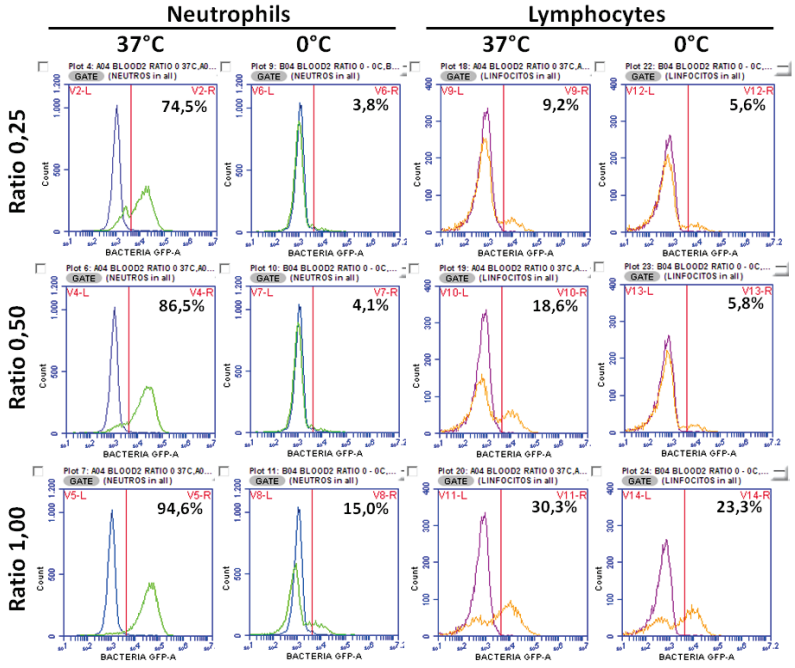

Figure 24: Histograms showing GFP fluorescence and percentages of positive cells after 30 min incubation with different bacteria to leukocyte ratios. Neutrophils and lymphocytes were gated from SSC vs CD45-APC dot plot. Blue and purple curves represent basal GFP levels (with no bacteria). Green and orange curves represent GFP fluorescence emission after incubation at each condition described.

Incubation at 0°C decreased markedly the phagocytic potential of neutrophils at any given ratio (Table 5). Furthermore, we analyzed a non-phagocytic leukocyte subpopulation (lymphocytes) to have a better estimation of the non-specific adherence at the different ratios and conditions assayed.

Ratio B:L	Neutrophils 37°C	Neutrophils 0°C	Lymphocytes 37°C	Lymphocytes 0°C
0.25	78.8 ± 10.0	5.4 ± 1.5	12.7 ± 3,3	7.7 ± 2.2
0.50	91.3 ± 4.8	9.5 ± 4.8	21.5 ± 2,6	13.1 ± 6.4
1.00	96.7 ± 2.2	20.7 ± 5.4	34.1 ± 4.0	28.7 ± 5.6

Table 5: Percentage of GFP+ positive cells (mean ± standard deviation) after incubation at the different conditions assayed.

Oxidative Burst Assays: Superoxide production by neutrophils was analyzed measuring hydroethidine oxidation as described previously. Three different HE concentrations were assayed incubated whole blood at a 0.25 bacteria to cell ratio. Figure 25 shows hydroethidine fluorescence histograms after staining whole blood samples with three different concentrations of HE and incubating for 30 minutes at a bacterium:leukocyte ratio equal to 0.25. The lowest concentration (3,3 µg/mL) produces the higher percentage of positive neutrophils. This is due to the fact that higher HE concentrations generate an increase in the HE basal fluorescence levels (without bacterial incubation).

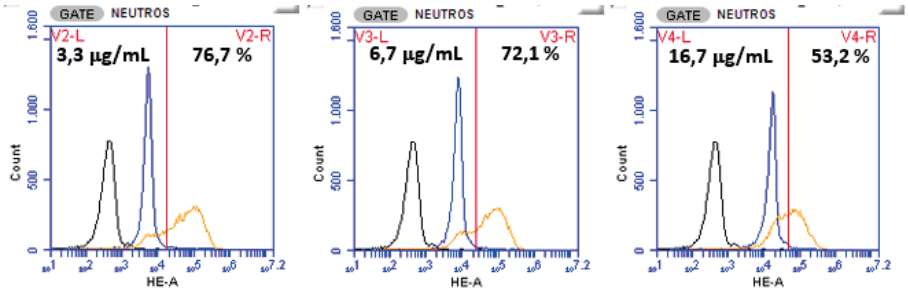

Figure 25: Hydroethidine titration: Black curves represent neutrophils autofluorescence, blue curves represent HE basal levels (without GFP-*E. coli* incubation) and orange curves represent HE fluorescence after incubating at a 1:4 bacteria to cell ratio for 30 minutes. The percentage of neutrophils positive for each condition is indicated in the upper right of the histogram.

The capability of GFP–*E. coli* to elicit radical oxygen species after 30 minutes incubation is similar to the effect of 200 nM PMA treatment, as shown in Figure 26. A marked shift in HE fluorescence intensity can be detected between untreated vs. PMA-stimulated neutrophils.

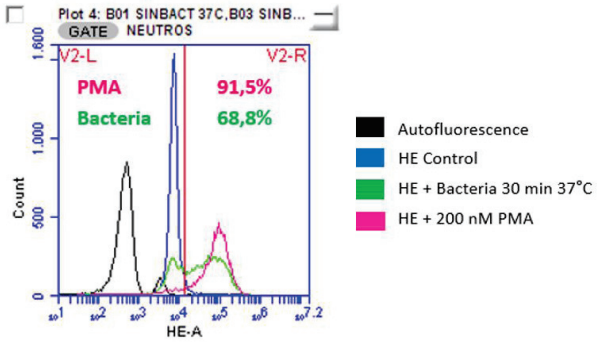

Figure 26: Overlay histogram showing hydroethidine fluorescence levels after incubating blood samples with: GFP-*E. coli* for 30 min (green), 200 nM PMA (pink). Black curve represents neutrophil autofluorescence and blue curve represents HE basal level.

Another parameter taken in consideration was the incubation time of whole blood samples. Figure 27 shows the percentages of neutrophils positive for GFP fluorescence after different incubation times. GFP positive cell percentages increased over time with longer incubation times, but no increase was observed after 30 minutes incubation. Furthermore, longer times than 60 minutes produce neutrophil degranulation and cell death, as observed by the decrease in neutrophil count after 60 minutes incubation with (green curve) or without (blue curve) GFP-*E. coli* bacteria.

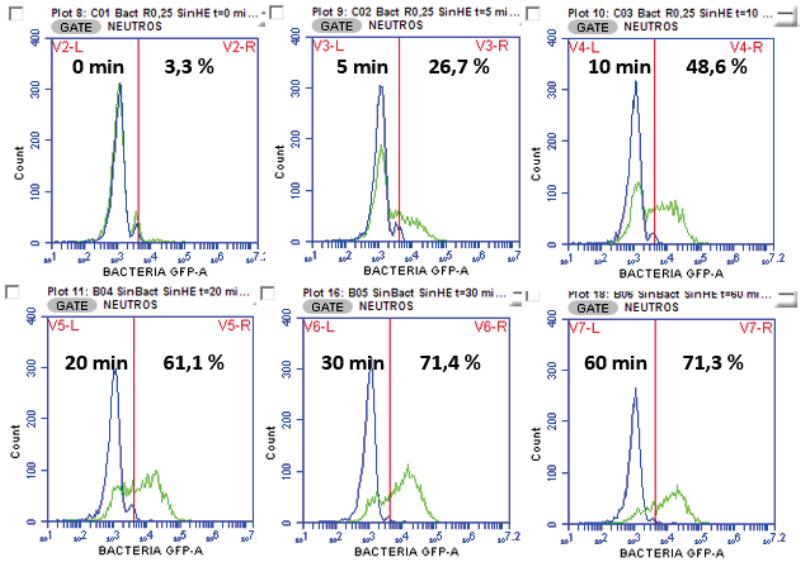

Figure 27: Effect of assay incubation length in GFP-*E.coli* internalization. Percentages of neutrophils positive for GFP after different incubation times at a bacterium:leukocyte ratio of 0.25. Blue curves represent basal GFP levels (with no bacteria) and green curves represent GFP fluorescence after the indicated time points.

Time course of Phagocytosis and Oxidative Burst: By plotting hydroethidine vs. GFP fluorescence intensities it is possible to track the progress of the phagocytic process. Percentages of neutrophils double positive for GFP and HE increased over time with longer exposure of leukocytes to bacteria (Figure 28).

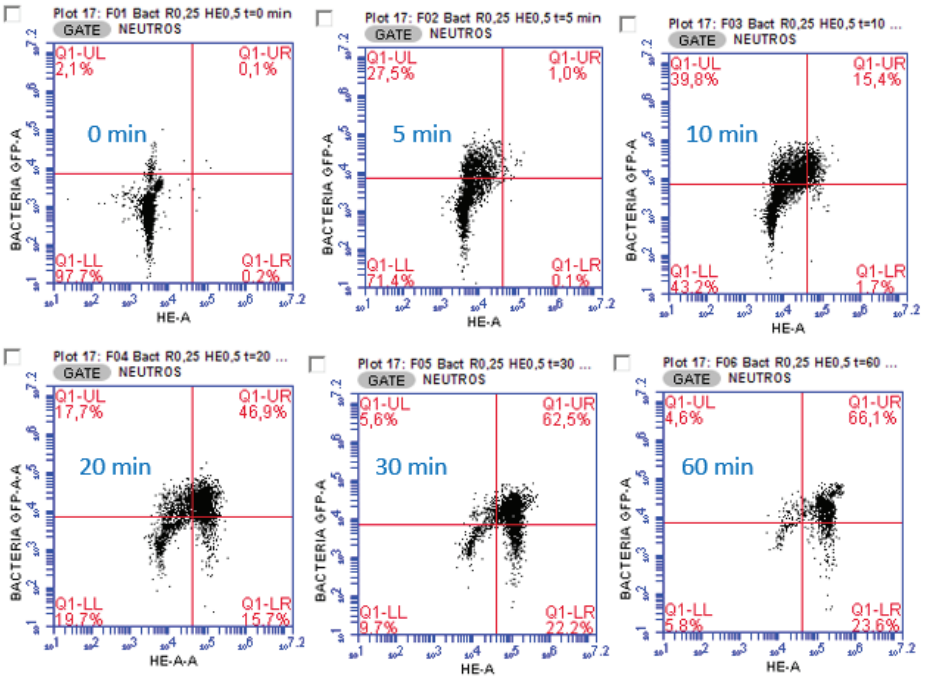

Figure 28: Hydroethidine (FL2) vs. GFP (FL1) fluorescence intensity dot plots after addition of GFP-*E.coli* bacteria at the indicated time points. Extracellular and/or adhered bacteria cannot be distinguished by conventional Flow Cytometry.

After 10 minutes incubation, an increase in the percentage of neutrophils positive for both HE and GFP can be detected. As the phagocytic process progresses, ingested pathogens are degraded in phagolysosomes, thereby resulting in decreased GFP fluorescence and lower percentages of GFP+ cells.

Figure 29 illustrates the percentage of the four different subpopulations based on GFP and hydroethidine positivity. The population of neutrophils GFP+/HE- decreased in a time-dependent manner (as a result of bacterial internalization and subsequent degradation) while GFP+/HE+ population increased due to oxidative burst response, which can be detected after 5 minutes incubation of whole blood with bacteria.

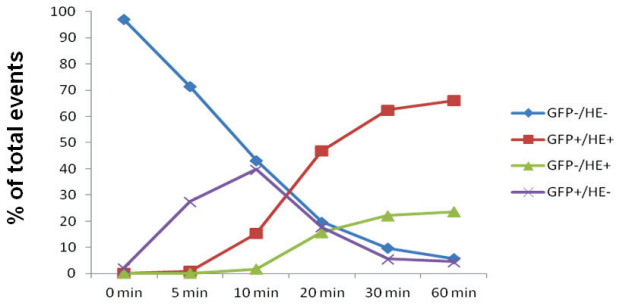

Figure 29: Time course of phagocytosis and oxidative burst by conventional Flow Cytometry.

Internalization Assays by Imaging Flow Cytometry: Leukocyte subpopulations were distinguished by their different side scatter and CD45-PE fluorescence intensities. Furthermore, image-based features are useful in the identification of the three subpopulations of interest. Lymphocytes have lower brightfield area and lower granularity (SSC) compared to neutrophils and monocytes (Figure 30).

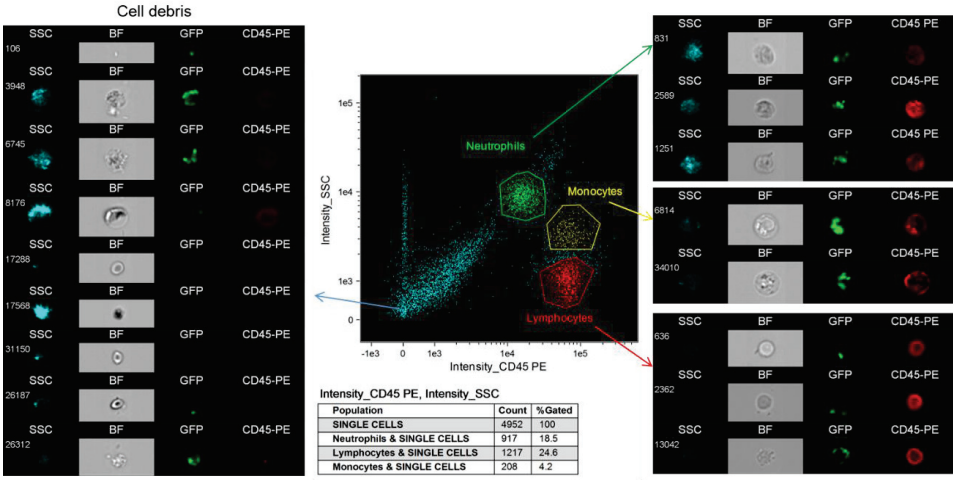

Figure 30: CD45-PE vs. SSC (Side Scatter) intensity dot plot showing identification of leukocyte subpopulations after 60 minutes incubation with GFP-*E. coli* at 37 °C. Each cell is represented by a row of images that includes: Side-scatter (SSC, blue), Brightfield (BF, grey), GFP-*E. coli* (green) and anti-human CD45-PE (CD45-PE, red).

In order to exclude the cells with GFP-*E. coli* bacteria adhered to the cell membrane, the centroids of the GFP and CD45-PE fluorescent images for each subpopulation were calculated (Figure 31). A centroid is the center of a fluorescent image location, in x and y pixel coordinates. Then the distance between both centroids was measured by using the Radial Delta centroid XY (RDC) feature, which computes the difference between both centers by using the Pythagorean Theorem to calculate the absolute distance.

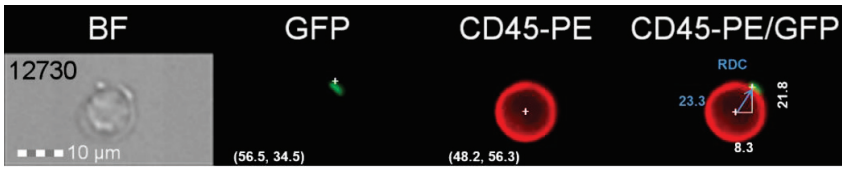

Figure 31: Cell stained with CD45 PE labeled antibody and positive for GFP-*E. coli*. The Radial Delta Centroid (RDC) value is the distance between both centroids of each image (23.3 pixels). The cell is represented by a row of images that includes: Brightfield (BF, grey), GFP-*E. coli* (GFP, green) and a composite overlay of GFP and CD45-PE channels. White crosses represent centroid coordinates for GFP and CD45-PE images. The scale bar shows 10 µm.

Non-phagocytic cells can be distinguished from phagocytes based on their low GFP fluorescence levels and high RDC values (Figure 32). Lymphocytes can be discriminated by their lower GFP fluorescence intensities and higher Delta centroid values. Neutrophils and monocytes show higher GFP fluorescence intensities and lower delta centroid distances.

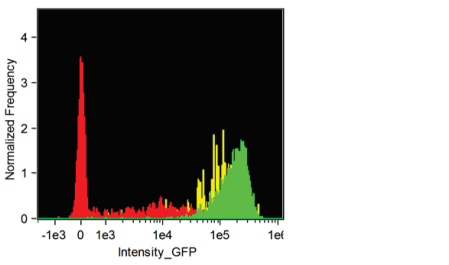

Intensity_GFP

Population	Count	%Gated	Mean
Neutrophils & SINGLE CELLS	917	100	189060.57
Lymphocytes & SINGLE CELLS	1217	100	6316.52
Monocytes & SINGLE CELLS	208	100	118396.48

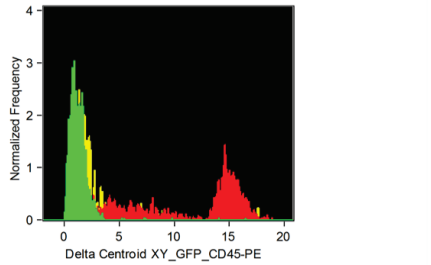

Delta Centroid XY_GFP_CD45-PE

Population	Count	%Gated	Mean
Neutrophils & SINGLE CELLS	917	100	1.28
Lymphocytes & SINGLE CELLS	1217	100	10.82
Monocytes & SINGLE CELLS	208	100	2.449

Figure 32: Histograms showing GFP-*E. coli* fluorescence intensity (left) and Delta Centroid XY distances (right) in the three subpopulations of interest (gated from Figure 30). Lymphocytes (red) can be discriminated by their lower GFP fluorescence intensity and dissimilar Delta centroid values. Neutrophils (green) and monocytes (yellow) show higher GFP fluorescence intensities and lower delta centroid distances.

To determine whether bacteria were surface-bound or internalized, the BF-GFP internalization feature was used in combination with the GFP-PE Delta Centroid (Figure 33). The internalization feature quantifies the degree of correlation between the bright pixels within the brightfield mask on a pixel-by-pixel basis. Positive values indicate that bright GFP pixels of bacteria are included in the brightfield mask, as measured by pixel coordinates.

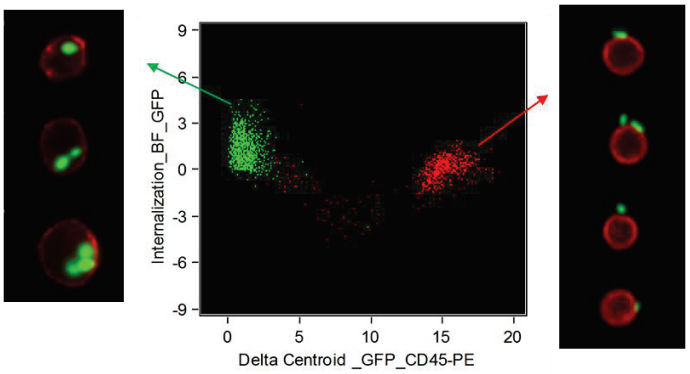

Figure 33: Dot plot showing GFP-PE Delta centroid feature vs BF-GFP internalization score. Cells with ingested bacteria are distinguished from those with extracellular bacteria adhered to their membrane by using imaged-based parameters. Lymphocytes with adhered bacteria have higher Delta centroid GFP-PE values and lower internalization scores compared to phagocytic cells.

Subsequently, the mean number of internalized bacteria per phagocyte was quantified by using the spot count feature, as observed in Figure 34. In order to have an estimation of the surface-bound bacteria in the assay, the mean number of spots was also calculated in lymphocytes, a non-phagocytic cell type.

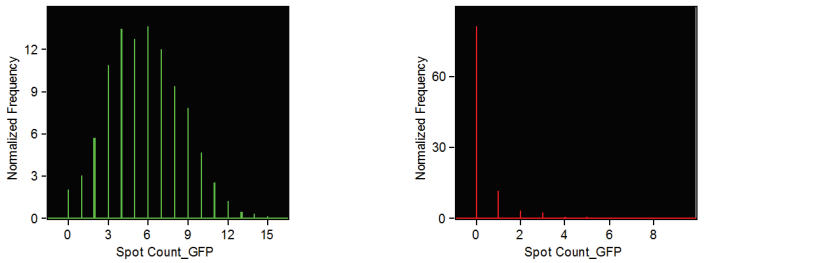

Spot Count_GFP

Population	Count	%Gated	Mean
Neutrophils & SINGLE CELLS	917	100	5.768

Spot Count_GFP

Population	Count	%Gated	Mean
Lymphocytes & SINGLE CELLS	1217	100	0.3262

Figure 34: Spot count histograms showing the mean spot number per cell in the neutrophil and lymphocyte subpopulations after 60 minutes incubation with GFP-*E. coli*.

Table 6 shows the mean number of ingested bacteria per neutrophil at different time points of phagocytosis. With longer exposure of bacteria to blood samples, the

percentage of GFP+ neutrophils increased, consistent with the increase of GFP fluorescence intensity of the intracellular bacteria observed in Figure 34. With the uptake of bacteria, the number of GFP spots per neutrophil increased in a time-dependent manner. After 60 minutes incubation a decrease in the spot number can be observed, which reflects bacterial degradation by phagolysosomes.

	% of GFP+ Neutrophils	GFP Fluorescence (AUF)	% of cells with Intern. GFP	Spot number per cell
15 min GFP-*E. coli* 0°C	22,5%	63,299±22,625	11.6%	1.9±0.6
15 min GFP-*E. coli* 37°C	49.7%	85,496±16,837	39.4%	2.7±1.3
30 min GFP-*E. coli* 37°C	65.2%	110,228±19,776	62.3%	3.1±1.8
45 min GFP-*E. coli* 37°C	60.2%	132,535±24,439	74.8%	4.3±2.2
60 min GFP *E. coli* 37°C	55.6%	180,223±25,013	90.2%	5.6±1.9
90 min GFP *E. coli* 37°C	52.3%	165,223±29,235	72.4%	4.5±2.4

Table 6: Percentages of neutrophils positive for GFP-*E.coli,* percentages of positive cells for the internalization score and mean spot number per cell after the indicated time points. Whole blood was stained with CD45-PE and incubated with GFP-*E. coli* at a 1:4 bacteria to cell ratio. Data represent mean ± SD of three independent experiments.

DISCUSSION

Phagocytosis and oxidative burst assays

In agreement with our previous data of GFP internalization assays by conventional flow cytometry, GFP fluorescence intensities of ingested bacteria and GFP positive cell percentages increased over time within the first 30 minutes following bacterial incubation. Imaging-Flow Cytometry enables the enumeration of individual bacteria associated with a cell. The number of bacteria per cell was determined by using the spot count feature in the subpopulation of cells positive for the BF-GFP internalization score. A continuous increase in the number of internalized bacteria was observed over time. Table 3 shows percentages of U937 cells positive for GFP-*E .coli* and the mean number of ingested bacteria at different time points of phagocytosis.

In order to obtain a more accurate measurement of phagocytosis, U937 cells were stained with hydroethidine to assess oxidative burst of the ingested bacteria by Imaging Flow Cytometry (Figure 20). Incubation at 0°C was performed as negative control. At this temperature phagocytosis is inhibited but not the non-specific adherence (van Eeden, Klut et al. 1999). Non-specific adherence between bacteria and the cell membrane interferes with the real measurement of internalized particles as shown in Table 4.

Imaging-Flow cytometry allows quantifying the degree of co-localization between the bacteria and sites of oxidative burst by measuring the degree of correlation between the bright GFP-*E. coli* pixels and the HE images on a pixel-by-pixel and cell-by-cell basis (Figure 21). Using conventional Flow Cytometry, precise determination of target locations relative to cell membranes (i.e., surface bound vs. fully internalized) during the phagocytic process is difficult to quantify (Figure 24).

Here, we describe a simple method using Imaging-Flow Cytometry that allows rapid and objective quantification of phagocytosis, as well as simultaneous determination of intracellular bacteria co-localized to sites of oxidative burst activity.

In the present study, we have established the usefulness of the U937 cell line as an *in vitro* model for GFP-*E. coli* phagocytosis and subsequent oxidative burst. Phagocytosis can be determined more exactly by counting the number of ingested bacteria per cell. Furthermore, membrane-attached bacteria can easily be identified and excluded from the measurement of phagocytosis, which by conventional flow cytometry is difficult. The spatial distribution of the oxidative burst dye hydroethidine can be determined, and an association to phagosomes can be visualized and quantified.

A number of fluorescence markers have been developed to determine oxidative burst, and HE is one of the most employed for this purpose. The spatial distribution of HE during *E. coli* phagocytosis in U937 cells has not been documented in detail.

Classically, dihydroethidium is considered to be converted to ethidium that binds to DNA, a fact that increases its fluorescence (Gomes, Fernandes et al. 2005). In our results with the U937 cell line, hydroethidine was mainly located not in the nucleus but in the cytoplasm and in phagosomes. While most cells did not show a high degree of co-localization, a minority had oxidative burst activity clustered at the bacteria-containing phagosome. This may reflect different states of activation of oxidative burst and/or different rates of bacterial degradation.

A bacterium:leukocyte ratio as low as 0.25 is enough to trigger phagocytosis and oxidative burst by neutrophils in whole blood samples. The capability of GFP–*E. coli* to elicit radical oxygen species is similar to PMA. Contrarily, incubation at 0°C decreased markedly the phagocytic potential of blood and U937 cells. Using Imaging-Flow Cytometry, the number of ingested bacteria per neutrophil can be determined, which is not possible by conventional Flow Cytometry (Hampton, Kettle et al. 1998). However this technique has some intrinsic limitations which must be considered. With increasing time of phagocytosis, ingested pathogens are degraded in phagolysosomes, thereby resulting in decreased GFP fluorescence. Therefore, time intervals of more than 30 minutes may underestimate the number of ingested bacteria.

Accurate analysis of phagocytosis requires knowledge about the type of targets and receptors involved and an accurate control of the initial bacteria to cell ratio. Based on the concentration of leukocytes, as measured by conventional Flow Cytometry, the concentration of bacteria can be calculated from the absolute FCM counts to establish the appropriate ratio. Combined measurements of oxidative burst and bacterial internalization improve the measurement of phagocytosis, which may be useful in cases of suspected dysfunction between phagocytosis and the oxidative burst response (e.g. in patients with CGD or LAD). Patients with CGD are sometimes infected with organisms that usually do not cause disease in people with normal immune systems. *E. coli* is one of the most common organisms that cause disease in CGD patients and therefore a natural target for studies of phagocytosis in patients with suspected CGD.

Phagocytosis is a tightly regulated, complex process by which particles are recognized, bound, and subsequently internalized by cells. The development of new methods for the study of the signaling processes and cellular activities involved at each stage will provide important information regarding phagocytic cell disorders. Here we describe the utility of image-based methods.

In conclusion, we describe an objective and rapid whole blood method for the analysis of viable GFP-*E. coli* phagocytosis and oxidative burst using Imaging-Flow Cytometry. This method broadens the obtainable information as compared to conventional approaches (Flow Cytometry and Microscopy). Advantages of this method include a more precise measurement of phagocytosis, quantitation of intracellular bacteria and co-localization of the oxidative burst activity in one assay. By

providing quantitative image analysis of cells imaged in flow, this technique allows a more comprehensive analysis of phagocytosis than can be done by traditional techniques.

5.2 NF-κB Immunotoxicity assays

5.2.1 Assay optimization in U937 cells

Image Analysis protocol: Firstly, to obtain the best nuclear in-focus images, the gradient RMS of the nuclear channel (7AAD) was used to measure the sharpness quality of the nuclear (Figure 35, A).
After gating on the subpopulation of cells with the best nuclear focus (bf, 98.8%), single U937 cells are located by plotting the area vs. the aspect ratio (the ratio of the width and height of the object) of the brightfield channel (Figure 35, B). Subsequently, double positive cells for both 7AAD and NF-κB were gated to measure the correlation between the NFκB-AF488 and nuclear fluorescent images. Then the NF-KB–7AAD Similarity score was used to analyze the degree of correlation between the NF-κB channel and nuclear channel images. In this analysis a larger score indicates a greater degree of signal and thus, translocation. The region drawn on the histogram represents the region for positive image correlation for both channels. Composites images of cells with low (left) and high (right) similarity values are shown.

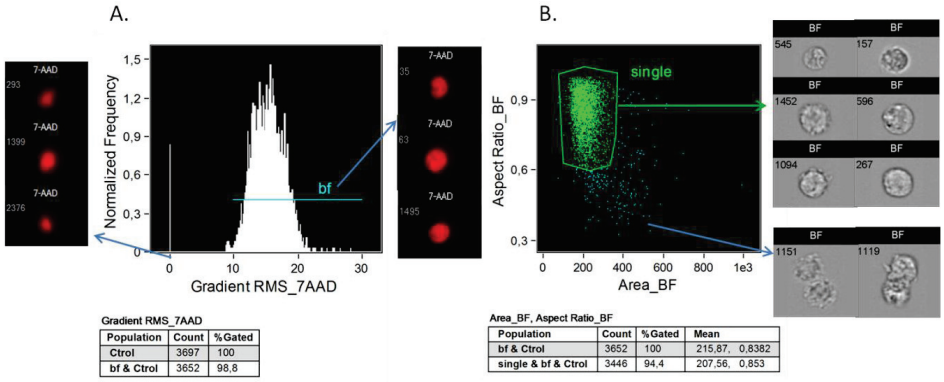

Figure 35: Image analysis protocol performed with IDEAS sofwtare showing the idenification of best nuclear-focused U937 cells (A). By plotting the area vs the Aspect Ratio (i.e, the shape) of the brighfield channel (BF) single cells can be separated from debris and multicellular aggregates.

Figure 36 indicates the basal level of NF-κB translocation in non-stimulated U937 cells (16.5 %). The image-based method for quantifying nuclear translocation employed here consists in the spectral isolation of NF-κB images from nuclear images by the ImageStream. All the cells were stained for anti-NF-κB/p50–AF488 and 7AAD for nuclear imaging. A mask was applied to determine the nuclear area based on 7AAD staining. Using this mask, the spatial relationship between the NF-κB-AF488 and

nuclear images was measured using the similarity algorithm (described previously in Figure 21).

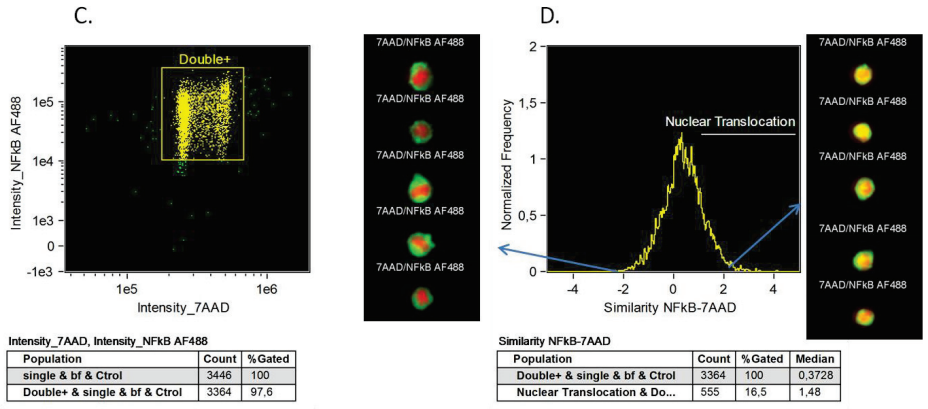

Intensity_7AAD, Intensity_NFkB AF488

Population	Count	%Gated
single & bf & Ctrol	3446	100
Double+ & single & bf & Ctrol	3364	97,6

Similarity NFkB-7AAD

Population	Count	%Gated	Median
Double+ & single & bf & Ctrol	3364	100	0,3728
Nuclear Translocation & Do...	555	16,5	1,48

Figure 36: Dot plot of 7AAD vs. NF-κB-AF488 fluorescence intensity (C) and Similarity histogram of unstimulated U937 cells (D).Images with low (left) and high values (right) for this score are shown above.

This algorithm measures the correlation between the pixels values of two image pairs and provides a measure of the degree of nuclear localization of NF-κB by computing the pixel intensity correlation between the NFκB-AF488 and 7AAD images. Cells with low similarity score exhibit no correlation of the images (hence, a cytoplasmic distribution of NF-κB), whereas cells with high scores exhibit a positive correlation (hence, a nuclear distribution).

Figure 37 shows the effect of 50 µg/ml LPS treatment on NF-κB translocation compared to the respective untreated sample after 2 hours incubation. As it can be observed, LPS incubation induced a shift in the distribution of the Similarity histogram of treated-cells (red curve), with 82% positive cells in the treated population vs. 16.5% in the untreated population.

Representative images from the indicated histogram bins of the treated group demonstrate a distinctly cytoplasmic NF-κB distribution in cells with low similarity values compared to a nuclear distribution in cells with high scores.

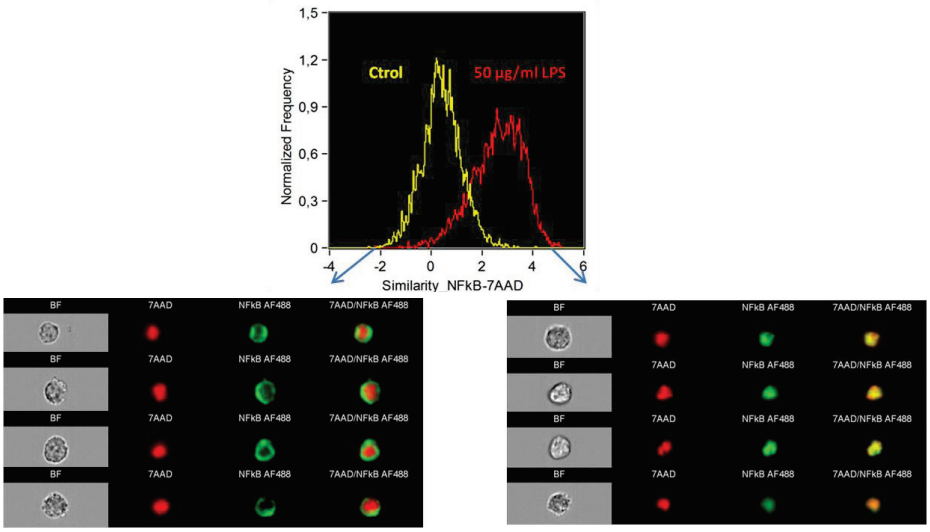

Figure 37: Histogram overlay showing the effect of LPS incubation in Control (yellow) vs. 50µg/ml LPS (red) after 2 hours treatment. Imagery of non-translocated cells (low similarity values, left) and translocated cells (high similarity values, right) are shown. Each cell is represented by a row of images that includes: Brightfield (BF, grey), 7-Amino-Actinomycin D (7AAD, red), antihuman-NF-κB-Alexa Fluor 488 (NFkBAF488, green) and a composite overlay of the NF-κB and nuclear channels.

At the time points assayed, LPS induces a higher dose-dependent response on NF-κB nuclear translocation in U937 cells compared to PMA (Figure 38). A concentration of 10 µg/ml LPS generates a 2-fold increase in the cell percentages showing NF-κB activation, this increase was prevented by pre-incubation of U937 cells with 200 µM PDTC. Pre-incubation of PDTC prior to LPS or PMA-treatment decreased partially NF-κB activation suggesting this antioxidant is a potent inhibitor for NF-κB /p50 activation.

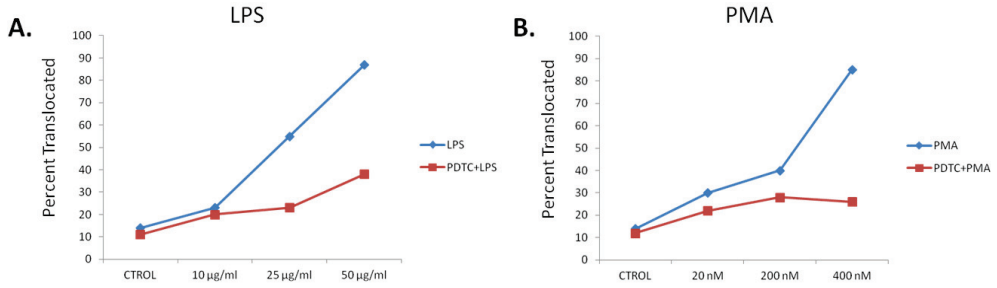

Figure 38: Effect of treatment with activating agents on NF-κB nuclear translocation in U937 cells. Samples pre-incubated for 1 hour with 200 µM PDTC (red) or without (blue) and treated with LPS (A) and PMA (B) for 2 hours.

Figure 39 demonstrates the effect of treatment with activating agents (LPS and PMA) pre-incubated with or without the inhibitor PDTC after 24 hours incubation. For longer

incubation times, LPS induced higher percentages of cells with NF-κB nuclear translocation compared to PMA.

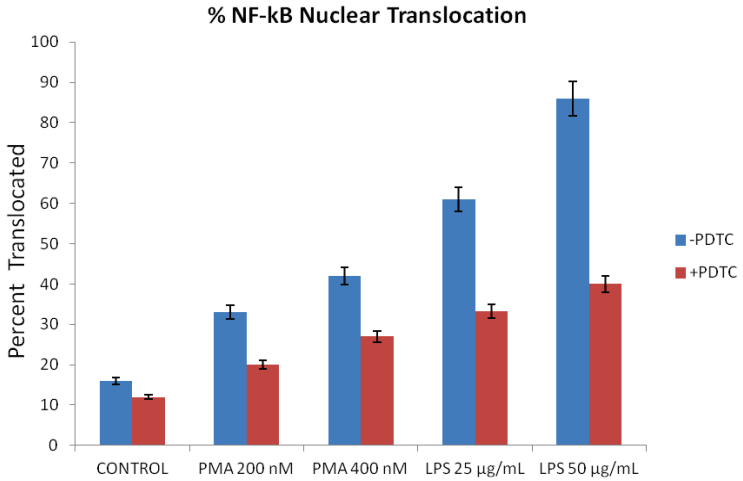

Figure 39: Percentages of NF-κB nuclear translocation in U937 cells pre-incubated with (red) or without 200 µM PDTC (blue) and treated with activating agents. All the treatments had a statistically significant effect (p-value<0.05) when compared with their respective controls.

A dose-response curve was then established to determine the optimal concentration of LPS. After evaluating the effect of different concentration of LPS in U937 cells, 25 and 50 µg/ml LPS dose induced the highest percentages of NF-κB activation in the preliminary experiments with the activating agents. LPS was chosen as positive control for the validation of the assay in whole blood samples.

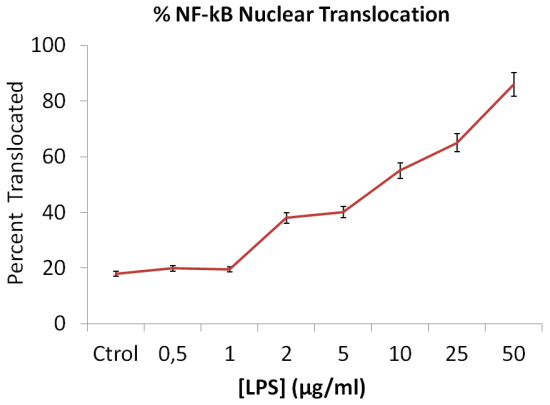

Figure 40: Dose response curve of nuclear translocation in U937 cells stimulated with LPS. Cells were incubated with the indicated dose of LPS for 24 hours at 37 °C, stained for NF-κB expression and 7-AAD, and run on the ImageStream.

To establish the concentration range of test compounds, IC50s of each compound were calculated by a flow cytometric viability assay with Propidium Iodide (Figure 41).

Based on these values, the range of concentrations for each compound was established by adding two concentrations below and one above to each IC50 dose.

CHEMICAL	IC50 (mM)
Mercury Chloride	$4.2x10^{-4}$
Hexachlorobenzene	0.075
Lindane	0.13
t-BHP	0.15

Figure 41: IC50 (mM) values for the tested compounds calculated by Propidium Iodide assay and assayed in the U937 cell line.

Figure 42 indicates the effect of Hexachlorophene treatment on NF-κB nuclear translocation after treatment for 24 hours. Hexachlorophene induced NF-κB activation in a dose dependent manner. The lowest concentration employed (a quarter of its IC50) caused a 5-fold increase compared to the untreated control sample. This effect was markedly prevented by pre-incubating samples with 200 µM PDTC.

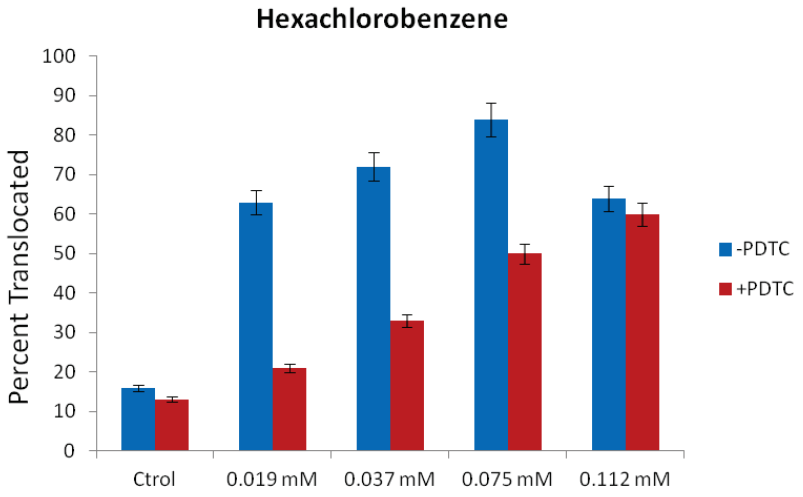

Figure 42: Percentages of NF-κB nuclear translocation in U937 cells pre-incubated with or without 200 µM PDTC and treated at the indicated dose for 24 hours. All the treatments had a statistically significant effect (p-value<0.05) when compared with their respective controls.

Lindane treatment caused a concentration-dependent increase in the NF-κB activation after 24 hours incubation, being this effect prevented by PDTC pre-incubation (Figure 43). The lowest concentration employed (a quarter of its IC50) induced a 3-fold increase compared with its respective control.

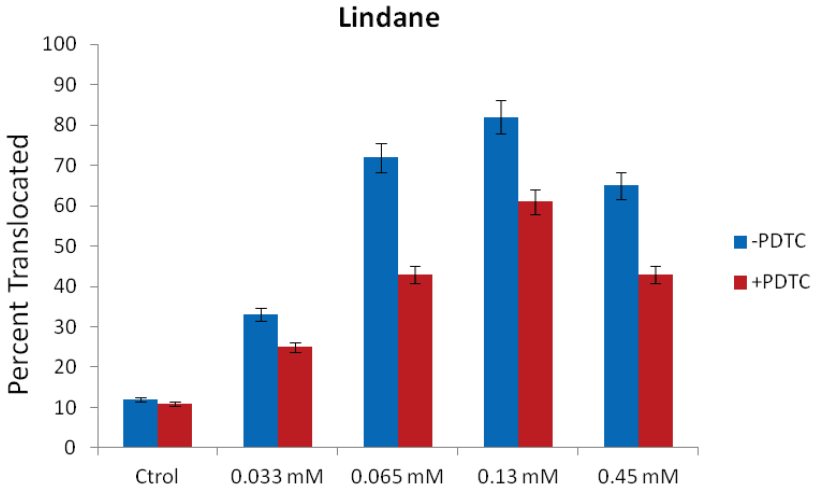

Figure 43: Percentages of NF-κB nuclear translocation in U937 cells pre-incubated with or without 200 μM PDTC and treated at the indicated dose for 24 hours. All the treatments had a statistically significant effect (p-value<0.05) when compared with their respective controls.

Figure 44 illustrates the effect of mercury chloride treatment on NF-κB activation. A dose as low as a quarter to the IC50 induced a 2.5-fold increase compared to the untreated control sample. Pre-incubation with PDTC partially decreased the effect of Mercury chloride treatment.

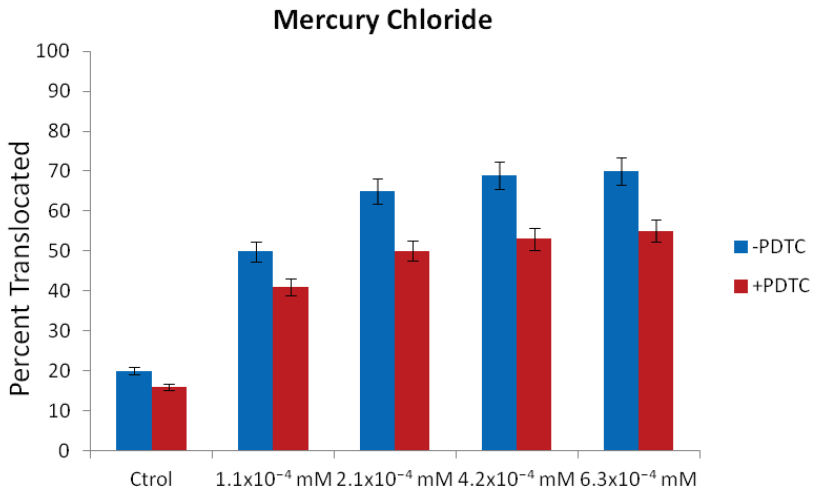

Figure 44: Effect of Mercury Chloride treatment on NF-κB nuclear translocation. U937 cells were pre-incubated with or without 200 μM PDTC and treated at the indicated dose for 24 hours. All the treatments had a statistically significant effect (p-value<0.05) when compared with their respective controls.

Treatment with tert-Butyl Hydroperoxide induced a strong effect on NF-κB activation, being this effect prevented by sample pre-incubation with PDTC. Incubation with the lowest concentration (a quarter of its IC50) generated a 5-fold increase vs. the untreated sample. Pre-incubation with PDTC prevented this effect notably.

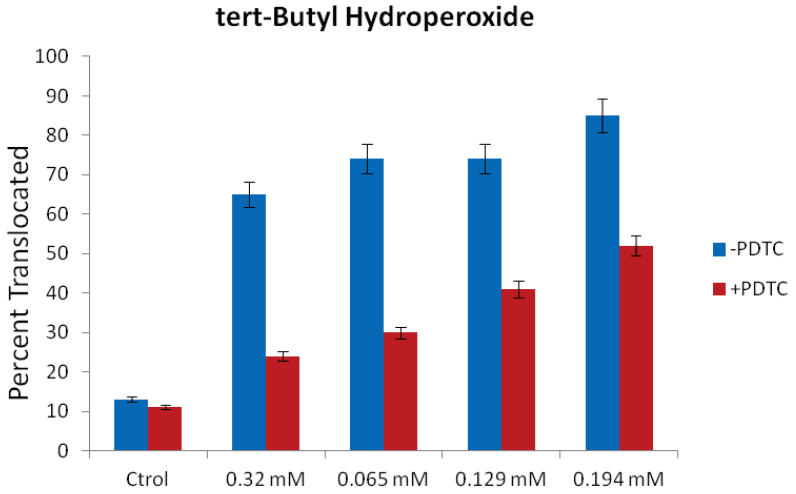

Figure 45: Effect of tert-Butyl Hydroperoxide treatment on NF-κB nuclear translocation. U937 cells were pre-incubated with or without 200 µM PDTC and treated at the indicated dose for 24 hours. All the treatments had a statistically significant effect (p-value<0.05) when compared with their respective controls.

5.2.2 Assay Validation in whole blood samples

The ability to quantify nuclear translocation in U937 cells afforded the possibility of quantifying translocation in human whole blood samples. After plotting CD14-Vio700 vs. SSC intensity, monocytes and lymphocytes were gated to measure the correlation between their NF-κB and nuclear images (Figure 46). All the cells were positive for NF-κB-AF488 and 7AAD.

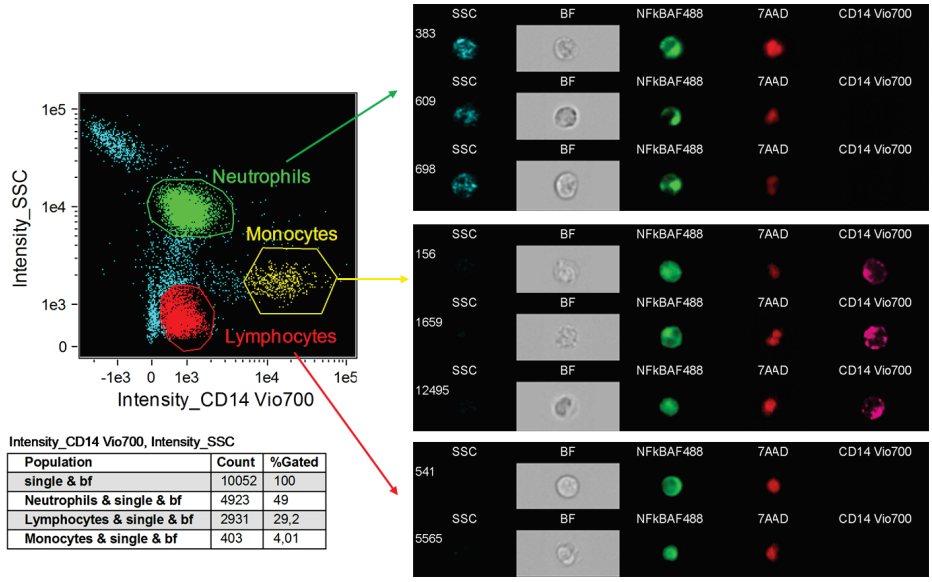

Intensity_CD14 Vio700, Intensity_SSC

Population	Count	%Gated
single & bf	10052	100
Neutrophils & single & bf	4923	49
Lymphocytes & single & bf	2931	29,2
Monocytes & single & bf	403	4,01

Figure 46: CD14-Vio700 vs. SSC (Side Scatter) intensity dot plot showing identification of leukocyte subpopulations after 24 hours treatment with 0.022 mM Mercury Chloride at 37 °C. Representative images of each subpopulation are shown. Each cell is represented by a row of images that includes: Side-scatter (SSC, blue), Brightfield (BF, grey), anti human NF-κB Alexa Fluor 488 (NFkBAF488, green), 7-Amino-Actinomycin D (7AAD, red) and anti-human CD14 Vio700 (CD14 Vio700, pink).

To establish the concentration range of test compounds in the whole blood assays, IC50s of each compound were calculated by calculated by MABA (Microplate Alamar blue assay) viability assay. Based on these values, the range of concentrations for each test compound was established by adding two concentrations below and one above to each IC50 dose (Figure 47).

CHEMICAL	IC50 (mM)
Diazepam	8.70 x10^{-4}
Hexachlorobenzene	1.51 x10^{-3}
Lindane	0.645
Mercury Chloride	0.091
t-BHP	6.129

Figure 47: Human whole blood IC50 (mM) values for the tested compounds calculated by MABA (Microplate Alamar blue assay).

Figure 48 indicates the effect of Lindane-treatment on NF-κB nuclear translocation in cell subpopulation of monocytes after incubating whole blood with a quarter of its IC50.

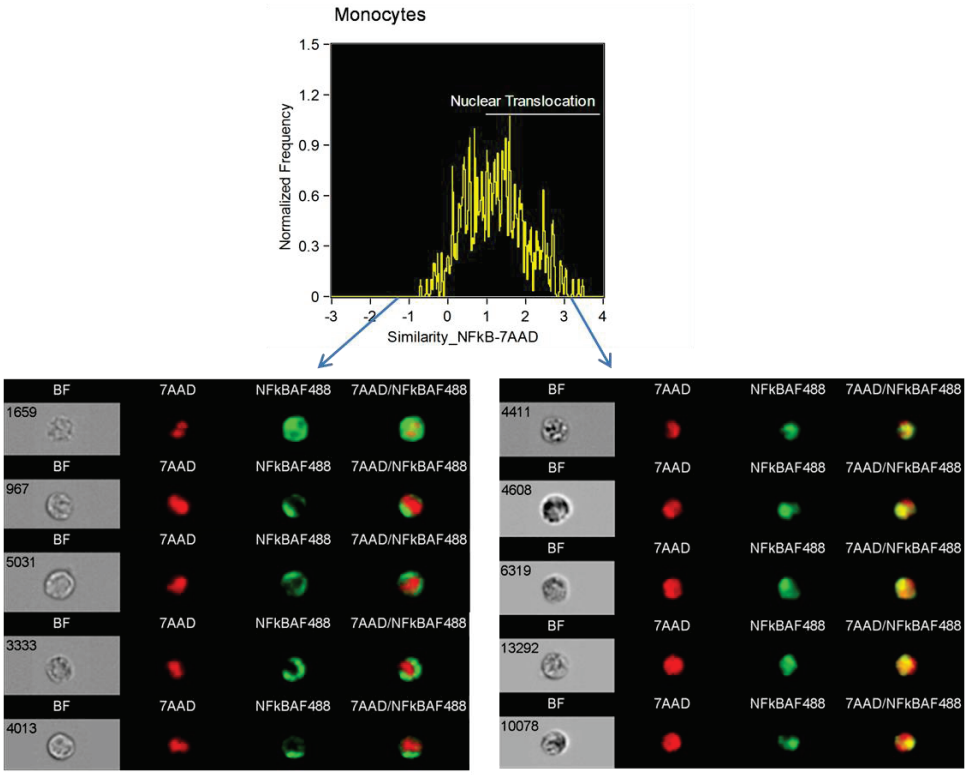

Figure 48: Similarity NFkB-7AAD histogram in human peripheral blood monocytes after treatment with 0.16 mM Lindane for 24 hours at 37 °C. Each cell is represented by a row of images that includes: Brightfield (BF, grey), 7-Amino-Actinomycin D (7AAD, red), anti-human NF-κB-Alexa Fluor 488 (NFkB AF488, green) and a composite overlay of the NF-κB and nuclear channels.

Figure 49 indicates the effect of Lindane-treatment on NF-κB nuclear translocation in cell subpopulation of lymphocytes after incubating whole blood with a quarter of its IC50. Figure 50 shows effect of 50 µg/ml LPS incubation on NF-κB nuclear translocation in the cell population of monocytes, lymphocytes and neutrophils.

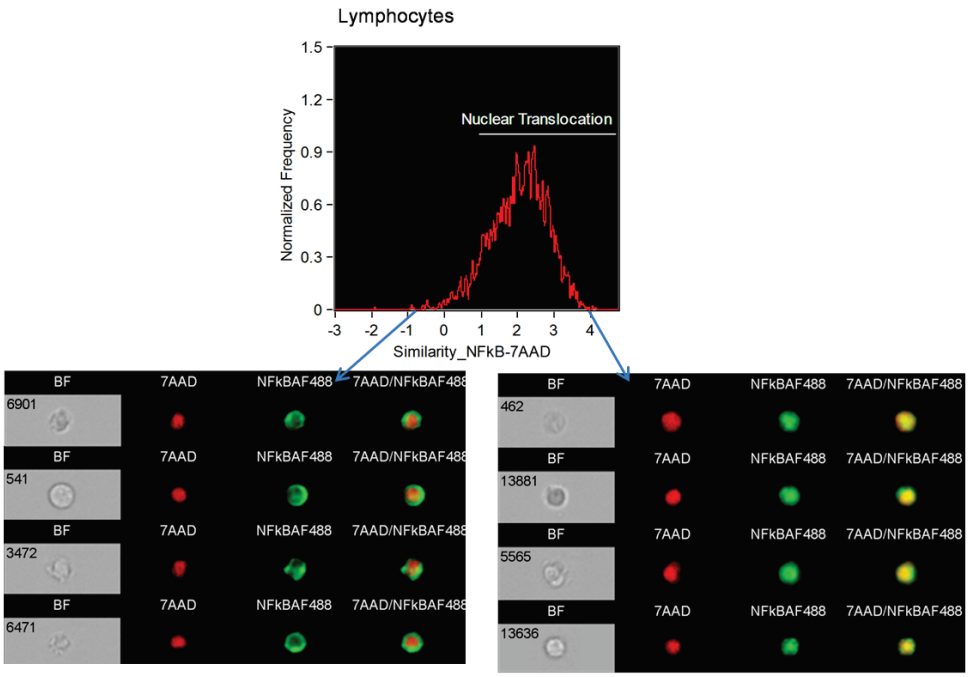

Figure 49: Similarity NFκB-7AAD histogram in human peripheral blood lymphocytes after treatment with 0.16 mM Lindane for 24 hours at 37 °C. Each cell is represented by a row of images that includes: Brightfield (BF, grey), 7-Amino-Actinomycin D (7AAD, red), anti-human NF-κB-Alexa-Fluor 488 (NFkB AF488, green) and a composite overlay of the NF-κB and nuclear channels.

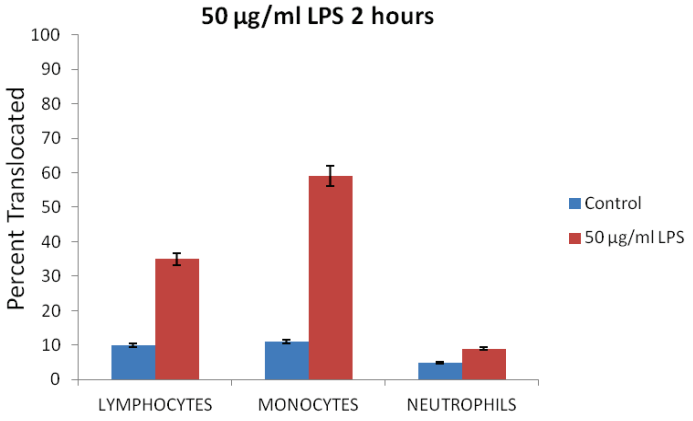

Figure 50: Effect of LPS on NF-κB nuclear translocation in leukocyte subpopulations (Lymphocytes, Monocytes and Neutrophils). Whole blood samples were treated with 50 µg/mL LPS for 2 hours at 37 °C.

LPS treatment had a statistically significant effect (p-value<0.05) in monocytes and lymphocytes when compared with their respective controls.

Pyrrolidine dithiocarbamate (PDTC) was shown to be an effective inhibitor of NF-κB in human lymphocytes and monocytes. No meaningful variation in the neutrophil percentages of NF-κB nuclear translocation was detected after 50 µg/ml LPS treatment. A slight decrease was observed after pre-incubating blood samples with PDTC at concentrations higher than 500 µM. (Figure 51)

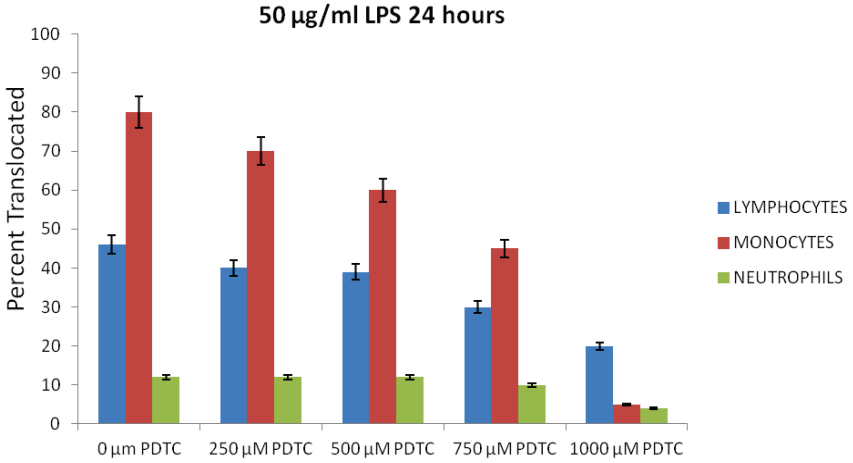

Figure 51: Inhibition of NF-κB activation by PDTC pre-incubation in blood samples: Percentages of NF-κB nuclear translocation in peripheral blood samples pre-incubated with different concentrations of PDTC for 2 hours and then treated with 50 µg/ml LPS for 24 hours at 37 °C. LPS treatment had a statistically significant effect (p-value<0.05) in the cell populations of monocytes and lymphocytes when compared with their respective controls.

Figure 52 shows the effect of test compounds on NF-κB nuclear translocation in the cell population of monocytes after 24 hours treatment. Mercury chloride and Diazepam showed a 5-fold increase with the lowest dose assayed (a quarter to their IC50) compared to their respective untreated controls.

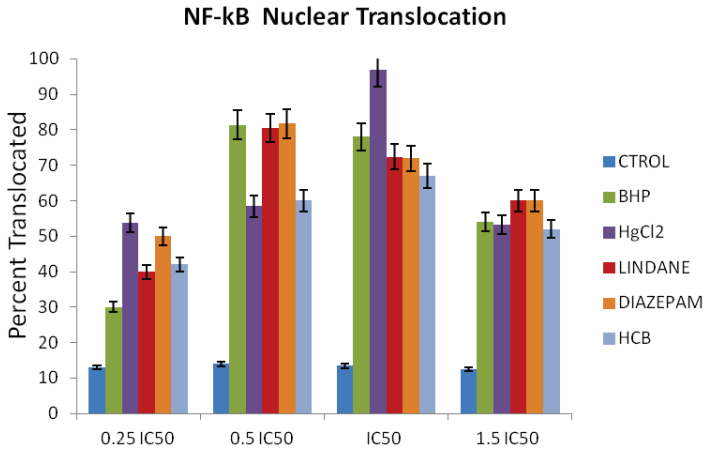

Figure 52: Effect of test compounds on human peripheral blood monocytes. Percentages of NF-κB nuclear translocation in peripheral blood monocytes after treatment with test compounds for 24h at 37 °C. Data represent the mean ± SD of three independent experiments. All the treatments had a statistically significant effect (p-value<0.05) when compared with their respective controls.

Figure 53 shows the effect of test compounds on NF-κB nuclear translocation in lymphocytes after 24 hours treatment. Diazepam showed an 8-fold increase after incubating with a half to the IC50 dose, compared to the respective untreated control.

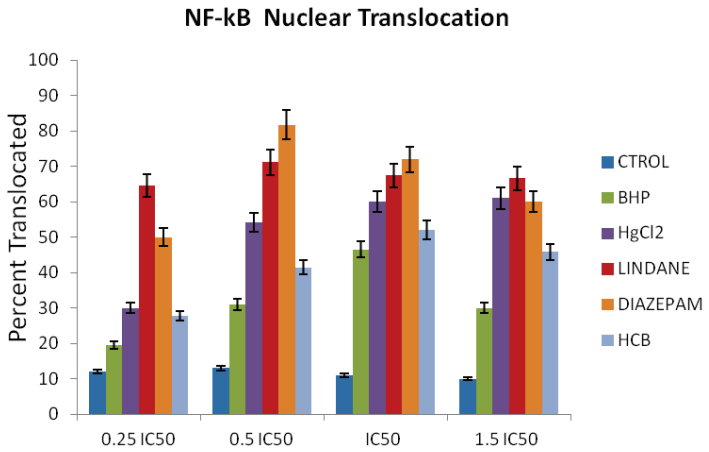

Figure 53: Effect of test compounds on human peripheral blood lymphocytes: Percentages of NF-κB nuclear translocation in peripheral blood lymphocytes after treatment with test compounds for 24h at 37 °C. Data represent the mean ± SD of three independent experiments. All the treatments had a statistically significant effect (p-value<0.05) when compared with their respective controls.

DISCUSSION

Identifying immunotoxicants is difficult because chemicals can cause a wide variety of complicated effects on immune function. Observations in humans and studies in rodents have clearly demonstrated that a number of environmental and industrial chemicals can adversely affect the immune system (Boverhof, Ladics et al. 2014).

Alternative testing methods to predict acute toxicity are required especially due to the implementation of new EU regulations. Regulation (EC) No 1907/2006 of the European Parliament and of the Council of 18 December 2006 concerning the Registration, Evaluation, Authorization and Restriction of Chemicals (REACH) aims to improve the protection of human health and the environment through the better and earlier identification of the intrinsic properties of chemical substances. The dramatic growth in chemicals production and trade has raised concern about the potential risk posed by dangerous chemicals and pesticides. (https://echa.europa.eu/es/reach)

The implementation of REACH will increase the number of laboratory animals used if alternative methods are not available. Meanwhile, REACH promotes the use of *in vitro* tests and therefore, a set of appropriated alternative testing methods and strategies are needed. The immune system can be a target for many chemicals including environmental contaminants and drugs with potential adverse effects on human health (Luebke 2012).

In vitro detection of human immunotoxicity is relevant to basic and regulatory toxicology but is usually complex (e.g., multiple cytokine detection, complex signaling pathways) while steps central to integrative processes may become simple and suitable endpoints. Abnormal activation of NF-κB is a promising therapeutic target in cancer biology and in immunotoxicity studies; therefore quantitative measurement of its activity is an important endpoint.

The aim of this work was to evaluate the suitability of a set of *in vitro* tests to detect NF-κB activation in U937 cells and whole blood samples. For each of the measured endpoints, IC50s values have been calculated. By establishing the dose range of toxic compounds based on their respective IC50 values, it is possible to compare the power of the different toxic compounds among them.

In this study, we report that *in vitro* exposure with the tested compounds to human blood samples differentially induced NF-κB activation at the different conditions assayed. Imaging-Flow Cytometry enabled quantifying NF-κB nuclear translocation in heterogeneous cell populations.

The localization of p65 as indicator of NF-κB activation was evaluated in U937 cells and whole blood samples treated with the indicated test compounds. Localization

of p65 in the cytoplasm indicates that the NF-κB heterodimer is still in its inactive form. In contrast, localization of p65 in the nucleus indicates that the NF-κB heterodimer has translocated into the nucleus and therefore is able to activate the transcription of NF-κB-dependent genes.

The dithiocarbamates represent a class of antioxidants showed to be potent inhibitors of Nf-κB *in vitro* (Schwartz, Moore et al. 1996). The metal-chelating properties of the diethyl derivates of dithiocarbamate have been used during decades for the treatment of metal poisoning in humans (Reisinger, Kern et al. 1990). Pyrrolidine dithiocarbamate (PDTC) was shown to be an effective NF-κB inhibitor as seen in Figure 51. The potential for modulating both cell activation and the effects observed on oxidants suggest that PDTC may offer therapeutic benefit in acute inflammatory conditions in which NF-κB activation plays a major role.

In most resting cells, other than neutrophils, NF-κB is present in the cytoplasm bound to the inhibitory protein IkBα. Cell stimulation with inflammatory signals leads to phosphorylation of the cytoplasmic IkBα, followed by its rapid ubiquitination and degradation by the proteasome. This process releases NF-κB to translocate into the nucleus and bind to the NF-κB responsive promoters. Miskolci et al demonstrated that human neutrophils differ from monocytic and other cells in that they contain predominant amounts of IkBα in the nucleus of resting cells (Miskolci, Rollins et al. 2007). In their work they also demonstrate that neutrophil stimulation with LPS induces early activation after 30-50 minutes treatment. However, the exact mechanisms by which nuclear IkBα regulates the NF-κB-dependent transcription remain unknown. Our results were consistent with their data: no differences in NF-κB subcellular localization (neither in cell percentages positive for NF-κB translocation) were detected in neutrophils after LPS stimulation at the time points assayed. For this reason, we focused the analysis of NF-κB subcellular localization on monocytes and lymphocytes.

Cytotoxicity of chemicals for components of the immune system may lead to altered host defense to infectious diseases. For this reason, it is important to screen for potential immunotoxicity within the context of acute toxicity testing. General parameters of the immune system (base-line pathway activation) are useful to identify potential immunotoxicity.

The cytoplasmic-nuclear transport of signaling proteins involved in signal transduction pathways is an important rate-limiting process in gene transcription. Thus, cellular localization of these proteins can be used not only as a measure of basal activation, but also of the effectiveness of therapy aiming to correct the pathway activity in disease conditions. This work demonstrates that Imaging-Flow Cytometry exhibits sensitivity and specificity in the measurement of NF-κB localization and that can distinguish heterogeneity amongst immunophenotypically defined subpopulations.

In the twelve years since the commercial introduction of the first Imaging-Flow Cytometer, this technology has been employed in over 500 peer-reviewed scientific studies (Basiji and O'Gorman 2015). As the literature has grown, the range of applications for the technology has expanded progressively and given rise to a need for development and standardization of new methods and practices for the use of this technology.

The application of automated image processing algorithms and classification tools allowed us to determine and quantify the precise number of cells that show NF-κB nuclear translocation. Significantly, analysis of NF-κB translocation by this methodology overcomes many of the limitations associated with conventional techniques (microscopy and western blot).

Our results show that Imaging-Flow Cytometry allowed us to quantify the effect of tested compounds and biological regulators on NF-κB nuclear translocation in the monoblastic leukemia cell line U937 and in whole blood samples.

CONCLUSIONS

Phagocytosis and oxidative burst assays

1. Analysis by Imaging Flow Cytometry of U937 cells and whole blood samples allows the discrimination between extracellular and ingested bacteria. Moreover, the number of bacteria per cell can be quantified.
2. This assay has been applied successfully to estimate the phagocytic potential of leukocytes in whole blood samples of normal subjects and it may provide a fast, simple and accurate protocol for diagnosing phagocytic disorders and toxic effects on phagocytic cells.

NF-κB Immunotoxicity assays

3. This is a fast and simple method for detecting immunotoxicity on processes associated with this molecular target. The present approach is not limited to NF-κB translocation and it could be used for any factor where regulation is associated with its intracellular location.
4. Automated image processing algorithms allowed us to calculate the percentage of lymphocytes and monocytes showing NF-kB nuclear translocation in each condition. IC50 values could be derived, thus classifying the immunotoxic potency of test compounds and allowing comparison with general cytotoxicity, as measured by PI assay and by the microplate Alamar Blue assay.

BIBLIOGRAPHY

Aderem, A. (2003). "Phagocytosis and the inflammatory response." J Infect Dis **187 Suppl 2**: S340-345.

Aderem, A. and D. M. Underhill (1999). "Mechanisms of phagocytosis in macrophages." Annu Rev Immunol **17**: 593-623.

Albert, M. L., J. I. Kim, et al. (2000). "alphavbeta5 integrin recruits the CrkII-Dock180-rac1 complex for phagocytosis of apoptotic cells." Nat Cell Biol **2**(12): 899-905.

Alevy, Y. G., J. Tucker, et al. (1993). "CD32C (Fc gamma RIIC) mRNA expression and regulation." Mol Immunol **30**(8): 775-782.

Alexander, C. and E. T. Rietschel (2001). "Bacterial lipopolysaccharides and innate immunity." J Endotoxin Res **7**(3): 167-202.

Ali, W. H., Q. Chen, et al. (2013). "Deficiencies of the lipid-signaling enzymes phospholipase D1 and D2 alter cytoskeletal organization, macrophage phagocytosis, and cytokine-stimulated neutrophil recruitment." PLoS One **8**(1): e55325.

Anderson, C. L., L. Shen, et al. (1990). "Phagocytosis mediated by three distinct Fc gamma receptor classes on human leukocytes." J Exp Med **171**(4): 1333-1345.

Anderson, H. A., C. A. Maylock, et al. (2003). "Serum-derived protein S binds to phosphatidylserine and stimulates the phagocytosis of apoptotic cells." Nat Immunol **4**(1): 87-91.

Andrews, T. and K. E. Sullivan (2003). "Infections in patients with inherited defects in phagocytic function." Clin Microbiol Rev **16**(4): 597-621.

Araki, N. (2006). "Role of microtubules and myosins in Fc gamma receptor-mediated phagocytosis." Front Biosci **11**: 1479-1490.

Ayatollahi, M., Z. Tabei, et al. (2006). "A fast and easy nitroblue tetrazolium method for carrier screening and prenatal detection of chronic granulomatous disease." Arch Iran Med **9**(4): 335-338.

Babior, B. M. (2000). "Phagocytes and oxidative stress." Am J Med **109**(1): 33-44.

Babior, B. M., R. S. Kipnes, et al. (1973). "Biological defense mechanisms. The production by leukocytes of superoxide, a potential bactericidal agent." J Clin Invest **52**(3): 741-744.

Bajno, L., X. R. Peng, et al. (2000). "Focal exocytosis of VAMP3-containing vesicles at sites of phagosome formation." J Cell Biol **149**(3): 697-706.

Baldwin, A. S., Jr. (1996). "The NF-kappa B and I kappa B proteins: new discoveries and insights." Annu Rev Immunol **14**: 649-683.

Barnham, K. J., C. L. Masters, et al. (2004). "Neurodegenerative diseases and oxidative stress." Nat Rev Drug Discov **3**(3): 205-214.

Basiji, D. and M. R. O'Gorman (2015). "Imaging flow cytometry." J Immunol Methods **423**: 1-2.

Basiji, D. A., W. E. Ortyn, et al. (2007). "Cellular image analysis and imaging by flow cytometry." Clin Lab Med **27**(3): 653-670, viii.

Baud, V. and M. Karin (2001). "Signal transduction by tumor necrosis factor and its relatives." Trends Cell Biol **11**(9): 372-377.

Bear, J. E., J. F. Rawls, et al. (1998). "SCAR, a WASP-related protein, isolated as a suppressor of receptor defects in late Dictyostelium development." J Cell Biol **142**(5): 1325-1335.

Beltran, B., P. Nos, et al. (2010). "Mitochondrial dysfunction, persistent oxidative damage, and catalase inhibition in immune cells of naive and treated Crohn's disease." Inflamm Bowel Dis **16**(1): 76-86.

Benov, L., L. Sztejnberg, et al. (1998). "Critical evaluation of the use of hydroethidine as a measure of superoxide anion radical." Free Radic Biol Med **25**(7): 826-831.

Bielski, B. H., R. L. Arudi, et al. (1983). "A study of the reactivity of HO2/O2- with unsaturated fatty acids." J Biol Chem **258**(8): 4759-4761.

Blystone, S. D., I. L. Graham, et al. (1994). "Integrin alpha v beta 3 differentially regulates adhesive and phagocytic functions of the fibronectin receptor alpha 5 beta 1." J Cell Biol **127**(4): 1129-1137.

Boverhof, D. R., G. Ladics, et al. (2014). "Approaches and considerations for the assessment of immunotoxicity for environmental chemicals: a workshop summary." Regul Toxicol Pharmacol **68**(1): 96-107.

Bozzaro, S. and L. Eichinger (2011). "The professional phagocyte Dictyostelium discoideum as a model host for bacterial pathogens." Curr Drug Targets **12**(7): 942-954.

Brinkmann, V., U. Reichard, et al. (2004). "Neutrophil extracellular traps kill bacteria." Science **303**(5663): 1532-1535.

Burch, P. M. and N. H. Heintz (2005). "Redox regulation of cell-cycle re-entry: cyclin D1 as a primary target for the mitogenic effects of reactive oxygen and nitrogen species." Antioxid Redox Signal **7**(5-6): 741-751.

Burhans, W. C. and N. H. Heintz (2009). "The cell cycle is a redox cycle: linking phase-specific targets to cell fate." Free Radic Biol Med **47**(9): 1282-1293.

Cadenas, E. and K. J. Davies (2000). "Mitochondrial free radical generation, oxidative stress, and aging." Free Radic Biol Med **29**(3-4): 222-230.

Cannon, G. J. and J. A. Swanson (1992). "The macrophage capacity for phagocytosis." J Cell Sci **101 (Pt 4)**: 907-913.

Clancy, D. and J. Birdsall (2013). "Flies, worms and the Free Radical Theory of ageing." Ageing Res Rev **12**(1): 404-412.

Collado, R., D. Ivars, et al. (2014). "Increased oxidative damage associated with unfavorable cytogenetic subgroups in chronic lymphocytic leukemia." Biomed Res Int **2014**: 686392.

Conner, S. D. and S. L. Schmid (2003). "Regulated portals of entry into the cell." Nature **422**(6927): 37-44.

Chen, S. H., J. K. Lin, et al. (2008). "Involvement of activating transcription factors JNK, NF-kappaB, and AP-1 in apoptosis induced by pyrrolidine dithiocarbamate/Cu complex." Eur J Pharmacol **594**(1-3): 9-17.

Choi, H., S. Kim, et al. (2001). "Structural basis of the redox switch in the OxyR transcription factor." Cell **105**(1): 103-113.

Daeron, M., O. Malbec, et al. (1994). "Tyrosine-containing activation motif-dependent phagocytosis in mast cells." J Immunol **152**(2): 783-792.

de Oliveira-Junior, E. B., J. Bustamante, et al. (2011). "The human NADPH oxidase: primary and secondary defects impairing the respiratory burst function and the microbicidal ability of phagocytes." Scand J Immunol **73**(5): 420-427.

de Oliveira Junior, M. R., A. L. Saud, et al. (2011). "Morphometrical analysis of the human mandibular canal: a CT investigation." Surg Radiol Anat **33**(4): 345-352.

Di Meo, S., T. T. Reed, et al. (2016). "Role of ROS and RNS Sources in Physiological and Pathological Conditions." Oxid Med Cell Longev **2016**: 1245049.

Dickinson, B. C. and C. J. Chang (2011). "Chemistry and biology of reactive oxygen species in signaling or stress responses." Nat Chem Biol **7**(8): 504-511.

Drevets, D. A. and P. A. Campbell (1991). "Macrophage phagocytosis: use of fluorescence microscopy to distinguish between extracellular and intracellular bacteria." J Immunol Methods **142**(1): 31-38.

Du Pasquier, L. (2004). "Innate immunity in early chordates and the appearance of adaptive immunity." C R Biol **327**(6): 591-601.

Duclos, S., R. Diez, et al. (2000). "Rab5 regulates the kiss and run fusion between phagosomes and endosomes and the acquisition of phagosome leishmanicidal properties in RAW 264.7 macrophages." J Cell Sci **113 Pt 19**: 3531-3541.

Dugas, B., P. Debre, et al. (1995). "Nitric oxide, a vital poison inside the immune and inflammatory network." Res Immunol **146**(9): 664-670.

El-Benna, J., M. Hurtado-Nedelec, et al. (2016). "Priming of the neutrophil respiratory burst: role in host defense and inflammation." Immunol Rev **273**(1): 180-193.

Erusalimsky, J. D. and S. Moncada (2007). "Nitric oxide and mitochondrial signaling: from physiology to pathophysiology." Arterioscler Thromb Vasc Biol **27**(12): 2524-2531.

Erwig, L. P. and P. M. Henson (2008). "Clearance of apoptotic cells by phagocytes." Cell Death Differ **15**(2): 243-250.

Ezekowitz, R. A., K. Sastry, et al. (1990). "Molecular characterization of the human macrophage mannose receptor: demonstration of multiple carbohydrate recognition-like domains and phagocytosis of yeasts in Cos-1 cells." J Exp Med **172**(6): 1785-1794.

Flannagan, R. S., V. Jaumouille, et al. (2012). "The cell biology of phagocytosis." Annu Rev Pathol **7**: 61-98.

Forman, H. J. (2016). "Redox signaling: An evolution from free radicals to aging." Free Radic Biol Med **97**: 398-407.

Forman, H. J., O. Augusto, et al. (2015). "Even free radicals should follow some rules: a guide to free radical research terminology and methodology." Free Radic Biol Med **78**: 233-235.

Foulds, S. (1997). "Novel flow cytometric method for quantifying nuclear binding of the transcription factor nuclear factor kappa B in unseparated human monocytes and polymorphonuclear cells." Cytometry **29**(2): 182-186.

Fridovich, I. (1998). "Oxygen toxicity: a radical explanation." J Exp Biol **201**(Pt 8): 1203-1209.

Fuchs, T. A., U. Abed, et al. (2007). "Novel cell death program leads to neutrophil extracellular traps." J Cell Biol **176**(2): 231-241.

Fuentes, E. and I. Palomo (2016). "Role of oxidative stress on platelet hyperreactivity during aging." Life Sci **148**: 17-23.

Gardiner, G. J., S. N. Deffit, et al. (2013). "A role for NADPH oxidase in antigen presentation." Front Immunol **4**: 295.

Gardner, R. M., J. F. Nyland, et al. (2010). "Differential immunotoxic effects of inorganic and organic mercury species in vitro." Toxicol Lett **198**(2): 182-190.

Ghezzi, P. and V. Bonetto (2003). "Redox proteomics: identification of oxidatively modified proteins." Proteomics **3**(7): 1145-1153.

Ghiran, I., S. F. Barbashov, et al. (2000). "Complement receptor 1/CD35 is a receptor for mannan-binding lectin." J Exp Med **192**(12): 1797-1808.

Gomes, A., E. Fernandes, et al. (2005). "Fluorescence probes used for detection of reactive oxygen species." J Biochem Biophys Methods **65**(2-3): 45-80.

Gordon, S. (2008). "Elie Metchnikoff: father of natural immunity." Eur J Immunol **38**(12): 3257-3264.

Greenberg, M. E., M. Sun, et al. (2006). "Oxidized phosphatidylserine-CD36 interactions play an essential role in macrophage-dependent phagocytosis of apoptotic cells." J Exp Med **203**(12): 2613-2625.

Gros, L., M. K. Saparbaev, et al. (2002). "Enzymology of the repair of free radicals-induced DNA damage." Oncogene **21**(58): 8905-8925.

Gross, H. J., B. Verwer, et al. (1993). "Detection of rare cells at a frequency of one per million by flow cytometry." Cytometry **14**(5): 519-526.

Halliwell, B. and M. Whiteman (2004). "Measuring reactive species and oxidative damage in vivo and in cell culture: how should you do it and what do the results mean?" Br J Pharmacol **142**(2): 231-255.

Hampton, M. B., A. J. Kettle, et al. (1998). "Inside the neutrophil phagosome: oxidants, myeloperoxidase, and bacterial killing." Blood **92**(9): 3007-3017.

Hampton, M. B. and C. C. Winterbourn (1999). "Methods for quantifying phagocytosis and bacterial killing by human neutrophils." J Immunol Methods **232**(1-2): 15-22.

Hanayama, R., M. Tanaka, et al. (2002). "Identification of a factor that links apoptotic cells to phagocytes." Nature **417**(6885): 182-187.

Havens, C. G., A. Ho, et al. (2006). "Regulation of late G1/S phase transition and APC Cdh1 by reactive oxygen species." Mol Cell Biol **26**(12): 4701-4711.

Hayashi, G. and G. Cortopassi (2015). "Oxidative stress in inherited mitochondrial diseases." Free Radic Biol Med **88**(Pt A): 10-17.

Hayden, M. S., A. P. West, et al. (2006). "NF-kappaB and the immune response." Oncogene **25**(51): 6758-6780.

Henchcliffe, C. and M. F. Beal (2008). "Mitochondrial biology and oxidative stress in Parkinson disease pathogenesis." Nat Clin Pract Neurol **4**(11): 600-609.

Herre, J., A. S. Marshall, et al. (2004). "Dectin-1 uses novel mechanisms for yeast phagocytosis in macrophages." Blood **104**(13): 4038-4045.

Hoffmann, A., G. Natoli, et al. (2006). "Transcriptional regulation via the NF-kappaB signaling module." Oncogene **25**(51): 6706-6716.

Holevinsky, K. O. and D. J. Nelson (1998). "Membrane capacitance changes associated with particle uptake during phagocytosis in macrophages." Biophys J **75**(5): 2577-2586.

Holland, S. M. (2010). "Chronic granulomatous disease." Clin Rev Allergy Immunol **38**(1): 3-10.

Holland, S. M. (2013). "Chronic granulomatous disease." Hematol Oncol Clin North Am **27**(1): 89-99, viii.

Huxford, T., S. Malek, et al. (1999). "Structure and mechanism in NF-kappa B/I kappa B signaling." Cold Spring Harb Symp Quant Biol **64**: 533-540.

Ibbotson, G. C., C. Doig, et al. (2001). "Functional alpha4-integrin: a newly identified pathway of neutrophil recruitment in critically ill septic patients." Nat Med **7**(4): 465-470.

Iijima, M., Y. E. Huang, et al. (2002). "Temporal and spatial regulation of chemotaxis." Dev Cell **3**(4): 469-478.

Imlay, J. A. (2013). "The molecular mechanisms and physiological consequences of oxidative stress: lessons from a model bacterium." Nat Rev Microbiol **11**(7): 443-454.

Ivanov, A. V., V. T. Valuev-Elliston, et al. (2016). "Oxidative Stress during HIV Infection: Mechanisms and Consequences." Oxid Med Cell Longev **2016**: 8910396.

Ivanova, D., Z. Zhelev, et al. (2016). "Overproduction of reactive oxygen species - obligatory or not for induction of apoptosis by anticancer drugs." Chin J Cancer Res **28**(4): 383-396.

Jang, J. Y., J. H. Min, et al. (2014). "Reactive oxygen species play a critical role in collagen-induced platelet activation via SHP-2 oxidation." Antioxid Redox Signal **20**(16): 2528-2540.

Jaumouille, V. and S. Grinstein (2011). "Receptor mobility, the cytoskeleton, and particle binding during phagocytosis." Curr Opin Cell Biol **23**(1): 22-29.

Jutras, I. and M. Desjardins (2005). "Phagocytosis: at the crossroads of innate and adaptive immunity." Annu Rev Cell Dev Biol **21**: 511-527.

Klebanoff, S. J., A. J. Kettle, et al. (2013). "Myeloperoxidase: a front-line defender against phagocytosed microorganisms." J Leukoc Biol **93**(2): 185-198.

Kobayashi, N., P. Karisola, et al. (2007). "TIM-1 and TIM-4 glycoproteins bind phosphatidylserine and mediate uptake of apoptotic cells." Immunity **27**(6): 927-940.

Krutzik, P. O. and G. P. Nolan (2003). "Intracellular phospho-protein staining techniques for flow cytometry: monitoring single cell signaling events." Cytometry A **55**(2): 61-70.

Li, S., H. Y. Tan, et al. (2015). "The Role of Oxidative Stress and Antioxidants in Liver Diseases." Int J Mol Sci **16**(11): 26087-26124.

Liegibel, U. M., S. L. Abrahamse, et al. (2000). "Application of confocal laser scanning microscopy to detect oxidative stress in human colon cells." Free Radic Res **32**(6): 535-547.

Lionaki, E., M. Markaki, et al. (2013). "Autophagy and ageing: insights from invertebrate model organisms." Ageing Res Rev **12**(1): 413-428.

Luebke, R. (2012). "Immunotoxicant screening and prioritization in the twenty-first century." Toxicol Pathol **40**(2): 294-299.

Manshian, B. B., A. M. Abdelmonem, et al. (2016). "Evaluation of quantum dot cytotoxicity: interpretation of nanoparticle concentrations versus intracellular nanoparticle numbers." Nanotoxicology **10**(9): 1318-1328.

Margulis, L. and D. Bermudes (1985). "Symbiosis as a mechanism of evolution: status of cell symbiosis theory." Symbiosis **1**: 101-124.

Marletta, M. A. (1994). "Nitric oxide synthase: aspects concerning structure and catalysis." Cell **78**(6): 927-930.

Martinez-Pastor, F., M. Mata-Campuzano, et al. (2010). "Probes and techniques for sperm evaluation by flow cytometry." Reprod Domest Anim **45 Suppl 2**: 67-78.

Massaad, C. A. and E. Klann (2011). "Reactive oxygen species in the regulation of synaptic plasticity and memory." Antioxid Redox Signal **14**(10): 2013-2054.

Miki, H., K. Miura, et al. (1996). "N-WASP, a novel actin-depolymerizing protein, regulates the cortical cytoskeletal rearrangement in a PIP2-dependent manner downstream of tyrosine kinases." EMBO J **15**(19): 5326-5335.

Miskolci, V., J. Rollins, et al. (2007). "NFkappaB is persistently activated in continuously stimulated human neutrophils." Mol Med **13**(3-4): 134-142.

Nakano, H., A. Nakajima, et al. (2006). "Reactive oxygen species mediate crosstalk between NF-kappaB and JNK." Cell Death Differ **13**(5): 730-737.

Navarro-Yepes, J., M. Burns, et al. (2014). "Oxidative stress, redox signaling, and autophagy: cell death versus survival." Antioxid Redox Signal **21**(1): 66-85.

Nicholls, S. J. and S. L. Hazen (2005). "Myeloperoxidase and cardiovascular disease." Arterioscler Thromb Vasc Biol **25**(6): 1102-1111.

Niedel, J. E., L. J. Kuhn, et al. (1983). "Phorbol diester receptor copurifies with protein kinase C." Proc Natl Acad Sci U S A **80**(1): 36-40.

Nolan, K., J. Kamrath, et al. (2012). "Lindane toxicity: a comprehensive review of the medical literature." Pediatr Dermatol **29**(2): 141-146.

O'Connor, J. E., R. C. Callaghan, et al. (2001). "The relevance of flow cytometry for biochemical analysis." IUBMB Life **51**(4): 231-239.

Oh, B., G. Figtree, et al. (2016). "Oxidative stress in prostate cancer patients: A systematic review of case control studies." Prostate Int **4**(3): 71-87.

Palazzolo, A. M., C. Suquet, et al. (2005). "Green fluorescent protein-expressing Escherichia coli as a selective probe for HOCl generation within neutrophils." Biochemistry **44**(18): 6910-6919.

Park, D., A. C. Tosello-Trampont, et al. (2007). "BAI1 is an engulfment receptor for apoptotic cells upstream of the ELMO/Dock180/Rac module." Nature **450**(7168): 430-434.

Park, H. S., D. Park, et al. (2006). "Molecular interaction of NADPH oxidase 1 with betaPix and Nox Organizer 1." Biochem Biophys Res Commun **339**(3): 985-990.

Park, S. Y., M. Y. Jung, et al. (2008). "Rapid cell corpse clearance by stabilin-2, a membrane phosphatidylserine receptor." Cell Death Differ **15**(1): 192-201.

Patel, S. N., L. Serghides, et al. (2004). "CD36 mediates the phagocytosis of Plasmodium falciparum-infected erythrocytes by rodent macrophages." J Infect Dis **189**(2): 204-213.

Perkins, N. D. and T. D. Gilmore (2006). "Good cop, bad cop: the different faces of NF-kappaB." Cell Death Differ **13**(5): 759-772.

Ploppa, A., T. C. George, et al. (2011). "ImageStream cytometry extends the analysis of phagocytosis and oxidative burst." Scand J Clin Lab Invest **71**(5): 362-369.

Rahal, A., A. Kumar, et al. (2014). "Oxidative stress, prooxidants, and antioxidants: the interplay." Biomed Res Int **2014**: 761264.

Rani, V., G. Deep, et al. (2016). "Oxidative stress and metabolic disorders: Pathogenesis and therapeutic strategies." Life Sci **148**: 183-193.

Ranoa, D. R., S. L. Kelley, et al. (2013). "Human lipopolysaccharide-binding protein (LBP) and CD14 independently deliver triacylated lipoproteins to Toll-like receptor 1 (TLR1) and TLR2 and enhance formation of the ternary signaling complex." J Biol Chem **288**(14): 9729-9741.

Reeves, E. P., H. Lu, et al. (2002). "Killing activity of neutrophils is mediated through activation of proteases by K+ flux." Nature **416**(6878): 291-297.

Reisinger, E. C., P. Kern, et al. (1990). "Inhibition of HIV progression by dithiocarb. German DTC Study Group." Lancet **335**(8691): 679-682.

Ritz, D. and J. Beckwith (2001). "Roles of thiol-redox pathways in bacteria." Annu Rev Microbiol **55**: 21-48.

Ross, G. D., W. Reed, et al. (1992). "Macrophage cytoskeleton association with CR3 and CR4 regulates receptor mobility and phagocytosis of iC3b-opsonized erythrocytes." J Leukoc Biol **51**(2): 109-117.

Roxo-Junior, P. and H. M. Simao (2014). "Chronic granulomatous disease: why an inflammatory disease?" Braz J Med Biol Res **47**(11): 924-928.

Saito, Y., K. Nishio, et al. (2006). "Turning point in apoptosis/necrosis induced by hydrogen peroxide." Free Radic Res **40**(6): 619-630.

Scheidereit, C. (2006). "IkappaB kinase complexes: gateways to NF-kappaB activation and transcription." Oncogene **25**(51): 6685-6705.

Schiff, D. E., L. Kline, et al. (1997). "Phagocytosis of gram-negative bacteria by a unique CD14-dependent mechanism." J Leukoc Biol **62**(6): 786-794.

Schwartz, M. D., E. E. Moore, et al. (1996). "Nuclear factor-kappa B is activated in alveolar macrophages from patients with acute respiratory distress syndrome." Crit Care Med **24**(8): 1285-1292.

Senftleben, U., Y. Cao, et al. (2001). "Activation by IKKalpha of a second, evolutionary conserved, NF-kappa B signaling pathway." Science **293**(5534): 1495-1499.

Siti, H. N., Y. Kamisah, et al. (2015). "The role of oxidative stress, antioxidants and vascular inflammation in cardiovascular disease (a review)." Vascul Pharmacol **71**: 40-56.

Speckmann, B., H. Steinbrenner, et al. (2016). "Peroxynitrite: From interception to signaling." Arch Biochem Biophys **595**: 153-160.

Splettstoesser, W. D. and P. Schuff-Werner (2002). "Oxidative stress in phagocytes--"the enemy within"." Microsc Res Tech **57**(6): 441-455.

Strober, W. (2001). "Trypan blue exclusion test of cell viability." Curr Protoc Immunol **Appendix 3**: Appendix 3B.

Stuart, L. M. and R. A. Ezekowitz (2005). "Phagocytosis: elegant complexity." Immunity **22**(5): 539-550.

Tamarit, J. (2014). Desarrollo de un ensayo de Fagocitosis en sangre entera mediante Citometría de Flujo con bacterias que expresan GFP. Universidad de Valencia.

Tarpey, M. M., D. A. Wink, et al. (2004). "Methods for detection of reactive metabolites of oxygen and nitrogen: in vitro and in vivo considerations." Am J Physiol Regul Integr Comp Physiol **286**(3): R431-444.

Thomas, C. A., Y. Li, et al. (2000). "Protection from lethal gram-positive infection by macrophage scavenger receptor-dependent phagocytosis." J Exp Med **191**(1): 147-156.

Tsai, J. C., M. Jain, et al. (1996). "Induction of apoptosis by pyrrolidinedithiocarbamate and N-acetylcysteine in vascular smooth muscle cells." J Biol Chem **271**(7): 3667-3670.

Underhill, D. M. and A. Ozinsky (2002). "Phagocytosis of microbes: complexity in action." Annu Rev Immunol **20**: 825-852.

Valko, M., D. Leibfritz, et al. (2007). "Free radicals and antioxidants in normal physiological functions and human disease." Int J Biochem Cell Biol **39**(1): 44-84.

Van Amersfoort, E. S. and J. A. Van Strijp (1994). "Evaluation of a flow cytometric fluorescence quenching assay of phagocytosis of sensitized sheep erythrocytes by polymorphonuclear leukocytes." Cytometry **17**(4): 294-301.

van den Berg, J. M., E. van Koppen, et al. (2009). "Chronic granulomatous disease: the European experience." PLoS One **4**(4): e5234.

van der Laan, L. J., E. A. Dopp, et al. (1999). "Regulation and functional involvement of macrophage scavenger receptor MARCO in clearance of bacteria in vivo." J Immunol **162**(2): 939-947.

van Eeden, S. F., M. E. Klut, et al. (1999). "The use of flow cytometry to measure neutrophil function." J Immunol Methods **232**(1-2): 23-43.

van Spriel, A. B., I. E. van den Herik-Oudijk, et al. (1999). "Effective phagocytosis and killing of Candida albicans via targeting FcgammaRI (CD64) or FcalphaRI (CD89) on neutrophils." J Infect Dis **179**(3): 661-669.

Vernon, P. J. and D. Tang (2013). "Eat-me: autophagy, phagocytosis, and reactive oxygen species signaling." Antioxid Redox Signal **18**(6): 677-691.

Vina, J., C. Borras, et al. (2007). "Theories of ageing." IUBMB Life **59**(4-5): 249-254.

Vos, J. G. (1986). "Immunotoxicity of hexachlorobenzene." IARC Sci Publ(77): 347-356.

Wardman, P. (2007). "Fluorescent and luminescent probes for measurement of oxidative and nitrosative species in cells and tissues: progress, pitfalls, and prospects." Free Radic Biol Med **43**(7): 995-1022.

Wei, M., L. Li, et al. (2010). "Suppressive effect of diazepam on IFN-gamma production by human T cells." Int Immunopharmacol **10**(3): 267-271.

Weinberg, J. B., M. A. Misukonis, et al. (1995). "Human mononuclear phagocyte inducible nitric oxide synthase (iNOS): analysis of iNOS mRNA, iNOS protein,

biopterin, and nitric oxide production by blood monocytes and peritoneal macrophages." Blood **86**(3): 1184-1195.

Zhang, Q. F., Y. W. Li, et al. (2016). "Exposure to mercuric chloride induces developmental damage, oxidative stress and immunotoxicity in zebrafish embryos-larvae." Aquat Toxicol **181**: 76-85.

Zhao, W., H. Feng, et al. (2017). "Tert-butyl hydroperoxide (t-BHP) induced apoptosis and necroptosis in endothelial cells: Roles of NOX4 and mitochondrion." Redox Biol **11**: 524-534.